COALESCENCE AND BREAK-UP OF DROPS AND BUBBLES

BY

LARS HAGESÆTHER

NORWEGIAN UNIVERSITY OF SCIENCE AND TECHNOLOGY
DEPARTMENT OF CHEMICAL ENGINEERING
N-7491 TRONDHEIM, NORWAY

THESIS SUBMITTED FOR THE DEGREE OF DR.ING. (Ph.D.)

MARCH 2002

Acknowledgement

This thesis is a result of a good number of years spent at the department, years which I have enjoyed greatly. Part of this time has been spent as a tutorial assistant, and to my surprise I liked it quite a lot.

This work was made possible through input from advisors, co-workers, friends and family. In particular I wish to thank professor Hugo A. Jakobsen. He has shown a huge interest in this work and he has pushed me forward when needed. Professor Hallvard F. Svendsen is also be mentioned, he got me started and has been an avid reader of my output, giving loads of suggestions.

A former Dr.ing. student and friend also pushed me into reading 'To Kill a Mockingbird'. Thus, the reader of this acknowledgement should at least read either my thesis or this great book by Harper Lee!

Financial support from the Norwegian Research Council is gratefully acknowledged.

Abstract

Fluid particle break-up and coalescence are important phenomena in a number of industrial processes.

A Lagrangian momentum balance model for the collision process between two fluid particles has been developed and tested favorably against experimental data. It is based on an earlier model developed in our department. Oscillations were introduced and the volume balances that are solved avoid earlier approximations. Film drainage was also implemented into the model based on a literature review given. It is believed this approach will lead to a more fundamental modeling of the coalescence process.

An improved break-up model has been developed. It is an extension of earlier work at the department and it introduces an additional criterion for break-up. This criterion gives a lower limit for the daughter fragment sizes in binary break-up, thus also limiting the break-up of smaller fluid particles, and is a more consistent model than the earlier one.

Two break-up models, original model by Luo (1993) and improved model, and a coalescence model have been implemented in a population balance as algebraic sink and source terms. This population balance is in turn included in an in-house CFD-code. The models have been tested against experimental data from a bubble column in our laboratory, and the improved break-up model compares favorably with the experimentally obtained accumulated mass distribution. Too few bubbles are predicted in the lower population classes, but it is shown that this may as well be a result of the coalescence model used as the improved break-up model.

Reference:

Luo, H. (1993). Coalescence, breakup and liquid circulation in bubble column reactors. Dr.Ing. Thesis, The Norwegian Institute of Technology, Trondheim.

Contents

Acknowledgement . . . . . **i**

Abstract . . . . . **iii**

CHAPTER 1 Introduction **1**

1.1 Motivation 1

1.2 Thesis outline 2

CHAPTER 2 The population balance model **5**

2.1 Basic number balance (population balance equation) 5

2.1.1 Break-up closure requirements 8

2.1.1.1 Maximum particle volume, ... 9

2.1.1.2 Daughter particle size distribution, ... 10

2.1.1.3 Number of daughter particle production, ... 10

2.1.1.4 Break-up frequency, ... 11

2.1.2 Coalescence closure requirements 12

2.1.2.1 Minimum particle volume, ... 12

2.1.2.2 Particle collision frequency, ... 13

2.1.2.3 Fluid particle coalescence efficiency, ... 13

2.2 Discretization of the particle size distribution 15

CHAPTER 3 Fluid particle coalescence efficiency **21**

3.1 Coalescence efficiency parameterizations, the relation to particle collision models . 21

3.1.1 Film rupture 22

3.1.2 Film drainage 22
3.1.2.1 Lubrication theory 22
3.1.2.2 Force, lubrication theory and drainage 31
3.1.2.3 Modification of the lubrication theory 34
3.1.2.4 Dimple in film 39
3.1.2.5 Surfactants or impurities 42
3.1.3 Fluid particle collision (force balance) 46
3.1.3.1 Drag force 52
3.1.3.2 Collision angle and off-centre collisions 52
3.1.4 Experimental studies 55
3.2 Coalescence efficiency 65

CHAPTER 4 Fluid particle collisions in turbulent flow 77
4.1 Introduction 77
4.2 Model description 78
4.3 Results and Discussion 83
4.4 Conclusion 89

CHAPTER 5 Fluid particle break-up 93
5.1 Introduction 93
5.2 Review and discussion of existing break-up model 94
5.2.1 The collision frequency 95
5.2.2 The collision outcome 98
5.3 The modified model 105
5.3.1 The surface energy probability 105
5.3.2 The energy density probability 107
5.4 Total break-up probability 112
5.5 Daughter size distribution 120
5.6 Numerical implementations 121
5.6.1 Eddy energy 121

5.6.2 Eddy classes 124
5.6.3 Daughter class distribution 125
5.7 Sensitivity analysis 126
5.8 Results 127
5.9 Possible model refinements 139
5.9.1 Activation energy 139
5.9.2 Surface energy criterion 141
5.9.3 Inertial subrange of turbulence 141
5.9.4 Fluid particle rest state 142
5.9.5 Number of daughter fragments 142
5.9.6 Collision frequency 143
5.9.7 Entropy 143
5.10 Conclusions 143

CHAPTER 6 Modeling of the dispersed phase size distribution in a bubble column 151

6.1 Introduction 151
6.2 The model 152
6.3 Numerical methods 162
6.4 Model validation 163
6.5 Multi-fluid modeling 167
6.6 Results and discussion 168
6.7 Conclusions 181

CHAPTER 7 Conclusions and recommendations for further work . . 189

7.1 General overview 189
7.2 General conclusions 190
7.3 Recommendations for further work 191

APPENDIX A Population balances 195

A.1 Finding the population balance like equation 195

A.2 Split into classes 196

A.3 Break-up 197

A.4 Coalescence 202

A.5 Break-up in population balance 202

A.6 Coalescence in population balance 206

A.7 Incorporation into the transport equation 209

CHAPTER 1

Introduction

1.1 Motivation

Fluid particle break-up and coalescence are important phenomena in a number of process units. Some industries with particular reactor examples in parentheses are listed below:

- Process industry (slurry columns, bubble columns, stirred vessels)
- Nuclear industry (reactors)
- Biological industry (fermentation)
- Metallurgical industry (electrolytic cells, refining units)
- Mining industry (extraction, flotation)
- Oil industry (scrubbers, gravity separators, cyclones)

Norway is the 9th largest oil producer and the 3rd largest net crude exporter in the world. However, gas will become more important in the future since the gas reserves will last much longer than the oil reserves with the current rate of production. Currently most of the produced gas on the Norwegian Continental Shelf is transported by pipelines to the continent. As reserves further to the north are produced this method will be less profitable and other alternatives will be more inter-

esting. These alternatives include subsea processing, piping to the coastal areas and further processing of natural gas to LNG or chemical conversion to hydrocarbons through GTL processes (e.g. Fischer-Tropsch). Thus our interest for fluid particle break-up and coalescence lies primarily with the oil companies, oil/water/gas separations and chemical conversion of natural gas. This interest has been reflected through a number of research programs by NFR (Norwegian Research Council) where these fundamental phenomena are featured. Examples are SPUNG (State R&D Program for Utilization of Natural Gas), Chemical Conversion of Gas, CARPET (CFD Applied to Reactor ProcEss Technology) and HiPGaS (High Pressure Gas Separation). These programs are in general co-sponsored by government and industry.

My own work is a continuation of an ongoing Ph.D program developing modeling tools for multiphase reactors that was started in 1987 at our institute. 5 Ph.D. projects have finished on related topics during these years. My project is sponsored by the NFR program: Chemical Conversion of Gas.

1.2 Thesis outline

In chapter 2 a general overview of population balances describing dispersed phases is provided. The continuous phase considered here is primarily a liquid and the dispersed phase may be either a liquid or a gas.

Chapter 3 contains a literature survey of the theories for fluid particle coalescence efficiency. This variable is assumed to be determined by particle collision mechanisms like film draining (lubrication theory), particle deformation and film rupture.

In chapter 4 a collision model for two colliding fluid particles that are oscillating is developed. The model solves a Lagrangian momentum balance for each of the two colliding fluid particles, and this involves the calculation of both the contact area and the film thickness between the particles.

In chapter 5 a fluid particle break-up model is developed that is an extension of an earlier model. The earlier model defines break-up based on only one criteria, i.e. when the energy applied to a fluid particle is greater than the change of surface energy due to a break-up. A new criterion is added for the energy density of the fluid particles and eddies. This criterion limits the lower possible size of daughter particles and as a consequence also the rate of break-up.

In chapter 6 the new fluid particle break-up model developed in chapter 5, together with the earlier one, and a coalescence model, are implemented into an in-house CFD code through a population balance. The distribution of bubbles is predicted for in a bubble column and compared to experimental data obtained in our laboratory.

In chapter 7 conclusions and suggestions for further work are presented.

CHAPTER 2

The population balance model

This chapter outlines the modeling framework that has been used to describe the fluid particle break-up and binary coalescence phenomena. It serves as a brief introduction to the population balance model in order to tie together the remaining parts of the thesis. First, an overview of the general population balance is presented. Second, the four source terms, i.e. the birth and death terms due to break-up and coalescence, are described. Third, the source term parameterizations used are discussed. Finally, the discretization of the particle size distribution is briefly outlined.

2.1 Basic number balance (population balance equation)

Several formulations of the population balance model exist. Ramkrishna (1985), Carrica, Drew, Bonetto & Lahey Jr. (1999) and Kocamustafaogullari & Ishii (1995) uses the Bolzmann transport equation as a starting point, others use continuum mechanics, Randolph & Larsson (1988). Randolph & Larsson (1988) start with a population balance in some fixed subregion of particle phase space and state

$$Accumulation = Input - Output + Net\ generation. \tag{2.1}$$

Considering a subregion, say R_1, to move convectively with particle phase space velocity v (i.e., take the Lagrangian viewpoint) then the population balance equation in the subregion may be stated as

$$\frac{d}{dt}\int_{R_1} n dR = \int_{R_1} (B - D) dR. \tag{2.2}$$

B represents the birth terms and D represents the death terms. $n(R, t)$ is considered an (m+3) dimensional particle distribution function defined over a region R consisting of the three spatial dimensions plus m independent internal property coordinates. The former term in (2.2) may be expanded to

$$\frac{d}{dt}\int_{R_1} n dR = \int_{R_1} \frac{\partial n}{\partial t} dR + \left(n\frac{d\boldsymbol{x}}{dt}\right)\Big|_{R_1} = \int_{R_1} \left[\frac{\partial n}{\partial t} + \nabla \cdot \left(\frac{d\boldsymbol{x}}{dt} n\right)\right] dR. \tag{2.3}$$

$\boldsymbol{x}$ is the set of internal and external coordinates comprising the phase space R,

$$\frac{d\boldsymbol{x}}{dt} = \boldsymbol{v} = \boldsymbol{v}_i + \boldsymbol{v}_e. \tag{2.4}$$

The population balance can be written for the Lagrangian region R_1, and since the region is arbitrary the integrand must vanish identically giving the differential population balance as

$$\frac{\partial n}{\partial t} + \nabla \cdot (\boldsymbol{v}_i n) + \nabla \cdot (\boldsymbol{v}_e n) - B + D = 0. \tag{2.5}$$

Diffusion has not been included in (2.5), and growth (or density changes) is part of the internal term.

Kocamustafaogullari & Ishii (1995) discusses the number balance transport equation and closure relations.

Applying the alternative approach based on the Boltzmann equation, more detailed formulations of the source terms are obtained. The procedure accounts for fluid particles entering and leaving a control system through different mechanisms

yielding the fluid particle number density transport equation of particles having volume ϑ:

$$\frac{\partial f}{\partial t} + \nabla \cdot (f\boldsymbol{v}_p) = \sum_{j=1}^{4} S_j + S_{ph}. \tag{2.6}$$

Equation (2.6) is seen to be equal to (2.5) when phase change is included in (2.5). Equation (2.6) is also called a population balance equation and was first introduced in chemical engineering by Hulburt & Katz (1964). In this equation $f(\boldsymbol{x}, \vartheta, t)$ is the particle density distribution function, which is assumed to be continuous and specifies the probable number density of fluid particles at a given time t, in the spatial range $d\boldsymbol{x}$ about a position $\boldsymbol{x}$, with particle volumes between ϑ and $\vartheta + d\vartheta$. $\boldsymbol{v}_p(\boldsymbol{x}, \vartheta, t)$ is the particle velocity of the same volumes. S_{ph} represent phase change terms (nucleation and condensation). The interaction term $\sum_{j=1}^{4} S_j$ represents the net rate of change in the number density distribution function, f, due to particle break-up and coalescence. A general representation of these source and sink terms are as follows, Kocamustafaogullari & Ishii (1995):

$$S_1(\boldsymbol{x}, \vartheta, t) = \int_{\vartheta}^{\vartheta_{max}} \beta(\vartheta', \vartheta) n(\vartheta') g(\vartheta') f(\boldsymbol{x}, \vartheta', t) d\vartheta', \tag{2.7}$$

which represent the formation of particles of size ϑ due to break-up of larger particles. $\beta(\vartheta', \vartheta)$ is the distribution of daughter particles produced upon break-up of a parent particle having volume ϑ'. $n(\vartheta')$ is the number of daughter particles produced upon break-up of a parent particle of ϑ' and $g(\vartheta')$ is the break-up frequency for particle ϑ'.

$$S_2(\boldsymbol{x}, \vartheta, t) = -g(\vartheta) f(\boldsymbol{x}, \vartheta, t) , \tag{2.8}$$

represent the loss rate of particles of size ϑ due to break-up into daughter fragments.

$$S_3(\boldsymbol{x}, \vartheta, t) = \int_{\vartheta_{min}}^{\vartheta/2} \lambda(\vartheta - \vartheta', \vartheta')h(\vartheta - \vartheta', \vartheta')f(\boldsymbol{x}, \vartheta - \vartheta', t)f(\boldsymbol{x}, \vartheta', t)d\vartheta', \quad (2.9)$$

represents the formation of particles of size ϑ due to coalescence of two particles of size ϑ' and $(\vartheta - \vartheta')$. $\lambda(\vartheta, \vartheta')$ is the coalescence efficiency once collision occurs between particles of volumes ϑ and ϑ'. $h(\vartheta, \vartheta')$ is the collision frequency of particles of volumes ϑ and ϑ'.

$$S_4(\boldsymbol{x}, \vartheta, t) = -\int_{\vartheta_{min}}^{\vartheta_{max}-\vartheta} \lambda(\vartheta, \vartheta')h(\vartheta, \vartheta')f(\boldsymbol{x}, \vartheta, t)f(\boldsymbol{x}, \vartheta', t)d\vartheta', \quad (2.10)$$

represents the loss of particles of size ϑ due to coalescence. The source term formulations given above, (2.7) to (2.10), are well known, e.g. Coulaloglou & Tavlarides (1977) and Lee, Ericson & Glasgow (1987b). The breakage terms were first given by Valentas, Bilous & Amundson (1966) and the coalescence terms were first given by Valentas & Amundson (1966). How to model the different functions in the source terms is another matter. Some models are described in the next section.

There are some requirements to the source term closures, (2.7) - (2.10), the following discussion of these are mainly based on Kocamustafaogullari & Ishii (1995).

2.1.1 Break-up closure requirements

The following variables are needed for the break-up source terms.

- Maximum particle volume, ϑ_{max}
- Daughter particle distribution, $\beta(\vartheta, \vartheta')$
- Number of daughter particle production, $n(\vartheta')$
- Break-up frequency, $g(\vartheta')$

The fluid particle break-up variables are discussed below:

2.1.1.1 Maximum particle volume, ϑ_{max}

The maximum particle size which is stable against break-up is found from a generalized break-up mechanism which can be expressed as a balance between external stresses, τ, that attempt to disrupt the fluid particle, and the surface stress, σ/d, resisting the particle deformation. This leads to a critical Weber number

$$We_{cr} = \tau d_{max}/\sigma \geq 1.0\,, \tag{2.11}$$

where d_{max} is the maximum stable fluid particle size.

The hydrodynamic condition responsible for break-up may be, Hinze (1955):

- Turbulent flow (local turbulence)
- Laminar flow (viscous shear)
- Interfacial instability (Rayleigh-Taylor and Kelvin-Helmholtz instabilities, Drazin & Reid (1981))

According to Kocamustafaogullari & Ishii (1995) the two last types of break-up may be neglected in most cases in chemical engineering processes due to high Reynolds numbers in such flows. For the turbulent flow the mean square spatial fluctuating velocity, $\overline{v_c'^2}$, describes the turbulent pressure forces of eddies of size d_{max} giving the critical Weber number as

$$We_{cr} = \rho_c \overline{v_c'^2} d_{max}/\sigma \geq 1.0\,. \tag{2.12}$$

According to Batchelor (1951)

$$\overline{v_c'^2} \cong (\varepsilon d_{max})^{2/3}\,. \tag{2.13}$$

Thus an approximation for d_{max} can be found. As this is just an average value it can at best be used as an aid for setting the upper limit for the size classes when discretizising the population balance equation.

2.1.1.2 Daughter particle size distribution, $\beta(\vartheta, \vartheta')$

A number of empirical functions exist for describing this distribution, as discussed by Hsia & Tavarides (1983) and Tsouris & Tavlarides (1994). Valentas *et al.* (1966) assume binary breakage with equal sized daughter particles which is a limiting case of the complex breakage process for which the breakage kernel is represented by a Kronecker delta function, Kreyszig (1988),

$$\beta(\vartheta, \vartheta') = \delta\left(\vartheta - \frac{1}{2}\vartheta'\right). \tag{2.14}$$

They alternatively use a normal density distribution function as they assumed it is reasonable to expect the distribution of daughter particles to be normal or approximately normal. Coulalogou & Tavlarides (1977) also assume that the daughter distribution follow a normal density function. Narsimhan, Gupta & Ramkrishna (1979) on the other hand assume a uniform daughter droplet size distribution.

Hesketh, Etchells & Russel (1991) observed bubble and droplet break-up in turbulent liquid flow in a pipeline. They found bubbles to break up into only two daughter fragments which had a higher probability for unequal rather than equal size. Two types of breakage was observed:

- Bubble or drop undergoing a large scale deformation resulting in break-up.
- Some kind of tearing mechanism resulting in a very small volume being torn from the original fluid particle.

Nambiar, Kumar, Das & Gandhi (1992) when modeling stirred tanks, also assumes unequal breakage in their model. Their model predicts that a large drop is reduced in size due to stripping of smaller fragments off it through unequal breakage. It is only when the drop is close to the value of the maximum stable drop diameter that it breaks into equal parts.

Many different daughter particle distribution functions have thus been proposed, that are not always consistent with each other.

2.1.1.3 Number of daughter particle production, $n(\vartheta')$

Various experimental data indicate 2-7 daughter particles as the norm from experimental data in liquid-liquid systems, Chatzi & Lee (1987). Bubble break-up on the other hand normally gives two daughter particles. Prince, Walters &

Blanch (1989) found two principal daughter bubbles and also a number of smaller daughter fragments. Narsimhan *et al.* (1979) assumed binary breakage in their model for stirred liquid-liquid dispersions.

2.1.1.4 Break-up frequency, $g(\vartheta')$

There are two types of flow regimes which heavily influence the break-up frequency models:

- Turbulent flow
- Laminar flow

Several phenomenological models exist for liquid-liquid dispersions, Kocamustafaogullari & Ishii (1995):

- Molecular decomposition analogy model
- Dispersion hydrodynamics break-up models
- Critical velocity break-up frequency model
- Drop oscillation break-up frequency model

Flow conditions decide the type of model to be used. For dispersions in turbulent flow, the kinetic energy transferred by eddies plays a dominant role in the break-up process.

Coulaloglou & Tavlarides (1977) proposed a model for $g(\vartheta)$ in turbulent flow based on dispersion hydrodynamics. The model uses eddy-drop collision frequency and energy dissipation and is given as

$$g(\vartheta') = c_1(\varepsilon^{1/3}/\vartheta'^{2/9})\exp[-c_2\sigma/(\rho_d\varepsilon^{2/3}\vartheta'^{5/9})]. \qquad (2.15)$$

c_1 and c_2 are adjustable constants, to be determined from experiments. According to Prince & Blanch (1990), (2.15) provides results that are in poor agreement with experimental data for air-liquid systems.

The break-up frequency, $g(\vartheta')$, may also be divided into collision frequency, $h(\vartheta, \lambda')$, and break-up probability, $\lambda(\vartheta, \lambda')$, even though it is not done so in S_1 and S_2. When divided it is assumed that

$$g(\vartheta') = h(\vartheta, \lambda')\lambda(\vartheta, \lambda'). \qquad (2.16)$$

Luo (1993) used such a division. Lee, Erickson & Glasgow (1987a) assume that the collision frequency is a Poisson process and they find the frequency function by using dimensional analysis.

2.1.2 Coalescence closure requirements

The following variables are needed for the coalescence source terms.

- Minimum particle volume, ϑ_{min}
- Particle collision frequency, $h(\vartheta, \vartheta')$
- Particle coalescence efficiency, $\lambda(\vartheta, \vartheta')$

The coalescence process can further be divided into three distinctive phenomena, Kocamustafaogullari & Ishii (1995):

- Collision between two or more fluid particles
- Surface flattening and film drainage between the fluid particles
- Film rupture giving coalescence

For bubbly two-phase flow the collision process may be due to the following phenomena, Kocamustafaogullari & Ishii (1995):

- Turbulent fluctuations
- Size dependent rise velocity differences
- Wake entrainment
- Shear layer induced velocity differences

The three latter are highly dependent on the particle size distribution and internal flow structure.

2.1.2.1 Minimum particle volume, ϑ_{min}

It is often assumed that there is a minimum stable particle size below which a pair of particles will coalesce upon colliding. By using the adhesion force and the kinetic energy of a fluid particle - fluid particle collision Shinnar & Church (1960) and Shinnar (1961) got the following expression for the minimum particle volume as a function of the diameter

$$d_{min} = C_1/(\rho_c^{3/8}\varepsilon^{1/4}), \tag{2.17}$$

where C_1 is a parameter defined upon critical rupture thickness, h_c, of the film between the particles. This view is based on an average kinetic energy level, thus not realistic for simulations where the spectrum of kinetic energy is used, but it gives an estimate for the lower range of the population balance discretization.

Thomas (1981) developed a similar model by replacing the adhesion force with the surface tension force acting at the time of rupture getting

$$d_{min} \sim 2.4(\sigma^2 h_c^2/(\mu_c \rho_c \varepsilon))^{1/4}. \tag{2.18}$$

This shows that there are several possible approximations of the minimum particle volume depending on the assumptions made.

2.1.2.2 Particle collision frequency, $h(\vartheta, \vartheta')$

For liquid-liquid dispersions Tavlarides & Stamatoudis (1981) gave the following frequency for collisions in a uniform shear flow (laminar)

$$h(d, d') = 1.366(d + d')^3(\partial v/\partial r). \tag{2.19}$$

For turbulent flow the gradient may be exchanged,

$$\partial v/\partial r \approx (\varepsilon/\vartheta)^{1/2}. \tag{2.20}$$

When the drop density is approximately equal to the density of the continuous phase, the collision frequency will be determined by local turbulent flow characteristics giving

$$h(d, d') = 0.618(d + d')^3(\varepsilon/\vartheta)^{1/2}. \tag{2.21}$$

When the drops are large compared to the turbulent eddies they are exposed to stresses in all directions. This results in a random drop motion and an analogy to kinetic theory of gases has been used.

2.1.2.3 Fluid particle coalescence efficiency, $\lambda(\vartheta, \vartheta')$

An empirical model based on average contact time and average coalescence time is widely used, Coulaloglou & Tavlarides (1977),

$$\lambda(\vartheta, \vartheta') = \lambda(d, d') = \exp[-t_{coa}(d, d')/t_{con}(d, d')]. \tag{2.22}$$

Population balance equations generally use volume as basis for the particle coalescence efficiency, Coulaloglou & Tavlarides (1977) uses fluid particle diameter. It is assumed that these two representations are interchangeable. Different models based on (2.22) exist for the coalescence efficiency in turbulent and laminar flow regimes. Coulaloglou & Tavlarides (1977) uses

$$t_{coa}(d, d') = \frac{\mu_c \rho_c \varepsilon^{2/3}(d + d')^{2/3}}{\sigma^2}\left(\frac{1}{h^2} - \frac{1}{h_0^2}\right)\left(\frac{dd'}{d + d'}\right)^2, \tag{2.23}$$

which is based on the drainage time of the film between the colliding fluid particles and the force of the collision itself in a turbulent environment. The average contact time is similarly given as

$$t_{con}(d, d') = \frac{(d + d')^{2/3}}{\varepsilon^{1/3}}. \tag{2.24}$$

Prince & Blanch (1990) uses

$$t_{coa}(d, d') = \frac{1}{32}\left(\frac{dd'}{d + d'}\right)^{3/2}\left(\frac{\rho_c}{\sigma}\right)\ln\left(\frac{h_0}{h}\right), \tag{2.25}$$

which is also based on the drainage time of the film between the colliding fluid particles. The further use

$$t_{con}(d, d') = \left(\frac{dd'}{4\varepsilon^2(d + d')}\right)^{2/3}, \tag{2.26}$$

which is based on dimensional considerations. Chesters (1991) and Luo (1993) use still other expressions for $t_{coa}(d, d')$ and $t_{con}(d, d')$. The model by Luo is given and used in chapter 6 and the implementation is explained in appendix A.

Low & List (1982) and Orme (1997) use another empirical model for the coalescence efficiency. This empirical model is found for raindrops and is based on what they define as the total collision energy, Orme (1997), or the total energy of coalescence, Low & List (1982). Starting with the change in surface energy as a result of coalescence

$$\Delta S_\sigma = S_T - S_C = \pi\sigma(d^2 + d'^2) - \pi\sigma(d^3 + d'^3)^{2/3}, \tag{2.27}$$

where S_T is the surface energy of the parent fluid particles and S_C is the surface energy of the coalesced fluid particle. Spherical shape is assumed for all fluid particles. Further, the collision kinetic energy is defined as

$$CKE(\vartheta, \vartheta') = \frac{\rho_d}{16}\left(\frac{\vartheta\vartheta'}{\vartheta + \vartheta'}\right)(U + U')^2 . \tag{2.28}$$

The total energy of coalescence is then defined as

$$E_T = CKE + \Delta S_\sigma . \tag{2.29}$$

The measurements collected from six coalescing drop pairs is then approximated as the empirical relation (with ϑ' representing the smallest drop)

$$\lambda(\vartheta, \vartheta') = \lambda(d, d') = a[1 + d'/d]^{-2}\exp\left[-\frac{b\sigma E_T^2}{S_C}\right] \text{ for } E_T < 5.0\ \mu J, \tag{2.30}$$

$$\lambda(\vartheta, \vartheta') = \lambda(d, d') = 0 \text{ for } E_T > 5.0\ \mu J, \tag{2.31}$$

with $a = 0.778$ and $b = 2.61\times10^6 J^{-2}m^2$.

2.2 Discretization of the particle size distribution

The population balance equation must be discretizised in order to be solved numerically. As this will be done for the source terms in chapter 6 and in appendix A, only the general form is given here as

$$N_i(t) = \int_{\vartheta_i}^{\vartheta_{i+1}} n(\vartheta, t)d\vartheta . \tag{2.32}$$

$N_i(t)$ is assumed to be concentrated at a representative size *i*, although N_i is the total number between ϑ_i and ϑ_{i+1}.

Notation

a	constant, $a = 0.778$, eq (2.30), -
B	birth term, eq (2.2), $1/(m^3 s)$
b	constant, $b = 2.61\times10^6$, eq (2.30), m^2/J^2
C_1	parameter defined upon critical rupture thickness, eq (2.17), -
c_1	adjustable constant, eq (2.15), -
c_2	adjustable constant, eq (2.15), -
$CKE(\vartheta, \vartheta')$	collision kinetic energy, eq (2.28), J
D	death term, eq (2.2), $1/(m^3 s)$
d, d'	diameters of fluid particles, eq (2.19), m
d_{max}	maximum stable fluid particle diameter size, eq (2.11), m
d_{min}	minimum particle diameter, eq (2.17), m
E_T	total energy of coalescence, eq (2.29), J
$f(\boldsymbol{x}, \vartheta, t)$	particle density distribution function, eq (2.6), $1/m^3$
$g(\vartheta')$	break-up frequency for particle ϑ', eq (2.7), $1/s$
$h(t)$	liquid film thickness, eq (2.23), m
h_0	initial liquid film thickness, eq (2.23), m
$h(\vartheta, \lambda')$	collision frequency between particle of volume ϑ and eddy of size λ', eq (2.16), $1/s$
$h(\vartheta, \vartheta')$	collision frequency of particles of volume ϑ and ϑ', eq (2.9), $1/s$
h_c	critical rupture thickness, eq (2.18), m
$N_i(t)$	total number of fluid particles between sizes ϑ_i and ϑ_{i+1}, eq (2.32), -
$n(R, t)$	m+3 dimensional particle distribution function, eq (2.2), $1/m^3$
$n(\vartheta')$	number of daughter particles from breakage of parent particle having volume ϑ', eq (2.7), $1/m^3$
$n(\vartheta, t)$	number density of particles of volume ϑ at time t, (2.32), $1/m^3$
R	region of integration, eq (2.2), m^3

R_1	sub-region of integration, eq (2.2), m^3
r	length axis, eq (2.19), m
$S_1(\boldsymbol{x}, \vartheta, t)$	birth term due to breakup, eq (2.7), $1/(m^3 s)$
$S_2(\boldsymbol{x}, \vartheta, t)$	death term due to breakup, eq (2.8), $1/(m^3 s)$
$S_3(\boldsymbol{x}, \vartheta, t)$	birth term due to coalescence, eq (2.9), $1/(m^3 s)$
$S_4(\boldsymbol{x}, \vartheta, t)$	death term due to coalescence, eq (2.10), $1/(m^3 s)$
S_C	surface energy of coalesced fluid particle, eq (2.27), J
S_T	surface energy of parent fluid particles, eq (2.27), J
S_j	source term, eq (2.6), $1/(m^3 s)$
S_{ph}	phase change terms, eq (2.6), $1/(m^3 s)$
t	time, eq (2.2), s
$t_{coa}(d, d')$	average coalescence time for two fluid particles of diameter sizes d and d', eq (2.22), s
$t_{con}(d, d')$	average contact time for two fluid particles of diameter sizes d and d', eq (2.22), s
U, U'	fluid particle velocities, eq (2.28), m/s
$\boldsymbol{v}$	set of internal and external velocities, eq (2.4), m/s
v	fluid velocity, eq (2.19), m/s
$\overline{v_c'^2}$	mean square spatial fluctuating velocity, eq (2.12), m^2/s^2
$\boldsymbol{v}_e$	set of external velocities, eq (2.4), m/s
$\boldsymbol{v}_i$	set of internal velocities, eq (2.4), m/s
$\boldsymbol{v}_p(\boldsymbol{x}, \vartheta, t)$	particle velocity, eq (2.6), m/s
We_{cr}	Critical Weber number, eq (2.11), -
$\boldsymbol{x}$	set of internal and external coordinates, eq (2.3)
$\beta(\vartheta', \vartheta)$	distribution of daughter particles produced upon break-up of parent particle of volume ϑ', eq (2.7), -

ΔS_σ	change in surface energy, eq (2.27), J
δ	Kronecker delta function, eq (2.14), -
ε	turbulent eddy dissipation, eq (2.13), m^2/s^3
ϑ	volume of fluid particle, eq (2.7), m^3
ϑ_{min}	minimum stable particle size below which coalescence occur, m^3
ϑ_{max}	maximum particle size stable against break-up, m^3
ϑ_i	volume of particle of class i, m^3
$\lambda(\vartheta, \lambda')$	break-up probability for particle of volume ϑ hit by eddy of size λ', eq (2.16), -
$\lambda(d, d')$	coalescence efficiency once collision occurs between particles of diameters d and d', eq (2.22), -
$\lambda(\vartheta, \vartheta')$	coalescence efficiency once collision occurs between particles of volumes ϑ and ϑ', eq (2.9), -
μ_c	viscosity of continuous phase, eq (2.18), $kg/(ms)$
ρ_c	density in continuous phase, eq (2.12), kg/m^3
ρ_d	density in dispersed phase, eq (2.15), kg/m^3
σ	surface tension, eq (2.11), N/m
τ	external stresses, eq (2.11), N/m^2

References

Batchelor, G.K. (1951). Pressure fluctuations in isotropic turbulence. *Proceedings of the Cambridge Phil. Society,* **47**, 359-374.

Carrica, P.M., Drew, D., Bonetto, F. & Lahey Jr., R.T. (1999). A polydisperse model for bubbly two-phase flow around a surface ship. *International Journal of Multiphase Flow,* **25**, 257-305.

Chatzi, E. & Lee, J.M. (1987). Analysis of interactions for liquid-liquid dispersion in agitated vessels. *Ind. Chem. Engng. Res.*, **26**, Vol 11, 2263-2267.

Chesters, A.K. (1991). The modelling of coalescence processes in fluid-fluid dispersions: A review of current understanding. *Trans IChemE*, **69**, Part A, 259-270.

Coulaloglou, C.A. & Tavlarides, L.L. (1977). Description of interaction processes in agitated liquid-liquid dispersions. *Chemical Engineering Science*, **32**, 1289-1297.

Drazin, P.G. & Reid, W.H. (1981). Hydrodynamic stability. Cambridge university press, Cambridge, USA, 14-22.

Hesketh, R.P., Etchells, A.W. & Russell, T.W.F. (1991). Experimental observations of bubble breakage in turbulent flow. *Ind. Eng. Chem. Res.*, **30**, 835-841.

Hinze, J.O. (1955). Fundamentals of the hydrodynamic mechanism of splitting in dispersion processes. *AIChE Journal*, **1**, No. 3, 289-295.

Hsia, M.A. & Tavlarides, L.L. (1983). Simulation and analysis of drop breakage, coalescence and micromixing in liquid-liquid stirred tanks. *Chem. Engng J.*, **26**, 189-199.

Hulburt, H.M. & Katz, S. (1964). Some problems in particle technology. *Chemical Engineering Science*, **19**, 555-574.

Kocamustafaogullari, G. & Ishii, M. (1995). Foundation of the interfacial area transport equation and its closure relations. *Int. J. Heat Mass Transfer*, **38**, No. 3, 481-493.

Kreyszig, E. (1988). Advanced engineering mathematics. John Wiley & sons, 6th ed., New York, USA, 219.

Lee, C.-H., Erickson, L.E. & Glasgow, L.A. (1987a). Bubble breakup and coalescence in turbulent gas-liquid dispersions. *Chem. Eng. Comm*., **59**, 65-84.

Lee, C.-H., Erickson, L.E. & Glasgow, L.A. (1987b). Dynamics of bubble size distribution in turbulent gas-liquid dispersions. *Chem. Eng. Comm*., **61**, 181-195.

Low, T.B. & List, R. (1982). Collision, coalescence and breakup of raindrops. Part I: Experimentally established coalescence efficiencies and fragment size distributions in breakup. *Journal of the atmospheric sciences*, **39**, 1591-1606.

Luo, H. (1993). Coalescence, breakup and liquid circulation in bubble column reactors. Doktor ingeniøravhandling, Institutt for kjemiteknikk, Univeritetet i Trondheim, Norway.

Nambiar, D.K.R., Kumar, R., Das, T.R. & Gandhi, K.S. (1992). A new model for the breakage frequency of drops in turbulent stirred dispersions. *Chemical Engineering Science*, **47**, 2989-3002.

Narsimhan, G., Gupta, J.P. & Ramkrishna, D. (1979). A model for transitional breakage probability of droplets in agitated lean liquid-liquid dispersions. *Chemical Engineering Science*, **34**, 257-265.

Orme, M. (1997). Experiments on droplet collisions, bounce, coalescence and disruption. *Prog. Energy Combust. Sci.*, **23**, 65-79.

Prince, M.J. & Blanch, H.W. (1990). Bubble coalescence and break-up in air-sparged bubble column. *A.I.Ch.E. Journal*, **36**, Vol 10, 1485-1499.

Prince, M.J., Walters, S. & Blanch, H.W. (1989). Bubble break-up in air-sparged biochemical reactors. In *First Generation of Bioprocess Engineering*. Edited by Ghose, T.K.

Ramkrishna, D. (1985). The status of population balances. *Chem. Engng.*, **3**, 49-95.

Randolph, A.D. & Larson, M.A. (1988). Theory of particulate processes. 2nd ed., Academic Press Inc., San Diego, USA.

Shinnar, R. (1961). On the behavior of liquid dispersions in mixing vessels. *J. Fluid Mech.*, **10**, 259-275.

Shinnar, R. & Church, J.M. (1960). Predicting particle size in agitated dispersions. *Ind. Engng. Chem.*, **52**, 253-262.

Tavlarides, L.L. & Stamatoudis, M. (1981). The analysis of interphase reactions and mass transfer in liquid-liquid dispersions. *Advances in Chemical Engineering*, **11**, 199-273.

Thomas, R.M. (1981). Bubble coalescence in turbulent flows. *Int. J. Multiphase Flow*, **7**, 709-717.

Tsouris, C. & Tavlarides, L.L. (1994). Breakage and coalescence models in turbulent dispersion. *A.I.Ch.E. Journal*, **40**, 395-406.

Valentas, K.J. & Amundson, N.R. (1966). Breakage and coalescence in dispersed phase systems. *I&EC Fundamentals*, **5**, No. 4, 533-542.

Valentas, K.J., Bilous, O. & Amundson, N.R. (1966). Analysis of breakage in dispersed phase systems. *I&EC Fundamentals*, **5**, No. 2, 271-279.

CHAPTER 3

Fluid particle coalescence efficiency

This chapter provides a literature overview of the parameterizations accounting for the mechanisms determining the binary fluid particle collision processes. The aim is to describe the coalescence efficiency through a fundamental lagrangian momentum balance model. Models describing the drainage of the film between two colliding particles are also considered. Other factors that may influence the efficiency are outlined. Finally, experimental data for collisions between fluid particles are discussed.

3.1 Coalescence efficiency parameterizations, the relation to particle collision models

The aim of this chapter is to describe an approach for finding the particle coalescence efficiency, $\lambda(\vartheta, \vartheta')$, and variables that may affect this efficiency. The goal is to develop a fundamental model for the efficiency starting with the coalescence closure requirements, Kocamustafaogullari & Ishii (1995):

- Collision between two or more fluid particles
- Surface flattening and film drainage between the fluid particles
- Film rupture giving coalescence

3.1.1 Film rupture

Film rupture is considered more or less instantaneous compared to the other two processes, Chesters (1991). Further, the film rupture does not happen at a specified film thickness. It seems that the rupture thickness may vary and that it is also affected by impurities in the film. Generally rupture occurs when the film at the initial rupture position is less than a few hundred Å for large fluid particles and a few tens for small ones, Chesters (1991).

3.1.2 Film drainage

A large number of studies has been published. Most use lubrication theory in order to describe the drainage process.

3.1.2.1 Lubrication theory

The basic lubrication theory is shown in detail. In order to derive the lubrication equation start with the Navier Stokes equations and the continuity equation, Bird, Stewart & Lightfoot (1960). Assumptions used are:

- Newtonian fluid
- ρ, μ are constants
- Axisymmetry
- Gravity is negligible

A sketch of the lubrication film is shown in figure 3.1.

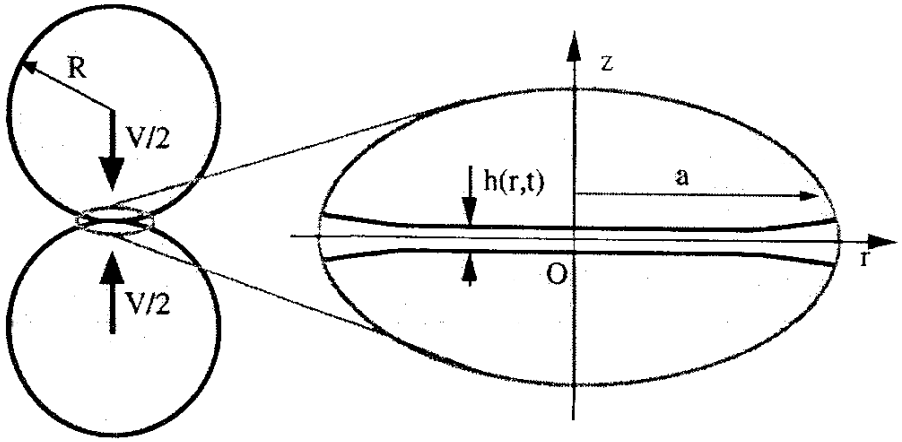

FIGURE 3.1: Definition sketch for two colliding fluid particles, Klaseboer, Chevaillier, Gourdon & Masbernat (2000). The film between the colliding particles is shown in detail.

In cylindrical coordinates the Navier Stokes in *r*-direction, *z*-direction, and continuity equations respectively, may be written as

$$\rho_c\left(\frac{\partial v_r}{\partial t} + v_r\frac{\partial v_r}{\partial r} + v_z\frac{\partial v_r}{\partial z}\right) = -\frac{\partial P}{\partial r} + \mu_c\left[\frac{\partial}{\partial r}\left(\frac{1}{r}\frac{\partial}{\partial r}(rv_r)\right) + \frac{\partial^2 v_r}{\partial z^2}\right], \tag{3.1}$$

$$\rho_c\left(\frac{\partial v_z}{\partial t} + v_r\frac{\partial v_z}{\partial r} + v_z\frac{\partial v_z}{\partial z}\right) = -\frac{\partial P}{\partial z} + \mu_c\left[\frac{\partial}{\partial r}\left(r\frac{\partial v_z}{\partial r}\right) + \frac{\partial^2 v_z}{\partial z^2}\right], \tag{3.2}$$

$$\frac{1}{r}\frac{\partial}{\partial r}(rv_r) + \frac{\partial v_z}{\partial z} = 0. \tag{3.3}$$

The lubrication approximation states that $h(r, t) \ll r_f$. In addition, the following assumptions are made, Lee & Hodgson (1968):

- $v_z \approx 0$, but $\frac{\partial v_z}{\partial z} \neq 0$

- $\frac{\partial v_r}{\partial t} = 0$, i.e. pseudo steady state.
- $v_r \frac{\partial v_r}{\partial r} \approx 0$, i.e. neglect the inertia term, this assumption is valid for creeping flow (typically $Re_p < 0.1$ for creeping flow).

The lubrication approximation shows that the flow between the boundaries may be assumed parallel since the distance between the boundaries is much less than the radial length of the boundaries. This in turn gives the assumption $\partial v_r / \partial z$ is $f(z)$ only. The first viscous term in eq (3.1) is proved negligible compared to the second term by inserting the continuity equation, eq (3.3), and comparing the terms. The equations (3.1) to (3.3) are reduced to

$$\frac{\partial P}{\partial r} = \mu_c \frac{\partial^2 v_r}{\partial z^2}, \tag{3.4}$$

$$\frac{\partial P}{\partial z} = 0, \tag{3.5}$$

$$\frac{1}{r}\frac{\partial}{\partial r}(r v_r) + \frac{\partial v_z}{\partial z} = 0. \tag{3.6}$$

Equations (3.4) to (3.6) are quite commonly used when solving for film drainage, see also Jain & Ivanov (1980) and Li (1996). In addition one has the following boundary conditions

- $v_r = 0$ at the surface ($z = 0.5h$)
- $v_z = 0.5 \partial h / \partial t$ at the surface
- $\frac{\partial h}{\partial t} + v_r \frac{\partial h}{\partial r} = v_z$ at the surface, and it is called the kinematic boundary condition, e.g. Slattery (1990)
- $\partial v_r / \partial z = 0$ at $z = 0$ due to symmetry

- $v_z = 0$ at $z = 0$ due to symmetry

where h is the thickness between the boundaries, and where $z = 0$ is in the centre of the film, thus the boundaries are at $-h/2$ and $h/2$. Note that h is a function of both r and t.

By integrating eq (3.4) twice we get

$$v_r = \frac{1}{2\mu_c}\frac{\partial P}{\partial r}z^2 + C_1 z + C_2 . \tag{3.7}$$

The integration constants are determined by using the boundary conditions, giving:

$$v_r = \frac{1}{2\mu_c}\frac{\partial P}{\partial r}\left(z^2 - \left(\frac{h}{2}\right)^2\right), \tag{3.8}$$

which is a parabolic velocity profile caused by the pressure gradient.

Integrating the continuity equation (3.6) over half the film and inserting eq (3.8) gives

$$\int_0^{h/2} \frac{1}{r}\frac{\partial}{\partial r}(rv_r)dz = \int_0^{h/2} \frac{1}{r}\frac{\partial}{\partial r}\left(\frac{r}{2\mu_c}\frac{\partial P}{\partial r}\left(z^2 - \left(\frac{h}{2}\right)^2\right)\right)dz = -\int_0^{h/2} \frac{\partial v_z}{\partial z}dz . \tag{3.9}$$

The Leibnitz theorem, Bird *et al.* (1960), is needed in order to integrate the left hand side of eq (3.9) (because h is a function of r in the integration limit):

$$\frac{d}{dt}\int_{a_1(t)}^{a_2(t)} f(x,t)dx = \int_{a_1(t)}^{a_2(t)} \frac{\partial f}{\partial t}dx + \left(f(a_2,t)\frac{da_2}{dt} - f(a_1,t)\frac{da_1}{dt}\right). \tag{3.10}$$

We have used $a_1(t) = 0$, $a_2(t) = h/2$, replaced dt with ∂r and replaced dx with dz. We also have

$$f = \frac{r}{2\mu_c}\frac{\partial P}{\partial r}\left(z^2 - \left(\frac{h}{2}\right)^2\right). \tag{3.11}$$

Using the Leibnitz theorem on the left hand term in the integrated continuity equation gives

$$\frac{1}{r}\int_0^{h/2}\frac{\partial}{\partial r}\frac{r}{2\mu_c}\left(\frac{\partial P}{\partial r}\left(z^2-\left(\frac{h}{2}\right)^2\right)\right)dz = \tag{3.12}$$

$$\frac{1}{r}\frac{\partial}{\partial r}\int_0^{h/2}\frac{r}{2\mu_c}\frac{\partial P}{\partial r}\left(z^2-\left(\frac{h}{2}\right)^2\right)dz-\frac{r}{2\mu_c}\frac{\partial P}{\partial r}\left[\left(\left(\frac{h}{2}\right)^2-\left(\frac{h}{2}\right)^2\right)\frac{\partial h}{\partial r}-\left(0-\left(\frac{h}{2}\right)^2\right)\frac{\partial 0}{\partial r}\right]$$

Computing the integral on the right hand side of eq (3.12)

$$\frac{1}{r}\frac{\partial}{\partial r}\int_0^{h/2}\frac{r}{2\mu_c}\left(\frac{\partial P}{\partial r}\left(z^2-\left(\frac{h}{2}\right)^2\right)\right)dz = \tag{3.13}$$

$$\frac{1}{2\mu_c r}\frac{\partial}{\partial r}\left[r\frac{\partial P}{\partial r}\left(\frac{1}{3}z^3-\left(\frac{h}{2}\right)^2 z\right)\right]\Bigg|_0^{h/2} = \frac{-1}{24\mu_c r}\frac{\partial}{\partial r}\left(rh^3\frac{\partial P}{\partial r}\right)$$

The second term in the continuity equation (3.6) gives

$$\int_0^{h/2}\frac{\partial v_z}{\partial z}dz = v_z\Big|_0^{h/2} = \frac{1}{2}\frac{\partial h}{\partial t}-0 = \frac{1}{2}\frac{\partial h}{\partial t}. \tag{3.14}$$

Combining eq (3.9), eq (3.12), eq (3.13) and eq (3.14) gives the lubrication equation

$$\frac{\partial h}{\partial t} = \frac{1}{12\mu_c r}\frac{\partial}{\partial r}\left(rh^3\frac{\partial P}{\partial r}\right), \tag{3.15}$$

which is the integrated form of the continuity equation. It is seen from eq (3.15) that in order to find the drainage rate the pressure gradient in the film between the two colliding fluid particles is needed.

By using the boundary condition $v_r = U_0$ at $z = h/2$, thus not assuming an immobile film, Danov, Gurkov, Dimitrova, Ivanov & Smith (1997), gives

$$v_r = \frac{1}{2\mu_c}\frac{\partial P}{\partial r}\left(z^2 - \left(\frac{h}{2}\right)^2\right) + U_0, \tag{3.16}$$

rather than eq (3.8) which in turn leads to

$$\int_0^{h/2} \frac{1}{r}\frac{\partial}{\partial r}\left(\frac{r}{2\mu_c}\frac{\partial P}{\partial r}\left(z^2 - \left(\frac{h}{2}\right)^2\right)\right)dz + \int_0^{h/2} \frac{1}{r}\frac{\partial}{\partial r}(rU_0)dz = -\int_0^{h/2} \frac{\partial v_z}{\partial z}dz. \tag{3.17}$$

The second term in eq (3.17) is solved with Leibnitz theorem, eq (3.10), since h is a function of r.

$$\int_0^{h/2} \frac{1}{r}\frac{\partial}{\partial r}(rU_0)dz = \frac{1}{r}\frac{\partial}{\partial r}\int_0^{h/2} rU_0 dz - \left[rU_0\frac{\partial h}{\partial r} - 0\right], \tag{3.18}$$

where $\partial h/\partial r \approx 0$ due to the lubrication approximation giving

$$\int_0^{h/2} \frac{1}{r}\frac{\partial}{\partial r}(rU_0)dz = \frac{1}{r}\frac{\partial}{\partial r}(rU_0 z)\Big|_0^{h/2} = \frac{1}{2r}\frac{\partial}{\partial r}(rU_0 h). \tag{3.19}$$

Combining eq (3.3), eq (3.14), eq (3.17) and eq (3.19) gives an expanded version of the lubrication as given by Klaseboer & Chevallier (1998)

$$\frac{\partial h}{\partial t} = -\frac{1}{r}\frac{\partial}{\partial r}(rU_0 h) + \frac{1}{12\mu_c}\frac{1}{r}\frac{\partial}{\partial r}\left(rh^3\frac{\partial P}{\partial r}\right), \tag{3.20}$$

where the second term is a plug flow part due to moving boundaries and the third term is the parabolic flow superimposed on the plug flow and this part is due to the pressure gradient in the film.

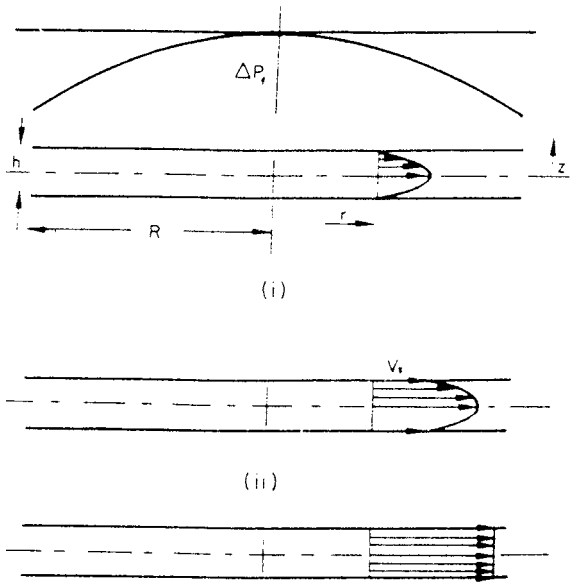

FIGURE 3.2: From Lee & Hodgson (1968), from above the figure shows immobile, partially mobile and fully mobile films. The form of the pressure distribution is also shown at the top.

As seen in figure 3.2 the upper plot is the situation assumed deriving equation (3.15), and the middle plot is given by (3.20).

Klaseboer & Chevaillier (1998) showed two film drainage models introducing few new improvements. They assumed viscous forces predominant and weak collisions. They further assumed a constant approach velocity for the collision making their models rather unrealistic, at least for rebounds. The first models assumes partially mobile films and plug flow. This may be an inconsistency in itself as one only expects plug flow with fully mobile films. The second model assumes immobile films and Poiseuille flow in the draining film. They use standard lubrication theory

$$\frac{\partial h}{\partial t} = -\frac{1}{r}\frac{\partial}{\partial r}(r v_r h) + \frac{1}{12\mu_c}\frac{1}{r}\frac{\partial}{\partial r}\left(r h^3 \frac{\partial P}{\partial r}\right), \tag{3.21}$$

where the first term on the right hand side is a Couette contribution (or plug flow contribution due to the moving interfaces) and the second term is a Poiseuille con-

tribution (a parabolic velocity profile contribution caused by a pressure gradient). The pressure is given as

$$P = \frac{2\sigma}{R} + \frac{\sigma}{2r}\frac{\partial}{\partial r}\left(r\frac{\partial h}{\partial r}\right), \tag{3.22}$$

where the second term on the right hand side is due to the curvature of the film.

Chesters & Hofman (1982) also started out with the Navier-Stokes equations and continuity to describe the collision between two colliding bubbles. They first assumed an inviscid liquid and later found out that for Re>100 this was a good approximation. They also assumed that the velocity at the outer edge of the collision zone is set to a constant. This combines to a poor representation of the physical system (especially the second assumption) and their results should probably be disregarded.

Chen, Hahn & Slattery (1984) included the London-van der Waals attraction force when solving for the film thickness. This force is according to them of importance when the film is less than 1000 Å. They assumed that the mutual force per unit mass b_m known as the London-van der Waals force is representable in terms of a scalar potential φ:

$$b_m = -\nabla\varphi. \tag{3.23}$$

At a planar fluid-fluid interface:

$$\rho_c\varphi = \rho_c\varphi_0 = \phi_B + \frac{B}{h^m}, \tag{3.24}$$

where $|B| \sim 10^{-21}\ J$ and $m = 3$ for a film thickness less than 120 Å. When the film thickness is more than 400 Å $|B| \sim 10^{-24}\ Jm$ and $m = 4$. No values are given for the intermediate range. When combined with interfacial tension they got:

$$-\frac{dh_r}{dt} = \frac{1}{\mu_c R}\left(\frac{0.406\sigma}{R^2}h_r^3 + \frac{B}{2h_r}\right) \text{ for } m = 3, \tag{3.25}$$

$$-\frac{dh_r}{dt} = \frac{1}{\mu_c R}\left(\frac{0.406\sigma}{R^2}h_r^3 + \frac{2B}{3h_r}\right) \text{ for } m = 4. \tag{3.26}$$

The film is above assumed to be immobile.

Hahn & Slattery (1985) followed up the article to Chen *et al.* (1984) by extending it to include the effects of surface viscosities. That is they solve for a partially mobile film and their new basic assumption is that the film drains slowly. This assumption may work for the gravity induced drainage where the contact time may be sufficiently long. For a collision of two fluid particles with a contact time far less than a second this assumption is not valid. Hahn & Slattery (1986) also included the effect of dimpling of the film. The resulting equation describes h as a function of time and radius.

Doubliez (1991) found that the viscous draining was too slow to explain the experimentally found drainage rate. An alternative model was presented. It is assumed that: 1- the film is plane-parallel, 2- gravity effects can be neglected in the flow, 3- axisymmetric flow without an azimuthal component, 4- the gas flow in the bubbles has no influence on the liquid flow, and 5- the radial velocity v_r is constant across the film, $\frac{\partial v_r}{\partial z} = 0$

By using the dimensionless variables

$r' = r/L$, $z' = z/H$, $v_r' = v_r/L$, $v_z' = v_z/W$, $t' = tW/H$,

the length scale ratio $\varepsilon = H/L = W/U$ and the Reynolds and Weber numbers

$$Re_f = \frac{\rho_c V_0 R}{\mu_c}, \quad We = \frac{\rho_c V_0^2 R}{\sigma} \text{ and } R_m = \left(\frac{4}{3}\frac{(\rho_c - \rho_d)g}{\gamma}R^4\right)^{1/2}, \qquad (3.27)$$

the Navier-Stokes equations may be expressed as (dimensionless form written without the apostrophes):

$$\frac{\partial v_r}{\partial t} + v_r\frac{\partial v_r}{\partial r} + v_z\frac{\partial v_r}{\partial z} = -\frac{\varepsilon^2}{We}\frac{\partial p}{\partial r} + \frac{\varepsilon}{Re_f}\left[\frac{\partial}{\partial r}\left(\frac{1}{r}\frac{\partial}{\partial r}(rv_r)\right) + \frac{1}{\varepsilon^2}\frac{\partial^2 v_r}{\partial z^2}\right], \qquad (3.28)$$

and

$$\frac{\partial v_z}{\partial t} + v_r\frac{\partial v_z}{\partial r} + v_z\frac{\partial v_z}{\partial z} = -\frac{1}{We}\frac{\partial p}{\partial z} + \frac{\varepsilon}{Re_f}\left(\frac{\partial^2 v_z}{\partial r^2} + \frac{1}{r}\frac{\partial v_z}{\partial r} + \frac{1}{\varepsilon^2}\frac{\partial^2 v_z}{\partial z^2}\right). \qquad (3.29)$$

With small fluid particles at terminal velocity $We \ll Re$ and initially $\varepsilon \sim 1$ the viscous parts are of minor importance, unlike the lubrication approximation.

Doubliez found the thickness of the film to be

$$h = \frac{4}{(t+2)^2}, \tag{3.30}$$

or in dimensional form

$$h = \frac{4h_0^3}{(V_0 t + 2h_0)^2}, \tag{3.31}$$

where initial conditions are needed

$$h_0 = \frac{\rho_c V_0^2 R^2}{4\sigma}\left(1 + \frac{4\mu_c}{\rho_c V_0 R}\right). \tag{3.32}$$

Two hypotheses can according to Doubliez explain the ending of this initial stage, the rebound process or the dimple formation, which will be looked into later.

3.1.2.2 Force, lubrication theory and drainage

The film drainage is in eq (3.15) and eq (3.20) above given as a function of the radial pressure gradient in the film. An alternative to using the pressure is to use the force between the fluid particles, or between a fluid particle and a solid surface as shown in figure 3.3.

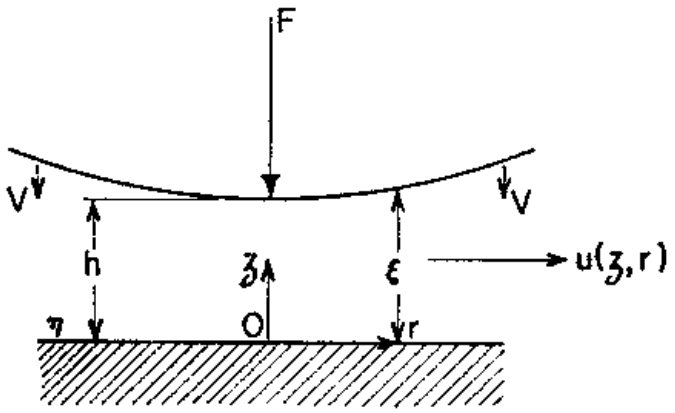

FIGURE 3.3: The close approach of a film to a surface in a viscous fluid, Charles & Mason (1960).

Charles & Mason (1960) found the rate of thinning between two interfaces as a function of the force between two fluid particles to be

$$v_z = \frac{dh}{dt} = \frac{F}{6\pi\mu_c \int_0^r \frac{r^3}{\xi^3} dr}. \tag{3.33}$$

where $\xi(r)$ is the thickness of the film, as seen in figure 3.3. They considered laminar flow in the radial direction, no flow in the *z* direction and negligible inertial effects. A no slip condition is applied at the interfaces, and a parabolic velocity profile is used in the *r* direction.

They further found an expression for the force, F, but there are two errors made during this development, the expression for the excess pressure found from Laplace's law and the volume balance. By assuming a parallel disc approach (3.33) can be simplified to

$$\frac{dh}{dt} = -\frac{2F}{3\pi\mu_c r^4} h^3, \tag{3.34}$$

by setting $\xi = h(t)$ (independent of r) and integrating equation (3.33). This equation is also called Reynolds equation, Reynolds (1886). Hartland (1967) found (3.34) by staring with the Navier Stokes equation in cylindrical coordinates for the radial direction, Bird *et al*. (1960), and neglecting the transient term, the inertia terms, assuming axis symmetry and removing the first viscous term by using the continuity equation and assuming that the velocity in the perpendicular direction is independent of the radial direction. By integrating (3.34) an expression is found for the drainage time that was first given by Stefan (1874)

$$t_{1,2} = \frac{3\pi\mu_c r^4}{4F}\left[\frac{1}{h_2^2} - \frac{1}{h_1^2}\right]. \tag{3.35}$$

This assumes that the force between the fluid particles is constant during the collision until breakage. Constant force is not expected due to several reasons. Firstly, this implies no drag between the fluid particles and the continuous medium. Secondly, it implies that the film will have constant contact area, which clearly cannot be the case. It further assumes that there is no loss due to dissipation during the collision itself and that the fluid particles are not oscillating.

Kirkpatrick & Lockett (1974) found that low approach velocities resulted in coalescence while higher velocities resulted in rebounds. They did experiments with bubbles rising to an interface. They wrote that with low approach velocity the rate of increase of the contact film area with time was sufficiently slow to allow the contact film to drain to rupture thickness before the bubble was brought to rest. When a bubble approach an interface, there is film drainage due to excess pressure in the film, and an increase in contact area. The latter decreases the rate of drainage. A model was given based on the Bernoulli equation (3.36) without friction, that is no shear at the film surfaces, and the continuity equation (3.37),

$$\frac{P_r}{\rho_c} + \frac{u_{r,r}^2}{2} = \frac{P_0}{\rho_c} + \frac{u_{r,0}^2}{2}, \tag{3.36}$$

$$\frac{dh}{dt} = \frac{-2u_r h}{r}. \tag{3.37}$$

By using that $P_0 = P_r + 2\sigma/R$ and combining for the edge of the collision radius they got

$$\frac{dh}{h} = -\left(\frac{16\sigma}{\rho_c R}\right)^{1/2}\frac{dt}{r_f}. \tag{3.38}$$

This can be considered an equation for the bottom case in figure 3.2 (fully mobile films).

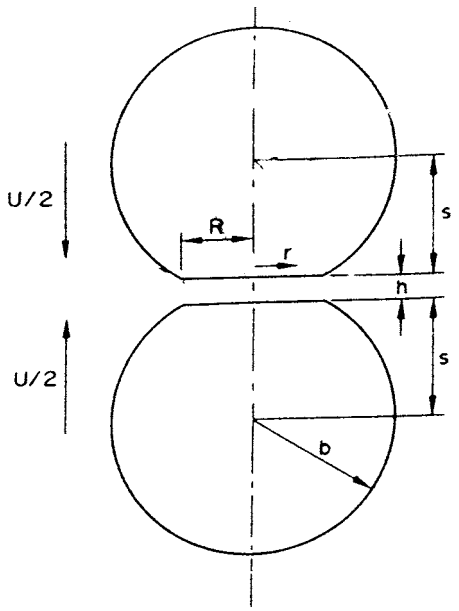

FIGURE 3.4: From Kirkpatrick & Lockett (1974), shows a collision model with a flat interface between the fluid particles.

3.1.2.3 Modification of the lubrication theory

Vaughn & Slattery (1995) and Slattery (1999) present a model based on the work by Bird *et al*. (1977). Creeping flow is assumed and it is postulated that

$$v_r = v_r(r, z, t), \tag{3.39}$$

$$v_z = v_z(z, t). \tag{3.40}$$

The momentum and continuity equations are simplified in accordance with eq (3.39), eq (3.40) and lubrication theory in general. An illustration of the liquid film between the two fluid particles is shown in figure 3.5.

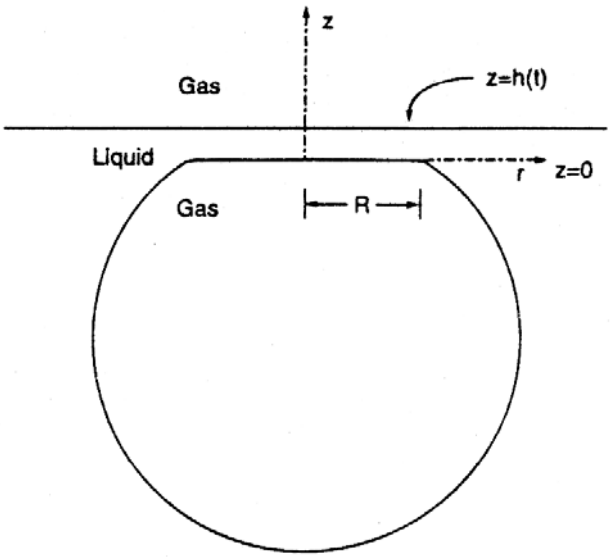

FIGURE 3.5: Idealized film formed as a small fluid particle, here gas, rises through a continuous liquid to an interface between the liquid and another fluid particle, here gas, by Vaughn & Slattery (1995). The film is observed in a frame of reference in which the interface between the fluid particle and the liquid is stationary.

Immobile interfaces:

The boundary conditions for immobile interfaces are:

$$z = 0 \rightarrow v_r = 0, v_z = 0, \tag{3.41}$$

$$z = h(t) \rightarrow v_r = 0, v_z = dh/dt, \tag{3.42}$$

$$r = 0 \rightarrow v_r = 0. \tag{3.43}$$

The reference frame is fixed to the lower fluid particle. $h(t)$ is the position of the upper interface. The upper interface can be another fluid particle, a wall or the interface of another continuous fluid.

It is postulated that

$$P = f_1(z, t) + f_2(r, t). \tag{3.44}$$

In view of eq (3.44), eq (3.1) can be integrated twice with respect to *z*, and by using the boundary conditions this gives

$$v_r = \frac{1}{2\mu_c}\frac{\partial P}{\partial r}(z^2 - hz). \tag{3.45}$$

The continuity equation, eq (3.3), is integrated with respect to *r*, and by using the boundary condition, eq (3.43), gives

$$v_r = -\frac{\partial v_z}{\partial z}\frac{r}{2}. \tag{3.46}$$

By eliminating v_r from eq (3.45) and eq (3.46) and integrating with respect to *z* gives

$$v_z = \frac{1}{\mu_c r}\frac{\partial P}{\partial r}\left(\frac{h}{2}z^2 - \frac{1}{3}z^3\right) + C_2. \tag{3.47}$$

Boundary condition eq (3.41) gives $C_2 = 0$, and using eq (3.42) gives

$$\frac{\partial P}{\partial r} = \frac{dh}{dt}\frac{6\mu_c r}{h^3}. \tag{3.48}$$

Combining eq (3.47) with (3.48) gives

$$v_z = \frac{1}{h^3}\frac{dh}{dt}(3hz^2 - 2z^3). \tag{3.49}$$

Finally by introducing eq (3.48) into eq (3.45) gives

$$v_r = -\frac{3r}{h^3}\frac{dh}{dt}(hz - z^2). \tag{3.50}$$

The dominant change in pressure (radial direction) and the velocities are now given as functions of the thinning rate of the film.

By using the boundary condition

$$r = r_f \rightarrow P = P_h, \tag{3.51}$$

where P_h is the hydrostatic pressure eq (3.48) can be integrated to give

$$P(r) = P_h + \frac{3\mu_c}{h^3}\frac{dh}{dt}(r^2 - r_f^2). \tag{3.52}$$

Note though that eq (3.51) is not consistent with the *z*-component of the momentum equation

$$\frac{\partial P}{\partial z} = \mu_c \frac{\partial^2 v_z}{\partial z^2}. \tag{3.53}$$

and eq (3.44), this inconsistency is disregarded. Further, by using eq (3.52) the force that the fluid exerts on the fluid particle is given as

$$F_z = 2\pi \int_0^{r_f} T_{zz}\big|_{z=0} r\,dr = 2\pi \int_0^{r_f} (P - P_d - S_{zz})\big|_{z=0} r\,dr \tag{3.54}$$

$$= -(P_d - P_h)\pi r_f^2 - \frac{3\pi r_f^4 \mu_c}{2h^3}\frac{dh}{dt}$$

where the normal stress S_{zz} is always zero for immobile interfaces and P_d is the pressure inside the fluid particle.

Mobile interfaces:

The boundary conditions for v_r, equations (3.41) and (3.42), are changed to

$$z = 0 \text{ and } z = h(t) \rightarrow \frac{\partial v_r}{\partial z} = 0. \tag{3.55}$$

In much the same way as for immobile interfaces the equations for mobile interfaces are found. Starting with eq (3.4), integrating it with regard to *z*, and using the boundary condition in eq (3.55) gives

$$\frac{\partial P}{\partial r} = 0. \tag{3.56}$$

Using the boundary condition in eq (3.51) gives

$$P = P_h. \tag{3.57}$$

Using the right hand side of eq (3.1),

$$-\frac{\partial P}{\partial r} + \mu_c\left[\frac{\partial}{\partial r}\left(\frac{1}{r}\frac{\partial}{\partial r}(rv_r)\right) + \frac{\partial^2 v_r}{\partial z^2}\right] = 0, \tag{3.58}$$

removing the first and third term (both zero), and inserting the continuity equation, eq (3.6) gives

$$\frac{\partial}{\partial r}\left(\frac{1}{r}\frac{\partial}{\partial r}(rv_r)\right) = \frac{\partial}{\partial r}\left(\frac{\partial v_z}{\partial z}\right) = 0. \tag{3.59}$$

Integrating the right hand part with respect to *r* and using boundary condition (3.42) gives

$$\frac{\partial v_z}{\partial z} = \frac{1}{h}\frac{dh}{dt}. \tag{3.60}$$

Inserting (3.60) into eq (3.46) gives the axial velocity

$$v_z = \frac{z}{h}\frac{dh}{dt}. \tag{3.61}$$

Integrating eq (3.60) and using boundary condition (3.41) gives the radial velocity

$$v_r = \frac{1}{2}\frac{r}{h}\frac{dh}{dt}. \tag{3.62}$$

The normal stress is now

$$S_{zz} = 2\mu_c\frac{\partial v_z}{\partial z} = \frac{2\mu_c}{h}\frac{dh}{dt}, \tag{3.63}$$

and the force that the fluid exerts on the fluid particle is given as

$$F_z = 2\pi\int_0^{r_f} T_{zz}\Big|_{z=h} r\,dr = 2\pi\int_0^{r_f} (P - P_d - S_{zz})\Big|_{z=h} r\,dr \quad . \tag{3.64}$$

$$= -(P_d - P_h)\pi r_f^2 - 2\pi r_f^2 \mu_c \frac{1}{h}\frac{dh}{dt}$$

The velocity distribution, the pressure distribution and the force exerted on the fluid particles are thus all found when using the approach described by Vaughn & Slattery (1995).

3.1.2.4 Dimple in film

The pressure gradient on the deformable interfaces suggests that it is impossible to have a plane parallel film since a flat film cannot support a gradient in the pressure. In order to support this pressure gradient the film needs to change to a curved shape. The increase in the pressure radially inward explains the experiments done by Derjaguin & Kussakov (1939), they found a dimple in the film. A dimple can be defined as a reverse curvature so that a central lens of liquid is entrapped by a thinner barrier ring. Frankel & Mysels (1962) were the first to model this dimple.

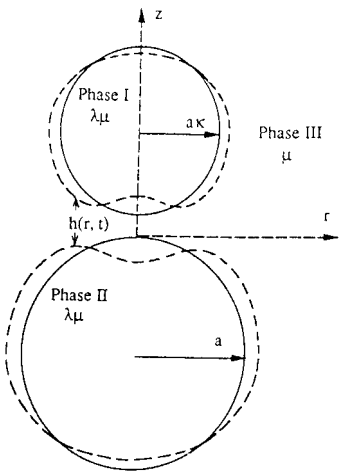

FIGURE 3.6: Taken from Yiantsios & Davis (1990), shows how the interface may change to a dimple which is marked with dashes.

They developed a hydrodynamic theory of the stability and evolution of the dimple which did not require any rigidity of any surface involved. They neglected double layer, structural and van der Waals effects. The model required that at least one of the surfaces involved does not dilate radially under the stresses involved. They found

$$\frac{d^3(z/b)}{d\left(\frac{r-r_0}{a}\right)^3} = \left(\frac{b}{z}\right)^3, \tag{3.65}$$

where $a = 3\mu_c Q n^2 r_0^4/(16\sigma T^4)$ and $b = 2Ta/r_0$.

Platikanov (1964) studied small air bubbles pressed against a glass plate submerged in various fluids, and by using an interference technique it was shown that the dimple is smaller than predicted by Frankel and Mysels. It must be noted that the time scale for this process is in order of minutes. Hartland (1967) wrote that a dimple is visible between about 1 and 10 min. He further noted that during the first minute drainage occurs in a film that is fairly uniform in thickness. Hartland though, used rather viscous systems, golden syrup and glycerol in sextol phthalate.

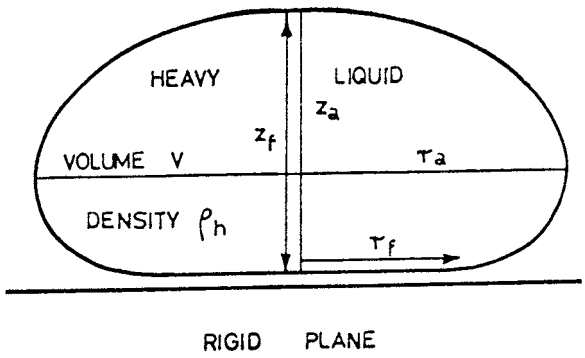

FIGURE 3.7: From Hartland (1969b), shows a drop resting on a rigid plane. A possible dimple is not included in the figure.

For a small drop resting on an interface, Lee & Hodgson (1968), showed that

$$r_{min} = R^2\left(\frac{2\Delta\rho g}{3\sigma}\right)^{1/2}, \tag{3.66}$$

and Chappelear (1961) gave the radius of the film as

$$r_f = 2R^2\left(\frac{\Delta\rho g}{3\sigma}\right)^{1/2}. \tag{3.67}$$

The ratio between these radiuses shows that the distance to the dimple is about 71% of the total collision radius.

Li (1996) extended the analysis of a dimpled film with immobile surfaces to account for the effects of dimpling and surface mobility. For the surface mobility the rate of mass transfer to the surfaces is controlled by diffusion. Li reduced the Navier-Stokes and continuity equations to eq (3.4) and eq (3.6). Li further assume the mass transfer do not effect the velocity distribution so that the z - velocity may be expressed as

$$v_z = \frac{\partial h_i}{\partial t} + \frac{\partial h_i}{\partial r} v_r \quad (i = 1, 2) \quad \text{at} \quad z = h_i, \tag{3.68}$$

thus the effect of the dimple is included in the second term on the right hand side of eq (3.68). These equations for the flow are solved together with an expression for σ at each surface.

This model should only be used for slow collisions or contacts that last much longer that the collisions one expect in a turbulent flow. In a turbulent flow one does not expect that a dimple will have time to develop in the contact film,

(1988).

3.1.2.5 Surfactants or impurities

Lee & Hodgson (1968) argued for three possible models of the film draining, namely the immobile, partly mobile and the fully mobile model, see figure 3.2. Complete immobility means that the fluid particle surface can support an infinite high shear stress. In reality it means that there must be a surfactant or an impurity in sufficient concentration to immobilize the surface. Complete mobility is obtained when the surface can not withstand shear stress. This is the case for very pure fluids and for the case where the impurities or surfactants are swept away from the interface due to partial mobility. In the latter case there will according to Lee & Hodgson (1968), be a back pressure from the swept away impurities due to a concentration difference. If a surface active third component is virtually insoluble and wholly confined to the surface its removal from the centre will increase the interfacial tension there and produce a gradient of interfacial tension between the periphery of the film and the centre. This can easily produce a shear stress sufficiently large to immobilize the film.

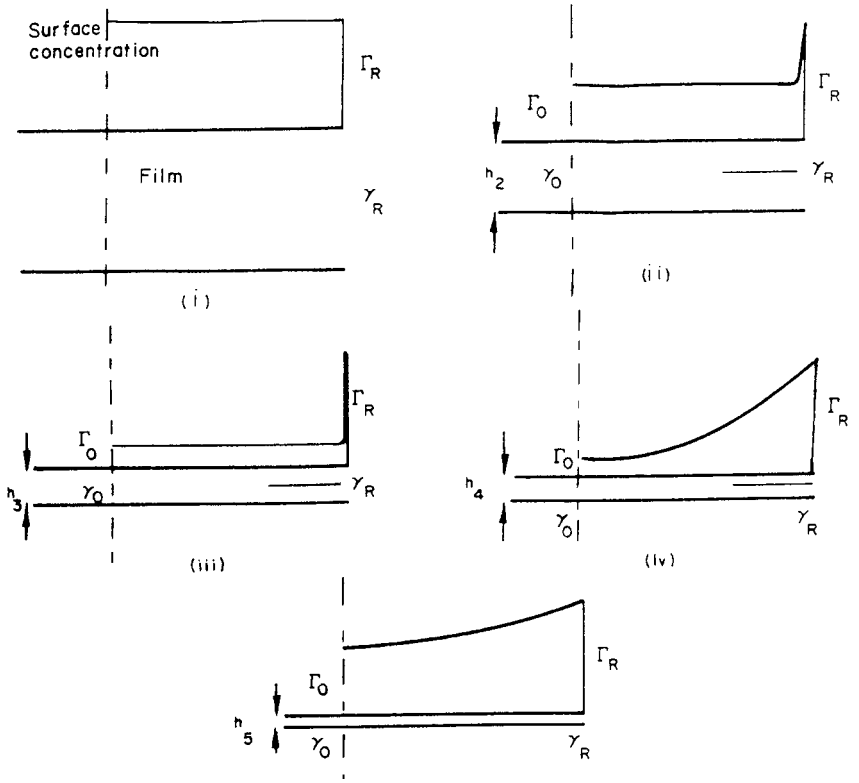

FIGURE 3.8: From Lee & Hodgson (1968), establishment of critical interfacial tension gradients. Starting with a initially uniform profile (i), then expansion (ii) and (iii), redistribution occurs and film is immobilized (iv) and further drainage with immobile film (v).

When the surface active third component is soluble it can diffuse to the surface when expansion occurs. The radial velocity in the film tends to sweep any surface active material to the periphery of the film, and this is accompanied by an expansion of an element of surface as it is moved radially outwards. The diffusion will result in a concentration of the surface active component that is between zero and the equilibrium value in the centre of the film. This provides a partial mobile film.

Lee & Hodgson (1968) found the critical interfacial tension difference promoting immobility for the parallel disk model to be

$$\Delta\sigma_0 = -\frac{1}{\pi}F\frac{h}{R^2}, \tag{3.69}$$

and for complete mobility they found

$$\Delta\sigma_0 = -\frac{1}{2\pi}F\frac{h}{R^2}, \tag{3.70}$$

which is only half the value of complete immobility. A possible scenario for the collision process between two fluid particles was given. The particles initially has an even distribution of the surface active agent and are initially fully mobile. The film will drain fast and the surface active agent will be redistributed radially due to the radial velocity causing depletion in the centre. The film will soon become fully immobile (going through a partial mobile phase). At full immobility the shear stress is balanced by the gradient of the surface active agent. The film will at this point drain very slowly. At some critical thickness the van der Walls force will cause instability and the film will again become mobile and drain fast until coalescence occurs. If this critical thickness is not reached, the fluid particles will generally rebound. MacKay & Mason (1963b) found the film drainage to be much faster below $0.2\ \mu m$ than predicted by the Reynolds equation (3.34). This suggest that the film changes from immobile to mobile at $0.2\ \mu m$ in their experiments, and it is in agreement with the suggestions Lee & Hodgson (1968) gave regarding changes of mobility. Hartland (1969b) also wrote that the rate of approach increases and that the final value is often close to that predicted by assuming a uniform film with no shear at the interface. Lee & Hodgson (1968) further argued that the film drainage process is laminar. Even in relatively inviscid liquids like water the smallest eddies are in order of $25\ \mu m$ which is generally much thicker than the draining film.

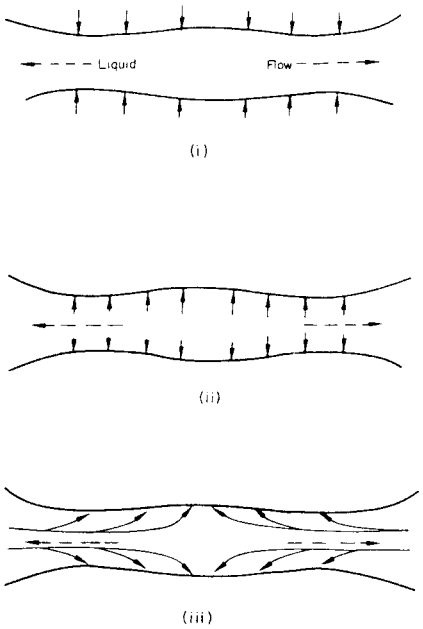

FIGURE 3.9: From Lee & Hodgson (1968), shows interface mobility with soluble surfactant. Expansion is determined by mass transfer. (i) Normal diffusion from outside film, (ii) normal diffusion from inside film and (iii) radial diffusion following depletion of film.

Mass transfer can play an important role in the rate of thinning of a liquid film between fluid dispersed particles. MacKay & Mason (1963a) wrote that the thinning rate was found to increase with the diffusion from the dispersed phase and decrease with the diffusion to the dispersed phase. The film thickness upon rupture appeared to be unchanged. Groothuis & Zuiderweg (1964) showed quantitatively that the coalescence rates can be enhanced twenty-fold by adding a relatively small amount of a third component to the dispersed phase. This agrees well with MacKay & Mason (1963a), who also showed a decrease in the film thinning by adding the third component to the continuous phase. A larger percentage was though needed in the continuous phase in order to get a similar percentage change in the rate of change of the film thickness. They argued that this may be due to their experimental setup.

3.1.3 Fluid particle collision (force balance)

The driving force for the film drainage is the pressure difference in the film, ΔP, or the force on the fluid particles resulting in the pressure difference. This section deals with the force driving the film drainage.

Chesters (1991) offers a review for the coalescence process and the article is an excellent reference and starting article for the subject. The collisions are divided into two categories, viscous and inertial collisions. For the viscous collisions the inertial part in the Navier-Stokes equations is neglected. This is expected to lead to a Stoke type expression

$$F \sim 6\pi\mu_c R(\dot{\gamma}R). \tag{3.71}$$

For viscous collisions in turbulent flow the strain rate, $\dot{\gamma}$, is replaced by $\dot{\gamma}_k$, a rate characteristic of flows in the smallest eddies:

$$\dot{\gamma}_k = (\varepsilon/\nu)^{1/2}. \tag{3.72}$$

For inertial collisions a characteristic velocity variation is given by

$$v_r = (\varepsilon d)^{1/3}, \tag{3.73}$$

with a typical force caused by the external flow on the fluid particles is given by

$$F_{ext} \sim \rho_c v_r^2 d^2 \sim \rho_c d^2 (\varepsilon d)^{2/3}. \tag{3.74}$$

Chesters (1991) further write that there is a virtual absence of viscous dissipation, giving a transfer of kinetic energy to surface energy during a collision. The assumption regarding the absence of viscous dissipation may not be correct for forceful collisions. For a forceful collision the collision interface radius, *a*, is of the same order of magnitude is the fluid particle radius, *R*, thus $a = O(R)$. A gentle collision on the other hand may be defined as $a \ll R$, see figure 3.10. Another important parameter that is addressed in the article is the virtual mass coefficient. It is listed as 2/3 for an isolated particle but it rises to about 1 for particles in close proximity. Normally this is not included in models and the virtual mass coefficient is assumed constant. Values below 2/3 is also common.

As for how to solve the collision problem, a conceptual solution procedure is given. This conceptual framework suggests solving the external flow and the internal

flow independently. The force applied in the internal flow (drainage) is given by the external flow. Chesters suggests that the contact time is given by the external flow, this may be true if there is no dissipation as assumed. With dissipation this is however unlikely since the dissipation is given by the internal flow and this again affects the amount of energy transferable to the fluid particles during the collision.

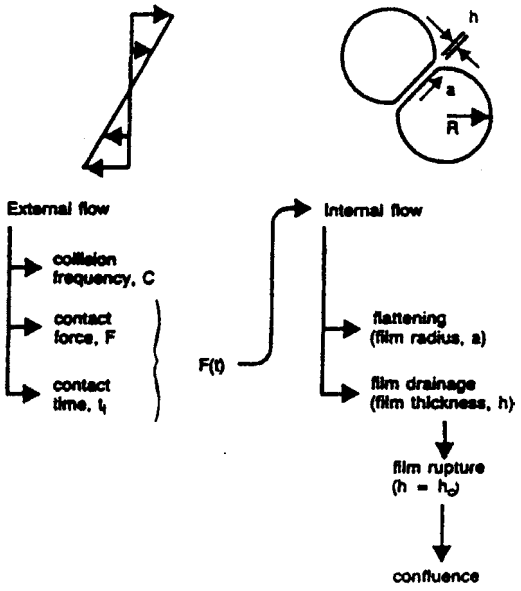

FIGURE 3.10: From Chesters (1991), showing a conceptual framework for coalescence modelling. External and internal flow is divided. Internal flow is here defined as flow between the collision surfaces.

It is further assumed that the deformation due to the collision, the a/R ration, is small. When comparing with the experimental data given by Scheele & Leng (1971), it is seen that this assumption is in error. They found experimental values up to $a/R \sim 0.7$. These collisions were not due to turbulent flow, but it still seems likely that the assumption is incorrect due to the high values found experimentally.

Ivanov & Traykov (1976) solved for the film thinning by solving the Navier-Stokes equations for both the film and in their case the droplets. They used three main assumptions. 1- film is much thinner than the collision interface radius, 2- the film is plane-parallel, and 3- the dissipation of energy due to liquid motion out from the film is negligible. The energy is according to them dissipated in a narrow region situated immediately about the collision zone of the droplets colliding. This dis-

sipation decreases sharply with thicker collision zones. They wrote the normal stress tensor as

$$T_{zz}(0) = -P(0) + 2\mu_c\left(\frac{\partial v_z}{\partial z}\right)_{\eta=0} \text{ with } \eta = \left(z - \frac{h}{2}\right)\sqrt{U/(r\nu)}, \qquad (3.75)$$

consisting of a pressure part and a viscous normal tensor. As most authors later on they only kept the pressure term when solving the equations, Middleman (1998). The Navier-Stokes equations are solved by using the simplifications above and they get the following expression for the critical film thickness

$$h_{cr}^{-2/3} - h_0^{-2/3} \approx 3.3\left(\frac{\Delta P^2}{R^4\rho_c\mu_c}\right)^{1/3}\Delta t, \qquad (3.76)$$

where h_0 is the initial thickness at which the film forms. ΔP is given from the collision between the fluid particles.

Jeelani & Hartland (1991a) solved for the movement of a fluid particle toward a flat interface (or another fluid particle):

$$m\frac{dv_z}{dt} = F_c - F - F_r, \qquad (3.77)$$

where $F_c = \beta\sigma a/R$ is the restoring force, $F_r = 12\pi\mu_c R v_z$ is the drag force and F is assumed a constant force. For a bubble or drop toward a horizontal interface F is the buoyancy force and in this case it is correct to assume that it is a constant. For a collision between two fluid particles F is normally called the outer force and it is normally not a constant. Jeelani and Hartland also included an added mass but did not assume a constant one. The added mass varied from 0.5 at infinite distance to 0.69 when the colliding surfaces were at contact. An approximation for the velocity was used based on the geometry of the problem

$$-v_z = -\frac{dz}{dt} = 0.5r\frac{d}{dt}\theta^2. \qquad (3.78)$$

This approximation only works well for small contact area compared to the cross-sectional area of the fluid particle. This becomes the following dimensionless linear second order differential equation

$$\frac{d^2A}{dT^2} + \lambda\frac{dA}{dT} + 2\pi\beta A = 2\pi f, \tag{3.79}$$

where $A = a^2/R^2$, $f = F/(\sigma R)$, $\lambda = 12\pi\mu_c R/\sqrt{m\sigma}$ and $T = t\sqrt{\sigma/m}$. When the drag term is neglected, the right hand side of eq (3.79), can be solved analytically and the analytical solution was given by Jeelani.

The film drainage, which is solved in addition to the movement of the particle itself, was divided into two parts. The inertial drainage being equal to the restoring force

$$\frac{k\rho_c v_z^2 a^2}{16\pi h^2} = \frac{\beta\sigma a}{R}, \tag{3.80}$$

and the viscous drainage being equal to the restoring force

$$\frac{3\mu_c n^2 a^2 v_z}{8\pi h^3} = \frac{\beta\sigma a}{R}, \tag{3.81}$$

where the k parameter in (3.80) allows for frictional resistance at the surface. This parameter is greater than or equal to unity. It was found that the viscous draining was too slow compared to the experimental data from Scheele & Leng (1971). This comparison is probably not very realistic since the contact areas in those experiments were in the order of 70% of the cross sectional areas. The small contact area approximation used by Jeelani and Hartland is thus violated. Further, the surface oscillation of the fluid particles in the experimental data is not accounted for.

Jeelani & Hartland (1991b) continued the work above by introducing shape oscillations. They used

$$m\frac{dv_z}{dt} = F_c - F_s - F_r, \tag{3.82}$$

where

$$\frac{F_s}{m} = \frac{dv_{z,s}}{dt} = F_0 e^{-\gamma t}\sin(\omega t + \delta_0) \text{ and } F_0 = \left.\frac{dv_{z,s}}{dt}\right|_0. \tag{3.83}$$

The fluid particles oscillate around the centre of mass when they are separate. Once two particles collide this translates into oscillation around the centre of mass. The experimental data given by Scheele & Leng (1971) is used for validation. The match with experimental data is very good. This is probably mostly due to the fact that five model parameters, $v_{z,s}$, F_0, γ, ω and δ_0, are fitted to each experimental run.

It is further noted in the article that the frictional losses at the surfaces of the collision area during inertial drainage may be extremely high. Reverse flow may thus occur in the drops when the oscillatory motion is directed away from the mid-plane of the collision interface. In their opinion the oscillation is very important for the coalescence process. This was also noted in the experiments done by Scheele & Leng (1971).

Luo & Svendsen (1996) offers a rather different view of the collision process between two fluid particles. They do not take the film drainage into account at all. The collision interface radius is found from a combination of the volume balances of each fluid particle and the total distance between the centres of mass of the particles

$$z_{tot} = \sqrt{R_1^2 - r_f^2} + \sqrt{R_2^2 - r_f^2} + \frac{3}{16} R_{10}\left(1 + \left(\frac{R_{10}}{R_{20}}\right)^3\right)\left(\frac{r_f}{R_{10}}\right)^4 . \qquad (3.84)$$

They also find a total collision time, but this time scale is questionable since no energy loss is accounted for during the collision process.

Svendsen & Luo (1996) uses a model similar to Luo & Svendsen (1996), in accordance with the previous work this model neglects the film drainage. The collision was split up in three distinct serial processes: the approach, the drainage and the interface rupture process. This view is rather doubtful, the drainage and the approach process are most likely simultaneous processes. Though, it may be that the approach process giving the interface area during the collision is approximately independent of the drainage. This also is rather doubtful initially, but as the interface starts to form the film between will quickly drain to a thin film compared to the radius of the contact area.

Two models are presented, one simple parallel-film model where the maximum collision area and the collision time for the maximum is found. An energy balance is used to find the potential energy stored in the collision, or internal kinetic energy as it is called in the article

$$E_{k,\,int} = \frac{1}{2}(m_1 v_{z,1}^2 + m_2 v_{z,2}^2) - \frac{1}{2}(m_1 + m_2) v_{z,um}^2, \tag{3.85}$$

where

$$v_{z,\,um} = \frac{m_1 v_{z,1} + m_2 v_{z,2}}{m_1 + m_2}, \tag{3.86}$$

is the velocity for the centre of mass for the two particles colliding. Further the increase in surface area can be approximated as

$$\Delta s = \Delta s_1 + \Delta s_2 = (\pi/4) r_f^4 (R_1^{-2} + R_2^{-2}). \tag{3.87}$$

This simplification is possible since the authors assume that $r_f \ll R$. They further assume that all internal kinetic energy is stored as an increase in the surface giving

$$\sigma \Delta s = E_{k,\,int}. \tag{3.88}$$

The maximum interface radius, r_{max}, is then found.

A more general collision model is also given. This model is based on a force balance for each fluid particle in order to track the location of both particles. Note that the models given can handle fluid particles of individually different sizes. The force balance for each particle is

$$m\frac{dv_z}{dt} = F \pm \frac{\beta \pi \sigma r_f^2}{R} - 12\pi\mu_c R v_z, \tag{3.89}$$

where F is the external force, it may be buoyancy, the next term on the right hand side is the restoration force and the last term is the drag force. In addition to the force equations, which is combined to a single one, an equation for the distance between the fluid particle mass centres is needed

$$\frac{z}{R_1} = \left(1 - \left(\frac{r_f}{R_1}\right)^2\right) + \frac{\left(1 - \xi^2\left(\frac{r_f}{R_1}\right)^2\right)^{1/2}}{\xi} + \frac{3}{16}(1 + \xi^3)\left(\frac{1}{R_1}\right)^4, \tag{3.90}$$

where $\xi = R_1/R_2$. The first two terms on the right hand side of (3.90) constitute the distance between the geometrical centres of the fluid particles and the third

term expresses the distance between the geometrical centres and the mass centres. The film area and velocity can then be plotted as a function of the collision time. Zero external force is assumed in these calculations and the results are compared with experimental data from Scheele & Leng (1971).

3.1.3.1 Drag force

The drag force may not be the most important one during a collision between two fluid particles, nevertheless a correct formulation should be used. Most authors use drag formulation found for a single sphere in a free flow. Hallouin, Gondret, Lance & Petit (1998) uses a modified formula for a sphere toward a rigid plane wall

$$F = 6\pi\mu_c R v_z \lambda, \tag{3.91}$$

where $\lambda = \lambda(h/R)$ is a correction to Stokes' low given by

$$\lambda = \tag{3.92}$$

$$\frac{4}{3}\sinh\alpha \sum_{n=1}^{\infty} \frac{n(n+1)}{(2n-1)(2n+3)} \left[\frac{2\sinh(2n+1)\alpha + (2n+1)\sinh 2\alpha}{4\sinh^2(n+1/2)\alpha - (2n+1)^2\sinh^2\alpha} - 1 \right]$$

where the parameter α depends on the ratio h/R by the relationship $\alpha = \cosh^{-1}(h/R - 1)$.

A good approximation that satisfies both limits $h/R \gg 1$ and $h/R \ll 1$ is

$$F = 6\pi\mu R v_z (1 + R/h). \tag{3.93}$$

3.1.3.2 Collision angle and off-centre collisions

Orme (1997) defines the collision angle, ψ, and the impact parameter, *b*, from figure 3.11.

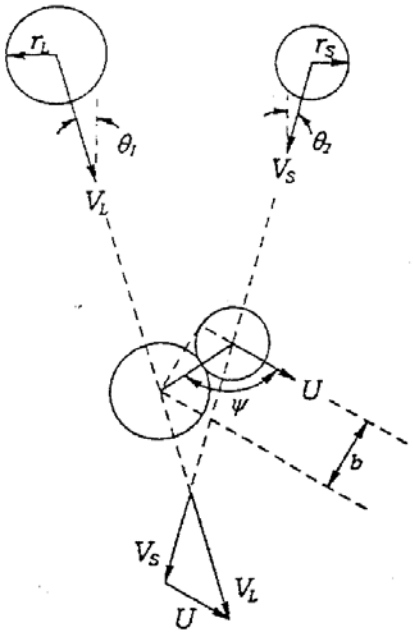

FIGURE 3.11: Nomenclature for the binary collision process by Orme (1977). *b* is the impact parameter, ψ is the collision angle, V_L and V_S are the velocities of the large and small fluid particles respectively. *U* is the relative velocity, r_L and r_S are the radii of the large and small particle respectively, and θ_1 and θ_2 are the trajectory angles measured from the reference of the gravitational vector.

The impact parameter, *b*, is thus the distance from the center of one fluid particle to the relative velocity vector placed on the center of the other fluid particle. The relative velocity between two fluid particles is given as

$$U = (U_1^2 + U_2^2 - 2U_1U_2\cos(\theta_1 + \theta_2))^{1/2}. \quad (3.94)$$

Examples of possible outcomes when the collision is not head on is given in figure 3.12. It was found that the coalescence probability is dependent on the collision angle and the impact parameter. Figure 3.12 also uses a ‘phasing parameter’. The impact parameter as described is used in the x-y plane, and the phasing parameter seem to be identical but in the y-z plane. The z-plane is aligned with the gravity vector.

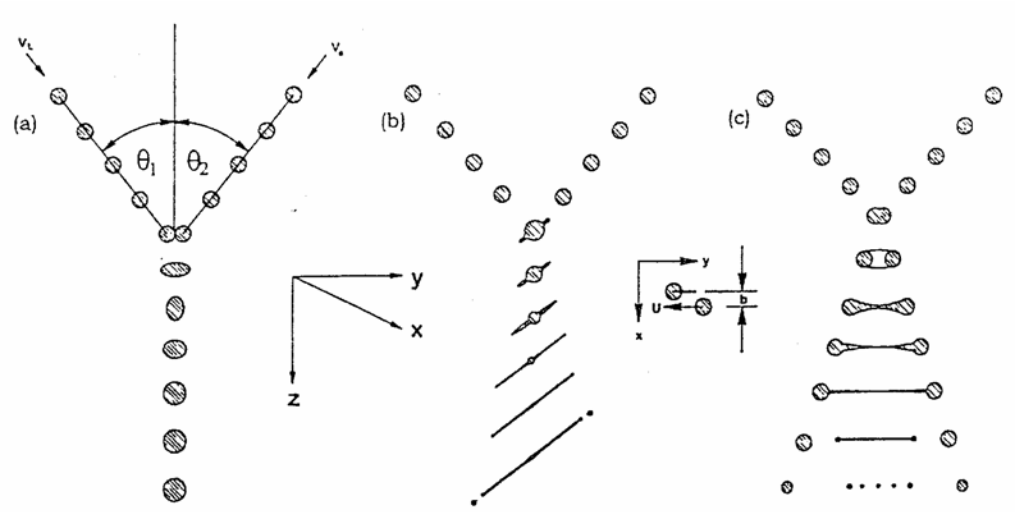

FIGURE 3.12: Examples of binary droplet collisions illustrating the effect of impact velocity and impact parameter, *b*, by Orme (1997): (a) low impact speed collision resulting in stable coalescence leading to fragmentation with zero impact and phasing parameter; (b) high impact speed collision resulting in unstable coalescence leading to fragmentation with zero impact parameter and finite phasing parameter; (c) high impact speed collision resulting in unstable coalescence leading to fragmentation with zero phasing parameter and finite impact parameter (grazing collision).

Not only do the two factors, collision angle and impact parameter, influence the coalescence probability, they also influence the outcome on collisions that experience temporary coalescence, as seen schematically in figure 3.12.

Ashgriz & Poo (1990) also shows that coalescence is dependent on the collision angle and an impact parameter, see figure 3.13. Figure 3.13 shows a coalescence situation which is only temporary due to a high impact parameter. The result of the head-on collision with a high impact parameter is a phenomena called a *stretching separation collision*. Notice that some mass is exchanged during such a collision.

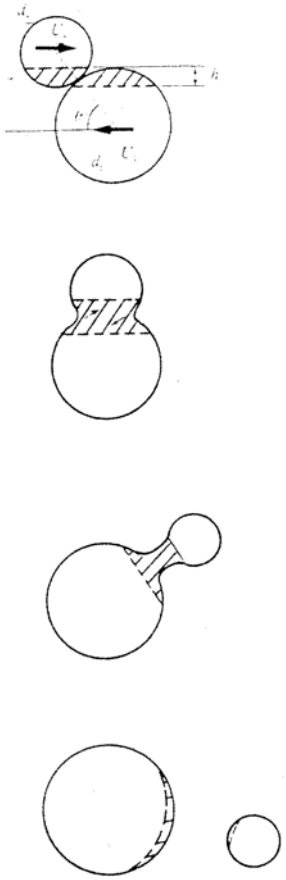

FIGURE 3.13: Schematic of the stretching separation collision of two fluid particles by Ashgriz & Poo (1990).

Figure 3.12 shows similar cases as figure 3.13, but for non head-on collisions.

3.1.4 Experimental studies

Chi & Leal (1989) lists a number of articles for methods of measuring the film thickness and a number of articles with such measurements. They pointed out that even though the literature is crowded with studies of the film drainage step of the coalescence process it is not clear that the full picture actually results. Most studies deal with initially placing a drop very close to an interface and measuring the

gravity approach. Such an approach ignores the dynamics of a collision process and some of the scales may be of different magnitudes. The time scale is one of them.

Scheele & Leng (1971) studied experimentally the collision of anisole drops of diameter 3.4 mm. in water. They used a magnetic variable pulse generator to shoot the colliding drops toward each other with approach velocities of 1.9 - 11.2 cm/s. They used mutually saturated liquids with freshly formed interfaces that oscillated due to the pulse generator generating the fluid particle. The collisions were recorded by high speed photography. The oscillation phase was found to be very important, that is the oscillation shape at contact. It was found that collisions starting in an initially elongated shape at first contact had a much higher chance of coalescing. They used the Stefan-Reynolds equation, also called Reynolds equation, (3.34), to test the drainage of the film. In all cases the Reynolds equation was found to give drainage of orders too slow, but it was found that the collisions resulting in coalescence drained somewhat more than the collisions that did not coalescence.

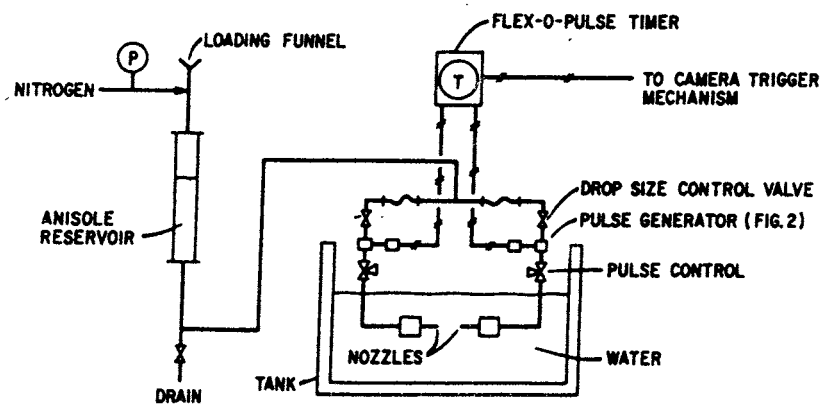

FIGURE 3.14: From Scheele & Leng (1971), shows the apparatus used to create the drop collisions measured experimentally.

Burrill & Woods (1973a) used various oil-water mixture combinations to study drainage mechanisms. Their results can be divided into three parts. First, a rapid approach from distances greater than 0.1 cm to film thicknesses at the deformed interface less than $3 \cdot 10^{-6}$ m in less than 0.1 s. The film then ruptures or the drop is arrested. Second, a dimple of water is formed if the drop is arrested. Third, dimple formation is followed by or occur simultaneously with drainage of water. They

wrote that the initially mobile film became dynamically immobile if transfer of kinetic energy to surface energy can be completed due to enough surfactant. If not, the film will become partially mobile and drain to coalescence in a relatively short time. A dimple is formed due to interfacial tension gradient exceeding the surface shear stress because the drop inertia that was partially responsible for setting up this gradient has been dissipated. The bulk interface then contracts and carries adsorbed surfactant inward which reduces the interfacial tension gradient along the bulk interface. If the interfacial velocity inward is large, it will carry with it bulk fluid and generate the dimple. After the initial rapid expansion and contraction of the bulk interface is over the shear stress can be written as

$$S = -\mu_c \left.\frac{\partial v_r}{\partial z}\right|_{interface} = \frac{d\sigma}{dr}. \tag{3.95}$$

Uneven drainage is according to Burrill & Woods (1973a) due to unsymmetrical outflow of fluid through the barrier ring caused by local interfacial mobility. This gives a large outflow of liquid and will continue until the equality between the surface shear stress and the interfacial tension gradient is again approached. Thus, the film will either rupture or regain an approximate symmertical shape.

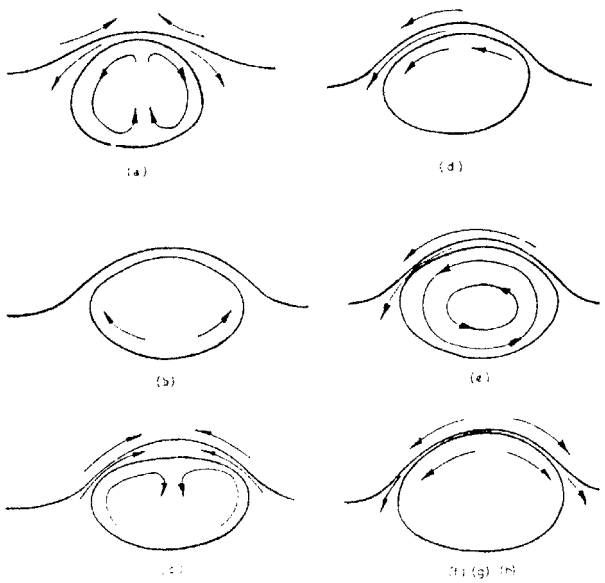

FIGURE 3.15: From Hartland (1969a), illustration of the flows and circulation patterns within a drop, draining film and bulk phase at different drainage times.

A somewhat different reason for uneven drainage was offered earlier. According to Hartland (1968) and Hartland (1969a) the unsymmetrical outflow is due to circulation patterns in the dispersed fluid. Hartland also notes that high concentration of surfactant gives symmetrical drainage and relatively uniform film, but this was due to immobility of the bulk interface causing no circulation. It was also noted that circulation in the dispersed drop has greater effect than circulation in the bulk. Also, measurements of interfacial tension indicate that it takes about one hour for the surface active molecules to reach their equilibrium surface concentration in the system studied by Hartland. For a drop to a bulk interface collision, Hartland found that surface active molecules collect to the bulk interface and are swept away from the drop interface during approach giving a collision with one mobile and one immobile interface.

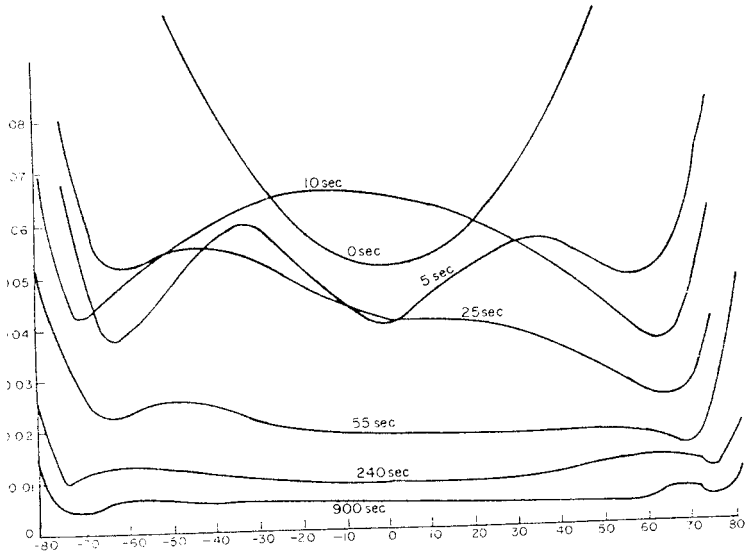

FIGURE 3.16: From Hartland (1969a), profiles of uneven drainage shown for different times.

Burrill & Woods (1973b) found that the interfacial concentration of adsorbed surfactant has an effect on the type of film drainage that occurred. For the low viscosity cases the film drained either evenly or unevenly. For other cases it can switch between even and uneven one or more times.

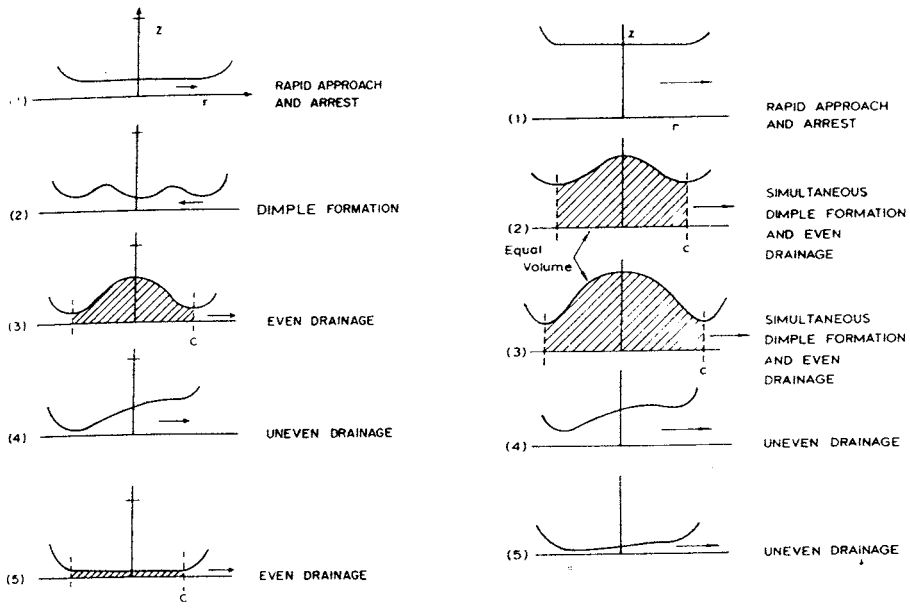

FIGURE 3.17: From Burrill & Woods (1973a), shows different versions of drainage and dimple formation. Left figure has small interfacial concentration of surfactant and right figure has large interfacial concentration of surfactant.

Experimental data for the drainage of the film for a collision between a bubble and a surface film is given by Doubliez (1991). Doubliez found that rebounds probability increase with surface ageing, with is not surprising since it is a well known fact that fluid particles collect impurities in the fluid after the particles are created. This gives rise to a less mobile film which in turn is responsible for the rebound probability increase. Similarly it was found for a given film thickness that the first stage of drainage thinning happened faster for the second bounce than for the first. This is probably due to the sweeping away of impurities at the interface during drainage. The film may then after the first bounce be looked upon as a more freshly formed fluid particle. Further, Doubliez noted that if bursting of the fluid particle takes place it more often takes place during the last stage when thickness is increasing. It is also interesting to note that it was experimentally found that higher approach velocities gives slower initial thinning rates. This is in agreement with what Chesters (1991) estimates for a parallel film model. The reason seems to be

that a higher initial velocity gives a faster increase in the surface area which in turn reduces the drainage rate.

Most articles reviewed about the collision phenomena considers models only and very few articles contain experimental data. Tsao & Koch (1997) presents some interesting data and conclusions drawn from this data. They found that a bubble toward a horizontal wall bounce further than a perfectly elastic bounce for a spherical bubble would account for. Two reasons for this were given, first reason is a release of energy associated with surface tension. This is due to the approaching bubble having a ellipsoidal shape due to terminal velocity while the rebounding bubble has a more spheroid shape. The second reason is due to a change in added mass with bubble shape. Both reasons transfers potential energy to kinetic energy giving a larger rebound.

An analysis of the collision with a wall shows that more energy is lost during a collision than what can be accounted for by drag alone. A possible mechanism for the additional loss is acoustic radiation of energy due to shape oscillations induced by the collisions, Tsao & Koch (1997). It also seems that most of the energy is lost during the rebound part of the collision, only 5% is lost when the bubble reaches its closest proximity to the wall and 59% is lost in total when the bubble reaches is maximum distance from the horizontal wall. This should be expected if the mechanism suggested is responsible for the energy loss observed, since it is assumed that the shape oscillations will occur after the rebound and before the bubble reaches its lowest point. On the other hand, it is seen from the collision radius reported by Scheele & Leng (1971) that a large part of the energy is lost during the rebound process itself. A second possible mechanism is a boundary layer separation from the rigid wall during the rebound, see figure 3.18.

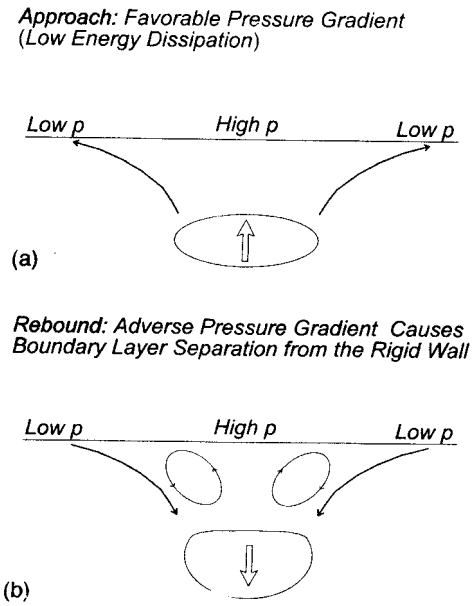

FIGURE 3.18: From Tsao & Koch (1997), schematic sketch of the bubble's approach to (a) and rebound from (b) a horizontal wall.

Tsao & Koch (1997) conclude that it is important to consider the surface energy and the changes in added mass during a bubble bounce. This should also be the case for a collision between two fluid particles.

Ashgriz & Poo (1990) found that in addition to normal coalescence when two fluid particles collide (in their case water droplets in air), the particles may experience unstable coalescence through two mechanisms, namely stretching separation (see figure 3.13) and reflexive separation (see figure 3.19).

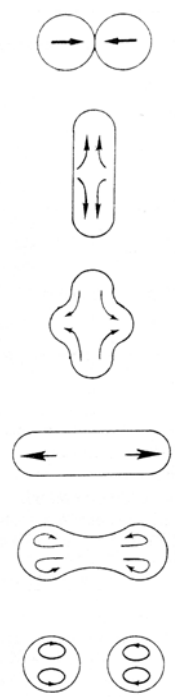

FIGURE 3.19: Schematic of reflexive separation for the head-on collision of two equal-sized fluid particles, Ashgriz & Poo (1990).

The impact parameter, *b*, is together with the force of the collision, by use of the Weber number, variables that give the kind of coalescence. The impact parameter, *b*, is defined in figure 3.11.

Experimental data showing the three kinds of coalescence is in figure 3.20 given for two equal sized droplets for the system water-air, i.e. collisions of water droplets in air.

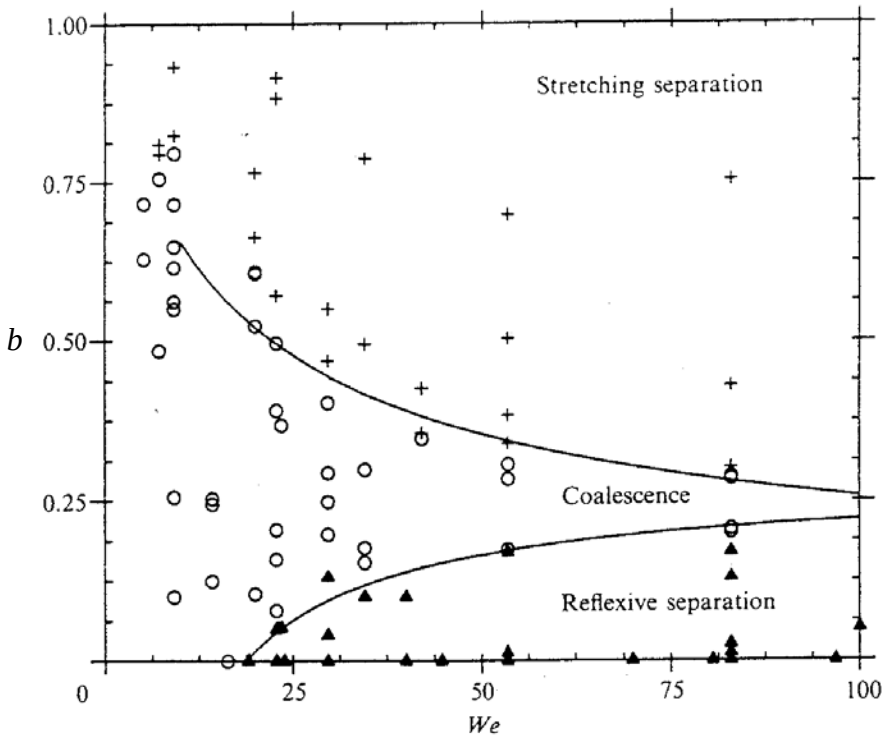

FIGURE 3.20: Regions obtained for coalescence, reflexive separation and stretching separation, Ashgriz & Poo (1990). Experimental data: '+' for stretching separation, 'o' for coalescence and filled triangles for reflexive separation. The fluid particles (water droplets) are of equal size.

Figure 3.21 gives similar experimental data as figure 3.20, but for one droplet being twice the diameter of the other one.

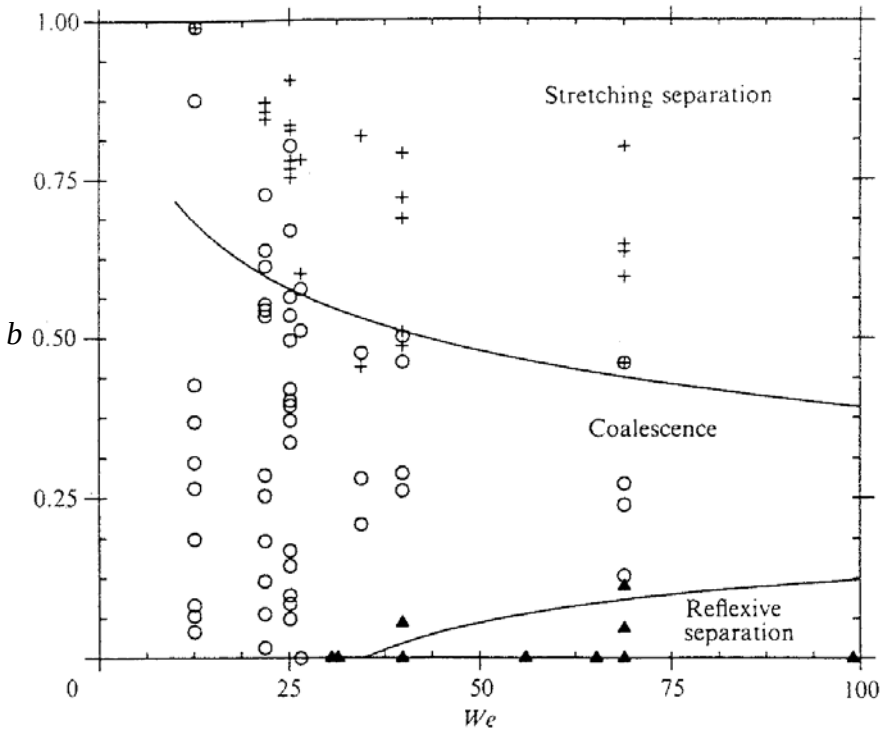

FIGURE 3.21: Regions obtained for coalescence, reflexive separation and stretching separation, Ashgriz & Poo (1990). Experimental data: '+' for stretching separation, 'o' for coalescence and filled triangles for reflexive separation. The largest fluid particle (water droplet) is twice the diameter of the other fluid particle (water droplet).

By comparing figure 3.21 with figure 3.20 it is seen that stable coalescence is more probable for the cases with unequal sized droplets. Further, Ashgriz & Poo (1990) mentions that for stretching separation the initially largest particle will become the smallest one after the collision. Thus, a large fraction of mass has been transferred.

3.2 Coalescence efficiency

It has been shown that it is very difficult to formulate a proper parameterization for the coalescence efficiency, $\lambda(\vartheta, \vartheta')$. As seen in chapter 2, several attempts have

been suggested in the literature, however, most of them are of very empirical nature. Our goal is to formulate a more fundamental model.

The following procedure for formulating the coalescence efficiency, $\lambda(\vartheta, \vartheta')$, emerges:

The thickness of the draining film seems to be one of the important variables determining the coalescence efficiency. The film drainage processes may be very different considering mobile and immobile interfaces, Lee & Hodgson (1968). In addition, as the film does not rupture at a specific thickness, a coalescence criterion may be estimated based on a probability density function for the rupture thickness, or one may simply have to determine a critical rupture thickness empirically. A third procedure could be developed based on mechanistical model simulations.

The thickness of the draining film between two colliding fluid particles can be calculated by use of a model formulation that couples the particle collision processes and the film draining. This may be obtained by combining the film draining models given by Vaughn & Slattery (1995) and Slattery (1999), with a particle collision model similar to the procedures used by Jeelani & Hartland (1991b) and Svendsen & Luo (1996).

Such a model should also take into account the size ration between the colliding particles as discussed by Ashgriz & Poo (1990). The fluid particles will oscillate in a turbulent environment, Montes, Galan & Cerro (1999), this effect should also be included because the oscillation phase together with the oscillation amplitude may be important for the coalescence probability, Scheele & Leng (1971). Further, the collisions may not be head-on, Ashgriz & Poo (1990), which will affect the coalescence probability. The kinetic energy in the collision may also vary resulting in a different coalescence probabilities, Low & List (1982) and Ashgriz & Poo (1990). A mechanistic model should take all these factors into account.

Notation

A	dimentionless area, eq (3.79), -
a	parameter, defined below eq (3.65), m
a	drainage film radius, defined below eq (3.77), m
$a_1(t)$	lower boundary in integration by Leibnitz theorem, eq (3.10)
$a_2(t)$	upper boundary in integration by Leibnitz theorem, eq (3.10)

B	constant, for different values see text after eq (3.24), J or Jm (see text after eq (3.24))
b	parameter, defined below eq (3.65), m
b	impact parameter, after eq (3.93)
b_m	London-van der Waals force, eq (3.23), N/kg
C_1	integration constant, eq (3.7), $1/s$
C_2	integration constant, eq (3.7), m/s
d	diameter of fluid particle, eq (3.73), m
$E_{k,\,int}$	internal kinetic energy, eq (3.85), $N \cdot m$
F	total force on film, eq (3.33), N
F	constant (or external) force, eq (3.77), N
F_0	initial amplitude, eq (3.83), m/s^2
F_c	restoring force, eq (3.77), N
F_{ext}	external force acting on fluid particle, eq (3.74), N
F_r	drag force, eq (3.77), N
F_s	shape oscillation force, eq (3.82), N
F_z	force fluid exerts on fluid particle, eq (3.54), N
f	dimentionless external force, eq (3.79), -
$f_1(z, t)$	function of z position and time, eq (3.44), Pa
$f_2(r, t)$	function of r position and time, eq (3.44), Pa
$f(x, t)$	function to be integrated by Leibnitz theorem, eq (3.10)
$f(z)$	function of z-direction only, after eq (3.3)
g	gravity constant, eq (3.27), m/s^2
H	length scale in axial direction, see text above eq (3.27), m
h	film thickness, after eq (3.6), m
$h(r, t)$	liquid film thickness, eq (3.3), m
h_0	initial liquid film thickness, eq (3.31), m
h_1	thickness at state 1, eq (3.35), m

h_2	thickness at state 2, eq (3.35), m
h_{cr}	critical film thickness, eq (3.76), m
h_i	film thickness for particle *i*, eq (3.68), m
h_r	film thickness at the rim, eq (3.25), m
k	parameter for frictional loss at surface of film, eq (3.80), -
L	length scale in radial direction, see text above eq (3.27), m
m	parameter, eq (3.24), -
m	mass, eq (3.77), kg
m_1, m_2	mass of fluid particle $1, 2$, eq (3.85), kg
n	number of non-dilating surfaces, see below eq (3.65), -
n	number of immobile interfaces bounding the film, eq (3.81), -
P	pressure, eq (3.1), Pa
$P(r)$	pressure as a function of radius, eq (3.52), Pa
P_0	pressure at center of radius of film, eq (3.36), Pa
P_d	pressure in dispersed phase, eq (3.54), Pa
P_h	hydrostatic pressure, eq (3.51), Pa
P_r	pressure at the rim of the film, eq (3.36), Pa
Q	flow through the barrier ring per unit length of periphery, see below eq (3.65), m^2/s
R	radius fluid particle, eq (3.22), m
R_1, R_2	radius fluid particle $1, 2$, eq (3.84), m
R_{10}, R_{20}	initial radius fluid particle $1, 2$, eq (3.84), m
R_m	film radius for bubble of radius R resting in equilibrium at a free surface, eq (3.27), m
Re	Reynolds number, $Re = (\rho v_z d)/\mu$, after eq (3.22), -
Re_f	Reynolds number, eq (3.27), -
Re_p	Reynolds number for particle, after eq (3.3), -
r	radial direction, eq (3.1), m

r	interface radius, eq (3.33), m
r’	dimensionless radius, see text above eq (3.27), -
r_0	radius of the barrier ring, eq (3.65), m
r_f	interface radius, eq (3.3) and (3.38), m
r_{max}	maximum interface radius, after eq (3.88), m
r_{min}	position of minimum film thickness, eq (3.66), m
S	shear stress, eq (3.95), N/m^2
S_{zz}	normal stress, $S_{zz} = 2\mu_c \partial v_z/\partial z$, eq (3.54), N/m^2
T	thickness in the middle of the dimple as a function of time, see below eq (3.65), m
T	dimensionless time, eq (3.79), -
T_{zz}	stress tensor, eq (3.54), N/m^2
t	time, eq (3.1), s
t’	dimensionless time, see text above eq (3.27), -
$t_{1,2}$	drainage time from state 1 to state 2, eq (3.35), s
U	velocity scale in radial direction, see text above eq (3.27), m/s
U	collision velocity between two particles, eq (3.94), m/s
U_1, U_2	scalar velocities for particles 1 and 2, eq (3.94), m/s
U_0	plug flow velocity, eq (3.16), m/s
$u_{r,0}$	velocity in radial direction at the centre of the film, eq (3.36), m/s
$u_{r,r}$	velocity in radial direction at the rim of the film, eq (3.36), m/s
V_0	relative approach velocity, eq (3.27), m/s
$v_r(r, z, t)$	radial velocity as a function of r and z positions and time, eq (3.39), m/s
v_r	velocity in radial direction, eq (3.1), m/s
v_r’	dimensionless radial velocity, see text above eq (3.27), -
v_z	velocity in axial direction, eq (3.1), m/s
v_z	oscillating velocity in axial direction, eq (3.83), m/s

$v_{z,1}, v_{z,2}$	axial velocity of fluid particle 1, 2 , eq (3.85), m/s
$v_{z,s}$	oscillating velocity to center of mass, eq (3.83), m/s
$v_{z,um}$	axial velocity of the centre of mass of the two colliding fluid particles, eq (3.85), m/s
v_z'	dimensionless axial velocity, see text above eq (3.27), -
$v_z(z, t)$	axial velocity as a function of z position and time, eq (3.40), m/s
W	velocity scale in axial direction, see text above eq (3.27), m/s
We	Weber number, eq (3.27), -
z	axial direction, eq (3.1), m
z	function of axial direction, eq (3.33)
z'	dimensionless axial length, see text above eq (3.27), -
z_{tot}	distance between mass centres of two colliding fluid particles, eq (3.84), m
α	parameter, after eq (3.92), -
β	parameter determining excess pressure in the film, eq (3.77), - = 1 for an approach to a deformable interface = 2 for an approach to a plane interface
γ	interfacial tension, eq (3.27), N/m
γ	amplitude decay rate constant, eq (3.83), $1/s$
$\dot{\gamma}$	strain rate, eq (3.71), $1/s$
$\dot{\gamma}_k$	strain rate for smallest eddies, eq (3.72), $1/s$
ΔP	$P_0 - P_h$, surplus pressure in the film, eq (3.76), Pa
Δs	increase in surface area due to collision, eq (3.87), m
Δs_1	increase in surface area for particle 1 due to collision, eq (3.87), m
Δs_2	increase in surface area for particle 2 due to collision, eq (3.87), m
Δt	$t_{cr} - t_0$, drainage time for the initial state to critical film thickness, eq (3.76), s
$\Delta\rho$	$\Delta\rho = \rho_1 - \rho_2$, eq (3.66), kg/m^3

$\Delta\sigma_0$	$\Delta\sigma_0 = \sigma_{0,1} - \sigma_{0,2}$, eq (3.69), N/m
δ_0	phase angle, eq (3.83), -
ε	turbulent eddy dissipation, eq (3.72), m^2/s^3
ε	dimensionless length scale ratio, see text above eq (3.27), -
η	dimensionless function, eq (3.75), -
θ	half angle subtended by the draining film, eq (3.78), -
θ_1, θ_2	trajectory angles measured with reference to gravitational vector, eq (3.94)
λ	dimensionless constant, defined below eq (3.79), -
λ	correction factor, eq (3.91), -
$\lambda(\vartheta, \vartheta')$	coalescence efficiency once collision occurs between particles of volumes ϑ and ϑ', -
μ_c	viscosity of continuous phase, eq (3.1), $kg/(ms)$
ν	kinematic viscosity, $\nu = \mu/\rho$, eq (3.72), m^2/s
$\xi(r)$	distance from curved particle interface to interface, eq (3.33), m
ξ	radius ratio, eq (3.90), -
ρ_c	density in continuous phase, eq (3.1), kg/m^3
ρ_d	density in dispersed phase, eq (3.27), kg/m^3
σ	surface tension, eq (3.22), N/m
ϕ_B	interaction potential per unit volume of a semi infinite film liquid in the limit as the fluid-fluid interface is approached, eq (3.24), J/m^3
φ	interaction potential energy per unit mass f the liquid in the film, eq (3.23), J/kg
φ_0	$= \varphi$ evaluated in the limit as the interface is approached, eq (3.24), J/kg
ψ	collision angle, after eq (3.93)
ω	frequency, eq (3.83), $1/s$

References

Ashgriz, N. & Poo, J.Y. (1990). Coalescence and separation in binary collisions of liquid drops. *J. Fluid Mech.*, **221**, 183-204.

Bird, R.B., Stewart, W.E. & Lightfoot, E.N. (1960). Transport phenomena. John Wiley & Sons, New York, USA, 83-85.

Burrill, K.A. & Woods, D.R. (1973a). Film shapes for deformable drops at liquid-liquid interfaces. II. The mechanisms of film drainage. *Journal of Colloid and Interface Science*, **42**, 15-34.

Burrill, K.A. & Woods, D.R. (1973b). Film shapes for deformable drops at liquid-liquid interfaces. III. Drop rest-times. *Journal of Colloid and Interface Science,* **42**, 35-51.

Chappelear, D.C. (1961). Models of a liquid drop approaching an interface. *Journal of Colloid Science,* **16**, 186-190.

Charles, G.E. & Mason, S.G. (1960). The coalescence of liquid drops with flat liquid/liquid interfaces. *Journal of Colloid Science,* **15**, 236-267.

Chen, J.-D., Hahn, P.S. & Slattery, J.C. (1984). Coalescence time for a small drop or bubble at a fluid-fluid interface. *AIChE Journal,* **30**, 622-630.

Chesters, A.K. (1991). The modelling of coalescence processes in fluid-fluid dispersions: A review of current understanding. *Trans IChemE*, **69**, Part A, 259-270.

Chesters, A.K. & Hofman, G. (1982). Bubble coalescence in pure liquids. *Applied Scientific Research*, **38**, 353-361.

Chi, B.K. & Leal, L.G. (1989). A theoretical study of the motion of a viscous drop toward a fluid interface at low Reynolds numbers, *J. Fluid Mech.*, **201**, 123-146.

Danov, K.D., Gurkov, T.D., Dimitrova, T., Ivanov, I.B. & Smith, D. (1997). Hydrodynamic theory for spontaneously growing dimple in emulsion films with surfactant mass transfer. *Journal of Colloid and Interface Science,* **188**, 313-324.

Derjaguin, B.V. & Kussakov, M. (1939). *Acta Physiochim. U.R.S.S.*, **10**, 25.

Doubliez, L. (1991). The drainage and rupture of a non-foaming liquid film formed upon bubble impact with a free surface. *Int. J. Multiphase Flow*, **17**, No 6, 783-803.

Frankel, S.P. & Mysels, K.J. (1962). On the dimpling during the approach of two interfaces. *J. Phys. Chem,* **66**, 190-191.

Groothuis, H. & Zuiderweg, F.J. (1964). Coalescence rates in continuous-flow dispersed phase system. *Chemical Engineering Science,* **19**, 63-66.

Hahn, P.-S. & Slattery, J.C. (1985). Effects of surface viscosities on the stability of a draining plane parallel liquid film as a small bubble approaches a liquid-gas interface. *AIChE Journal*, **31**, 950-956.

Hahn, P.-S. & Slattery, J.C. (1986). Effects of surface viscosities on the thinning and rupture of a dimpled liquid film as a small bubble approaches a liquid-gas interface. *AIChE Symposium Series*, **82**, No. 252, 100-118.

Hallouin, E., Gondret, P., Lance, M. & Petit, L. (1998). On the motion of a sphere toward a plane surface: From lubrication to bouncing regime. *Third International Conference on Multiphase Flow, ICMF'98*, Lyon, France.

Hartland, S. (1967). The approach of a liquid drop to a flat plate. *Chemical Engineering Science*, **22**, 1675-1687.

Hartland, S. (1968). The coalescence of a liquid drop at a liquid-liquid interface. Part V: The effect of surface active agent. *Trans. Instn. Chem. Engrs.*, **46**, T275-T282.

Hartland, S. (1969a). The effect of circulation patterns on the drainage of the film between a liquid drop and a deformable liquid-liquid interface. *Chemical Engineering Science*, **24**, 611-613.

Hartland, S. (1969b). The profile of the draining film beneath a liquid drop approaching a plane interface. *Chemical Engineering Progress Symposium Series* **91**, 82-89.

Ivanov, I.B. (1988). Thin liquid films fundamentals and applications. Marcel Dekker, New York, USA, 391.

Ivanov, I.B. & Traykov, T.T. (1976). Hydrodynamics of thin films. Rate on thinning of emulsion films from pure liquids. *Int. J. Multiphase Flow* **2**, 397-410.

Jain, R.K. & Ivanov, I.B. (1980). Thinning and rupture of ring-shaped films. *J.C.S. Faraday II*, **76**, 250-266.

Jeelani, S.A.K. & Hartland, S. (1991a). Effect of approach velocity on binary and interfacial coalescence. *Trans IChemE*, **69**, 271-281.

Jeelani, S.A.K. & Hartland, S. (1991b). Collision of oscillating liquid drops. *Chemical Engineering Science*, **46**, 1807-1814.

Kirkpatrick, R.D. & Lockett, M.J. (1974). The influence of approach velocity on bubble coalescence. *Chemical Engineering Science*, **29**, 2363-2373.

Klaseboer, E. & Chevaillier, J.Ph. (1998). Drainage of the liquid film between drops colliding at constant approach velocity. *Third International Conference on Multiphase Flow, ICMF/98*, Lyon, France.

Klaseboer, E., Chevaillier, J.Ph., Gourdon, C. & Masbernat, O. (2000). Film drainage between colliding drops at constant approach velocity: Experiments and modeling. *Journal of Colloid and Interface Science*, **229**, 274-285.

Kocamustafaogullari, G. & Ishii, M. (1995). Foundation of the interfacial area transport equation and its closure relations. *Int. J. Heat Mass Transfer*, **38**, No. 3, 481-493.

Lee, J.C. & Hodgson, T.D. (1968). Film flow and coalescence - I Basic relations, film shape and criteria for interface mobility. *Chemical Engineering Science*, **23**, 1375-1397.

Li, D. (1996). Coalescence between small bubbles: Effects of bulk and surface diffusion. *Chemical Engineering Science*, **51**, 3623-3630.

Low, T.B. & List, R. (1982). Collision, coalescence and breakup of raindrops. Part I: Experimentally established coalescence efficiencies and fragment size distributions in breakup. *Journal of the atmospheric sciences*, **39**, 1591-1606.

Luo, H. & Svendsen, H.F. (1996). Modeling and simulations of binary approach by energy conservation analysis. *Chem. Eng. Comm.*, **145**, 145-153.

MacKay, G.D.M. & Mason, S.G. (1963a). Some effects of interfacial diffusion on the gravity coalescence of liquid drops. *Journal of colloid science*, **18**, 674-683.

MacKay, G.D.M. & Mason, S.G. (1963b). The gravity approach and coalescence of fluid drops at liquid interfaces. *The Canadian Journal of Chemical Engineering*, **41**, 203-212.

Middleman, S. (1998). An introduction to fluid dynamics. John Wiley & Sons, New York, USA, 341-342.

Montes, F.J., Galan, M.A. & Cerro R.L. (1999). Mass transfer from oscillating bubbles in bioreactors. *Chemical Engineering Science*, **54**, 3127-3136.

Orme, M. (1997). Experiments on droplet collisions, bounce, coalescence and disruption. *Prog. Energy Combust. Sci.*, **23**, 65-79.

Platikanov, D. (1964). *J. Phys. Chem.*, **68**, 3619.

Reynolds, O. (1886). On drops floating on the surface of water. *Phil. Trans. Roy. Soc. (London)*, **A177**, 157.

Scheele, G.F. & Leng, D.E. (1971). An experimental study of factors which promote coalescence of two colliding drops suspended in water - I. *Chemical Engineering Science*, **26**, 1867-1879.

Slattery, J.C. (1990). Interfacial transport phenomena. Springer-Verlag, New York, USA.

Slattery, J.C. (1999). Advanced transport phenomena. Cambridge university press, USA.

Stefan, J. (1874). *Sitzber. Akad. Wiss. Wies, Math.-naturw. Kl.***69**, 713.

Svendsen, H.F. & Luo, H. (1996). Modeling of approach processes for equal or unequal sized fluid particles. *The Canadian Journal of Chemical Engineering*, **74**, 1-10.

Tsao, H.-K. & Koch, D.L. (1997). Observations of high Reynolds number bubbles interacting with a rigid wall. *Phys. Fluids*, **9**, 44-56.

Vaughn, M.W. & Slattery, J.C. (1995). Effects of viscous stresses in thin draining films. *Ind. Eng, Chem. Res.*, **34**, 3185-3186.

Yiantsios, S.G. & Davis, R.H. (1990). On the buoyancy-driven motion of a drop towards a rigid surface or a deformable interface. *J. Fluid Mech.*, **217**, 547-573.

CHAPTER 4

Fluid particle collisions in turbulent flow

This chapter is based on the paper 'Theoretical analysis of fluid particle collisions in turbulent flow' by Hagesaether, Jakobsen & Svendsen, printed in Chem. Eng. Sci.

4.1 Introduction

Bubble and drop coalescence phenomena observed in many industrial separation processes and in multiphase chemical reactors such as bubble columns and stirring vessels, often have a significant influence on the process performance. Even though a number of sophisticated modelling concepts have been presented in the literature over the years, the chemical and physical mechanisms involved are still not satisfactory understood. Among the most promising methods applicable for elucidating these phenomena are the 'volume of fluid (VOF)' and the direct numerical simulation (DNS) methods. On the other hand, the multifluid models have been found to represent a trade-off between accuracy and computational efforts for practical applications. In these multifluid models constitutive equations are needed to describe the coalescing process, and due to the limited understanding of these phenomena we still have to resort to empirical correlations.

The present model belongs to the latter class and deals with the collision process between two fluid particles. The intention is to formulate a constitutive model that can be applied for determining whether the particles coalesce or not. The model should be applicable for both in phenomenological reactors models and in CFD based reactor models. Turbulence is included by using collision time scales generally less that a second, and by including fluid particle shape oscillations.

4.2 Model description

The model describes a head on collision for two oscillating rotational ellipsoids of any volume and velocities. We expect the model to be valid for a large range of velocities but the lack of experimental data limits our validation of the model. The same model can also predict side collisions, but the physics of the rolling motion is not yet accounted for. Off-line collisions, that is collisions not strictly head-on, may be simulated by using the velocity component in the head-on direction only. An off-line collision has a higher probability for uneven drainage, Hartland (1969), this possible effect is not included in the model. Note that with minor changes, it is also possible to simulate a tail-end collision with the equations derived, that is a collision due to one fluid particle catching up and colliding with another.

The force balance for each particle is

$$m\frac{du_z}{dt} = F = F_{Drag} + F_{D,form} + F_C, \tag{4.1}$$

where m includes added mass:

$$m = \frac{4}{3}\pi\rho_c a_0 b_0^2\left(\frac{\rho_d}{\rho_c} + \gamma\right), \tag{4.2}$$

where γ is the added mass parameter and we have used $\gamma = 0.5$, Luo & Svendsen (1996). Other values are also possible. Cook & Harlow (1986) used 0.25 for the air/water system, and 0.5 to 0.8 is given by Jeelani & Hartland (1991b) as a normal range. A sensitivity analysis has been performed for the γ parameter. The directions of the two drag forces in eq (4.1) are always opposite to the fluid particle velocity, and the restoring surface force is always negative.

Force balances are solved simultaneously for the individual fluid particles. In these balances steady drag, lubrication form drag and particle deformations are accounted for. The drag coefficient parameterisation is taken from Clift, Grace & Weber (1978) and gives the standard steady drag

$$F_{Drag} = \frac{1}{2}\pi\rho_c u_z^2 C_D, \tag{4.3}$$

where C_D is dependent on the Reynolds number. This drag is for rigid spheres and is thus inaccurate for two fluid particles. However, the steady drag term is found to be the least important force in the system. The restoring surface force is described by

$$F_C = \beta\pi\sigma r^2/R, \tag{4.4}$$

where β is a parameter determining the excess pressure in the film, Jeelani & Hartland (1991b). By using the Kelvin equation for spheres, Mørk (1991), the excess pressure is given as

$$\Delta P = 2\sigma/R_s. \tag{4.5}$$

This can be combined to

$$F = A\Delta P = 2\pi\sigma r^2/R_s, \tag{4.6}$$

giving $\beta = 2$ for spherical fluid elements. In this work the same value of β has been used for ellipsoids. R in the equation for the deformation is taken to be the radius of the particle at the border of the collision zone and can be expressed as

$$R = (h^2 + r^2)^{1/2}. \tag{4.7}$$

In addition comes an expression for the lubrication form drag. This force describes the extra form drag caused by the flattening of the colliding surface. According to Middleman (1998) this can be written as

$$F_{D,form} = 2\pi\int_0^r T_{zz}\big|_{z=f/2} r\,dr, \tag{4.8}$$

where z is the collision direction and the total normal stress tensor is given by

$$T_{zz} = P - 2\mu_c \frac{\partial u_z}{\partial z}, \tag{4.9}$$

where P is the pressure in the film.

In earlier work, Middleman (1998), Jeelani & Hartland (1991b) and Lee & Hodgson (1968), the viscous normal stresses have been considered negligible compared to the pressure term. This assumption is found to be questionable due to the short time scales involved in the collisions and as the resulting models contain inconsistencies, Middleman (1998).

A number of other approaches exists, Colin, Kamp & Chesters (1998) neglect the viscous energy dissipation and find the interaction time from a total energy conservation equation. This approach may work for mobile films, but the model will underpredict the viscous energy dissipation for immobile films occurring in most practical applications. Klaseboer, Chevallier, Masbernat & Gourdon (1998), as several others, apply the lubrication equation to study drainage of liquid films between fluid particles colliding at a prescribed approach velocity. The coupling between film drainage and movement of the approaching particles is not accounted for by the model, thus it has limited application for our purpose. Also time scales for turbulent collisions are far less than a second while current film drainage models operate with time scales of minutes.

If one considers the extreme case when all the initial kinetic energy of the fluid particles dissipate during collision, then only the viscous contribution to the total normal stress tensor remains. Assuming flat interfaces gives $\partial u_z / \partial z = f(z)$, Lee & Hodgson (1968) and we obtain,

$$F_{D,form}^{Viscous} = -2\pi\mu_c r^2 \left.\frac{\partial u_z}{\partial z}\right|_{z = f/2}. \tag{4.10}$$

In many practical situations this relationship will be a good approximation of the lubrication form drag, provided that the value of the parameter $\partial u_z / \partial z|_{z = f/2}$ is fitted to experimental data. If one considers the other extreme case where $T_{zz} = P$, Middleman (1998), one get a force term due to the excess pressure in the film

$$F_{D,form}^{Pressure} = \frac{3\pi r^4 \mu_c \partial f/\partial t}{2f^3}. \tag{4.11}$$

We combine these two asymptotic expressions for the total lubrication form drag.

In addition to the force equations some geometric relations are needed, see figure 4.1):

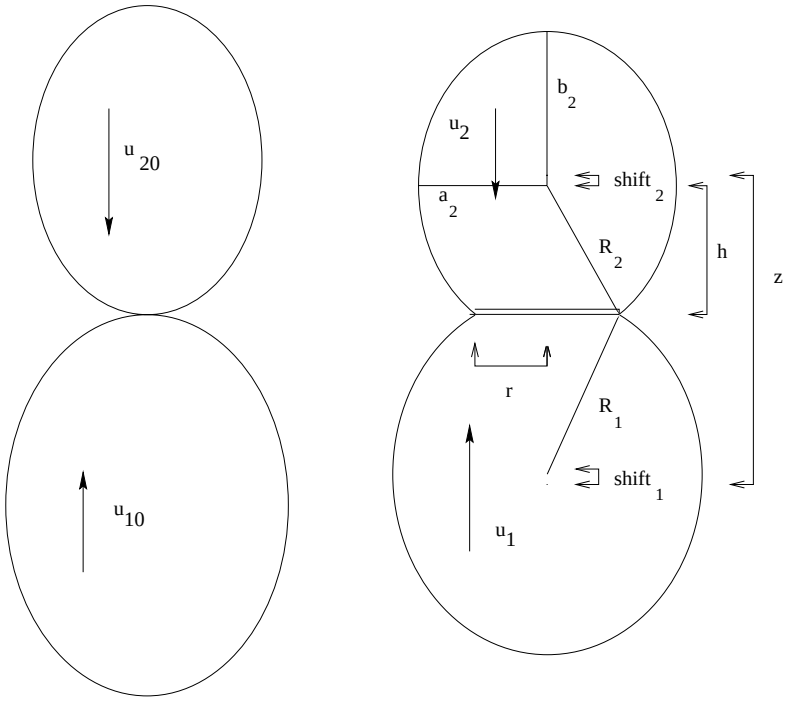

FIGURE 4.1 : Model sketch. Velocities and length variables are shown. The model is developed for oscillating rotational ellipsoids of different sizes.

The volume of the ellipsoid where *b* is rotated is

$$V = \frac{4}{3}\pi a_0 b_0^2. \tag{4.12}$$

Subscript *0* indicates the original shape of the particles, that is when the fluid particles are just touching each other, b is the radius in the collision direction, and a is the perpendicular radius. Assuming a flat interface between the colliding fluid particles and integrating, gives

$$V = \pi b^2\left(\frac{2}{3}a + h - \frac{h^3}{3a^2}\right) \text{ where } h = \left(a^2\left(1 - \frac{r^2}{b^2}\right)\right)^{1/2}. \tag{4.13}$$

In this formula the particle volume is retained, whereas, is earlier work, Svendsen & Luo (1996) and Chesters (1991), the flattening volumes have been disregarded. No exchange of mass between the fluid particles and the surrounding fluid have been assumed and the particles has been assumed incompressible. This volume balance implies that when the particles collide, the size of a, b or both has to increase. Assuming that the a/b ratio remains the same, the following equation is valid

$$a/b = a_0/b_0. \tag{4.14}$$

The total distance between the mass centres is found by adding the distances between the geometric centres and the interfaces, the distances between the mass centres and the geometric centres due to the deformation, and the film thickness f,

$$z = \left[h + \frac{3}{4}\frac{b^2}{a_0 b_0^2}\left(\frac{h^4}{4a^2} - \frac{1}{2}h^2 + \frac{1}{4}a^2\right)\right]_1 + \left[h + \frac{3}{4}\frac{b^2}{a_0 b_0^2}\left(\frac{h^4}{4a^2} - \frac{1}{2}h^2 + \frac{1}{4}a^2\right)\right]_2 + f. \tag{4.15}$$

The indexes specify each fluid particle. By dividing the mass integral by the volume integral we get the distance between the mass centre and the geometric centre of the rotational ellipsoid. In bubble columns and agitated reactors the turbulence motion induces fluid particle shape oscillations, Montes, Galan & Cerro (1998). To account for these oscillations, it is assumed that the collision axis can be modelled as a decaying sine function, Hagesaether, Luo & Svendsen (1996) and Jeelani & Hartland (1991a),

$$b = b_0(1 + \alpha\sin(\omega t + \theta\pi/180 + \pi/2)e^{-\delta t}). \tag{4.16}$$

The other length variable, *a*, is found from the volume balance. An equation for the variation in distance between the centres of mass for the two fluid particles is also needed and is expressed as

$$\frac{dz}{dt} = u_{z,1} + u_{z,2}. \tag{4.17}$$

Finally, a model describing the film drainage is developed in line with Kirkpatrick & Lockett (1974). A material balance for the film is combined with Bernoulli's equation along a streamline. In contrast to earlier work we include a friction term in the Bernoulli equation due to laminar flow in the film

$$\frac{P_0}{\rho_c} + \frac{u_{r,0}^2}{2} = \frac{P_r}{\rho_c} + \frac{u_r^2}{2} + \frac{F_{Friction}}{A\rho_c}, \tag{4.18}$$

where subscript *0* is for the centre of the film and *r* is for the radius *r*. The friction term is written as

$$F_{Friction} = n_0 \mu_c u_r r^3 / f^2. \tag{4.19}$$

The equations combined gives a second order equation for u_r that is solved and combined with the continuity equation for the film, giving the change of film thickness.

The resulting set of equations represents a DAE system that is solved in MATLAB using ODE15S for the differential equations (force balances) and BROYDEN for the algebraic equations.

4.3 Results and Discussion

Detailed experimental data on fluid particle collision is scarce and the only useful ones found are data given by Scheele & Leng (1971). These are used for model validation. The parameters α, θ, ω and δ in eq (4.16) are all found from experimental data and are not fitted. As mentioned earlier only one parameter in the lubrication form drag, eq (4.10), has been tuned to the experimental data. The same parameter value has been used in all simulations.

The experiments can be divided into two parts. Collisions that result in coalescence and collisions that result in a rebound. All simulations performed on collisions that result in rebounds, show that the energy dissipation caused by the lubrication form drag is dominant. Without it almost symmetrical rebound profiles are obtained, and the time scales of the collisions are much smaller than that found experimentally. When the lubrication form drag is included, the fit to experimental data is quite good.

In fig 4.2A is shown the collision radius, *r*, as a function of time during the collision process. It is seen that the simulations predict well the modular form of the *r*-response caused by the oscillations of the particles, shown in fig 4.2C. Also the departure process is well predicted. It should be noted that the agreement between simulations and experimental values is just as good for all the 4 experimental cases resulting in rebound. The experimental data comprise collision velocities in the range 2 - 11 cm/s, and oscillation phase angles at contact in the range 150 - 345^o. Maximum elongation along the collision axis is arbitrarily set as 0^o. Since the estimation of the collision velocity is uncertain, a 10% increase has been simulated and shown by the dotted line in fig 4.2A. The change is not dramatic indicating that the collision velocity is not a critical parameter in the approach process. Note that the film thickness profile, fig 4.2D, is hardly changed by the increase in velocity. This may be due to the assumption of immobile films. In fig 4.2B, the distance between the mass centres is given as function of time and shows how the particles approach each other and then depart. A sensitivity analysis of the added mass parameter, γ, showed that an increase of γ from 0.5 to 0.8 gave rise to an increased collision radius, *r*, of the order similar to that found for a 10 percent velocity rise. Lowering γ to 0.25 gave a corresponding reduction of the collision radius.

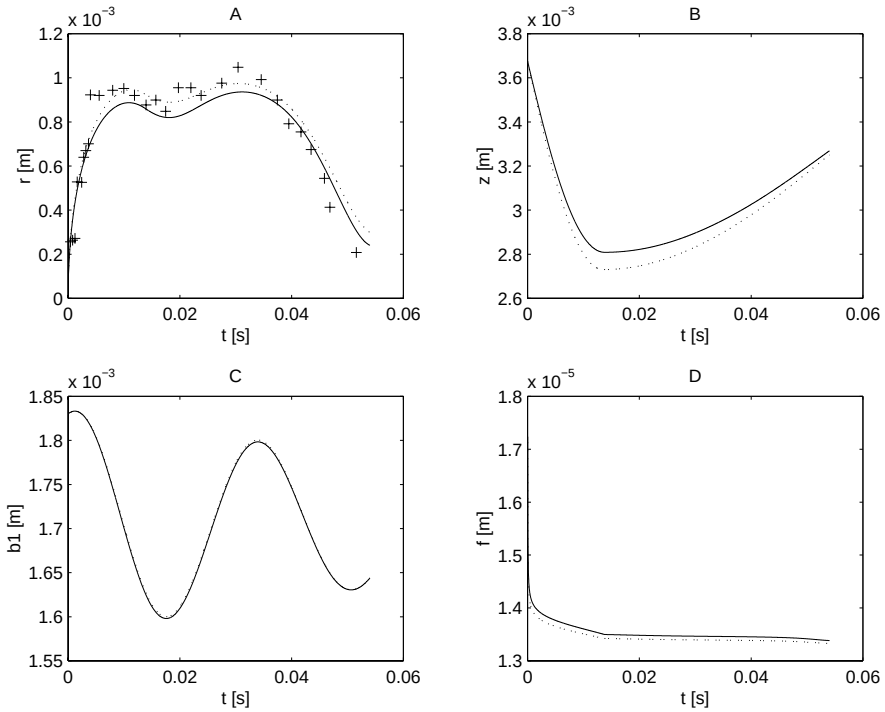

FIGURE 4.2 : Simulation of run 14 by Scheele & Leng (1971). Dotted curves for 10% increase in collision velocity. A - interface radius as a function of time, B - total distance between mass centres as a function of time, C - oscillating length variable, *b*, as a function of time. D - film thickness, *f*, as a function of time. The oscillation amplitude is 7.93 percent.

The energy dissipation during the collision process is supported by Tsao & Koch (1997) who found that there is a large energy loss during the collision process, 50% or more of the energy is generally lost. They attributed this to turbulence during the rebound process due to large pressure gradients. In all experimental rebounds we have found that the lubrication form drag can explain this loss completely. Other possible losses are friction in the liquid film during drainage and the kinetic energy spent in the drained continuous fluid. These contributions, however, have been found to be negligible, implying that the fluid particle approach process can be regarded as independent of the drainage processes in the film.

Dimple formation in the film between the fluid particles is reported by Princen (1963), Hartland & Robinson (1977) and Klaseboer *et al.* (1998), both in modelling studies and in experiments. For comparison with turbulent flow cases, how-

ever, the time scale is of crucial importance. In a collision between two fluid particles in turbulent flow, the time scale may be in the order of 0.1 second. For most drop-settling experiments and modelling studies the time scales have been of the order minutes. This may also be the reason why the whole lubrication form drag has not, to our knowledge been introduced before. Ivanov (1988) reports that in order for a dimple to occur, then $f \geq F/(2\pi\sigma)$. The initial film thickness used in our simulations is much lower indication that it is reasonable to assume a flat collision interface.

Fig 4.3 shows an example of an approach process resulting in coalescence. The agreement between simulations and experimental data is fair. Three of the four sets of experimental data show this fair agreement. The last one is a special case where coalescence takes place after several oscillation periods. The thickness of the film between the particles is governed by the film drainage model given by eq (4.18) and (4.19) where a friction factor, n_0, has been introduced as an adjustable parameter. Another parameter in the film model is the film thickness at initial contact.

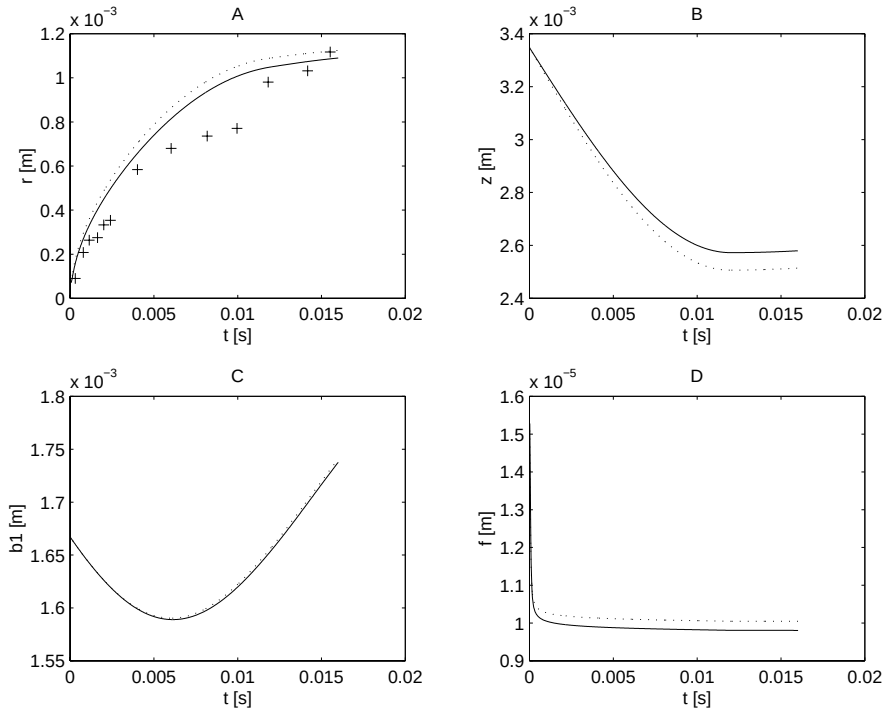

FIGURE 4.3 : Simulation of run 16 by Scheele & Leng (1971). Dotted curves for 10% increase in collision velocity. A - interface radius as a function of time, B - total distance between mass centres as a function of time, C - oscillating length variable, *b*, as a function of time. D - film thickness, *f*, as a function of time. The oscillation amplitude is 7.47 percent.

From figs 4.2D and 4.3D, it is seen that the film thickness very rapidly decreases to values around 10 μm and then remains almost constant. This is the case for all simulations and also for any choice of initial film thickness. Changing n_0 has a significant impact on the film thickness, as would be expected. However, the profiles are similar to those shown in figs 4.2D and 4.3D and the differences between the various simulations remain the same. The simulations show that the film thickness, after it has levelled off, is consistently 30-50% higher in the rebound cases compared to the coalescence cases. It is; however, to early to speculate whether this can be used as a criterion for coalescence. Apart from this no clear difference between the coalescence and rebound cases has been found. Scheele & Leng (1971) claimed that there was a correlation between the initial oscillation phase angle and coa-

lescence. A closer analysis shows that this finding is not generally valid for all experiments.

As mentioned earlier, in the literature, normally the viscous term in the total lubrication form drag; is disregarded, whereas the pressure term is believed to dominate. This was tested using the simulation model and a typical result is shown in fig 4.4. The graph shows clearly that the viscous term dominates the process. This was the case for all simulations. For the coalescence process however we speculate that the pressure contribution should have the important effect of increasing the film drainage compared to the rebound process situations.

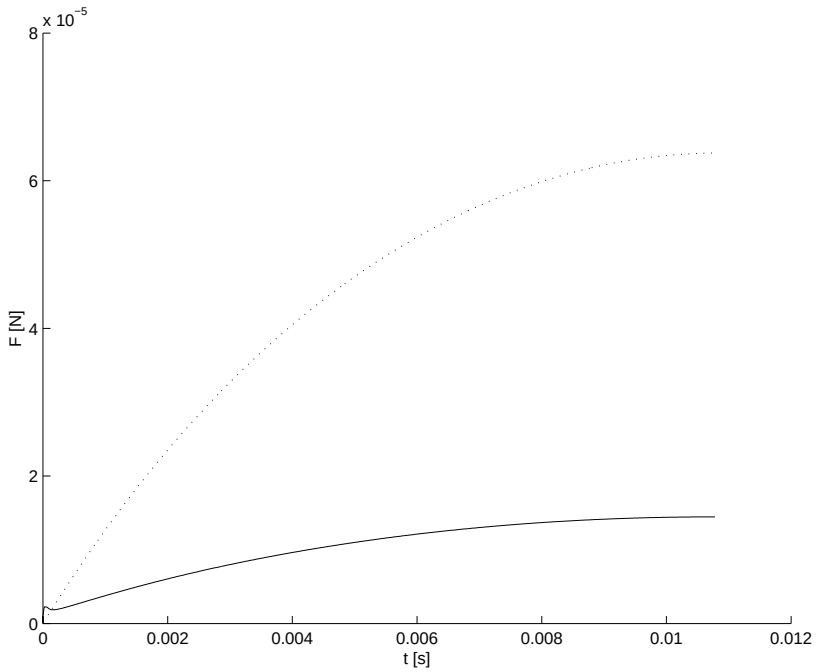

FIGURE 4.4 : Simulation of run 14 by Scheele & Leng (1971). The two parts of the lubrication form drag are compared. Dotted curve for the viscous term and continuous curve for the pressure term.

4.4 Conclusion

A model for the approach process between two oscillating particles has been formulated. The model includes a viscous lubrication form drag in the film that has been disregarded in earlier literature. It has been shown that this term dominates the approach process together with the surface restoration force.

Simulations have been compared with experimental data for oscillating particles and good agreement was obtained.

It is found that the particle approach process can be regarded as independent of the film drainage processes. However, the opposite is not true.

More experimental data is needed to further verify and improve the model. The immobile film assumption used may be incorrect when the film is drained to below some thickness.

Notation

A	area of interface, m^2
a	ellipsoid radius, non collision axis, m
b	ellipsoid radius, collision axis, m
C_D	drag coefficient, -
F	force, N
F_C	restoring surface force, N
$F_{D,form}$	form drag (due to flattening of the collision surface), N
$F_{D,form}^{Viscous}$	viscous form drag (due to viscous dissipation in the film), N
$F_{D,form}^{Pressure}$	pressure form drag (due to excess pressure in the film), N
F_{Drag}	drag force, N
$F_{friction}$	friction in the film draining process, N
f	thickness of liquid film, m

h	distance from geometric centre to interface, see fig 4.1, m
m	mass of fluid particle, kg
n_0	parameter in friction force term, -
P	pressure, Pa
P_0	pressure in the center of the film, Pa
P_r	pressure at the outer rim of the film, Pa
R	radius for fluid particle, m
r	radius of collision interface, m
shift	fig 4.1, distance between mass and geometric centres, m
T_{zz}	total normal stress tensor, Pa
t	time, s
u_r	radial velocity of fluid particle, m/s
u_z	axial velocity of fluid particle, m/s
V	volume, m^3
z	distance between mass centres, m
α	amplitude of drop oscillation, -
β	parameter for excess pressure in film, -
γ	added mass coefficient, -
δ	damping factor for oscillations, -
θ	phase angle at first contact, degrees
μ	viscosity, $Pa \cdot s$
ρ	density, kg/m^3
σ	surface tension, N/m

ω	frequency, rad/s

Subscripts:

c	continuous phase
d	dispersed phase
s	spherical shape
0	initial state / start of integration
1, 2	fluid particle 1, 2

References

Chesters, A.K. (1991). The modelling of coalescence processes in fluid-fluid dispersions: a review of current understanding. *Trans IchemE* **69**, 259-270.

Clift, R., Grace, J.R. & Weber, M.E. (1978). Bubbles, drops, and particles. Academic Press, Inc., San Diego, USA, 112.

Colin, C., Kamp, A.M. & Chesters, A.K. (1998). Measurement and prediction of bubble coalescence in turbulent pipe flows. Third International Conference on Multiphase Flows, ICMF98.

Cook, T.L. & Harlow, F.W. (1986). Vortices in bubble two phase flow. *Int. J. Multiphase Flow* **12**, 35-61.

Hagesaether, L., Luo, H. & Svendsen, H.F. (1996). The modelling of coalescence of oscillating liquid drops. *CHISA'96* Ref. No. 0383.

Hartland, S. (1969). The effect of circulation patterns on the drainage of the film between a liquid drop and a deformable liquid-liquid interface. *Chemical Engineering Science* **24**, 611-613.

Hartland, S. & Robinson, J.D. (1977). A model for an axisymmetric dimpled draining film. *Journal of Colloid and Interface Science* **60**, 72-81.

Ivanov, I.B. (1988). Thin liquid films fundamentals and applications. Marcel Dekker, Inc., New York, USA, 391.

Jeelani, S.A.K. & Hartland, S. (1991a). Collision of Oscillating Liquid Drops. *Chemical Engineering Science* **46**, 1807-1814.

Jeelani, S.A.K. & Hartland, S. (1991b). Effect of approach velocity on binary and interfacial coalescence. *Trans IchemE* **69**, 271-281.

Kirkpatrick, R.D. & Lockett, M.J. (1974). The influence of approach velocity on bubble coalescence. *Chemical Engineering Science* **29**, 2363-2373.

Klaseboer E., Chevaillier J.Ph., Masbernat O. & Gourdon C. (1998). Drainage of the liquid film between drops colliding at constant approach velocity. Third International Conference on Multiphase Flows, *ICMF98*.

Lee, J.C. & Hodgson, T.D. (1968). Film flow and coalescence - I. Basic relations, film shape and criteria for interface mobility. *Chemical Engineering Science* **23**, 1375-1397.

Luo, H & Svendsen, H.F. (1996). Modeling and simulation of binary approach by energy conservation analysis. *Chem. Eng. Comm* **145**, 145-153.

Middleman, S. (1998). An introduction to fluid dynamics. John Wiley & Sons, Inc., New York, USA, 339.

Montes, F.J., Galan, M.A. & Cerro, R.L. (1998). Mass transfer from oscillating bubbles in bioreactors. *ISCRE 15*, Reference 17-A.

Mørk, P.C. (1991). Overflate og kolliodkjemi. Institutt for industriell kjemi NTH, Trondheim, Norway, 47.

Princen, H.M. (1963). Shape of a fluid drop at a liquid-liquid interface. *Journal of Colloid Science* **18**, 178-195.

Scheele, G.F. & Leng, D.E. (1971). An experimental study of factors which promote coalescence of two colliding drops in suspended water - I. *Chemical Engineering Science* **26**, 1867-1879.

Svendsen, H.F. & Luo, H. (1996). Modeling of approach processes for equal or unequal sized fluid particles. *The Canadian Journal of Chemical Engineering* **74**, 1-10.

Tsao, H.-T. & Koch, D.L. (1997). Observations of high Reynolds number bubbles interacting with a rigid wall. *Phys. Fluids* **9**, 44.

CHAPTER 5

Fluid particle break-up

This chapter is a based on the paper 'A model for turbulent binary breakup of dispersed fluid particles' by Hagesaether, Jakobsen & Svendsen, accepted for puplication in Chem. Eng. Sci. A model for fluid particle break-up is developed.

5.1 Introduction

Luo & Svendsen (1996) developed a model for fluid particle break-up based on principles of molecular collision, isotropic turbulence and probability. Unlike earlier work this bubble breakage rate model contained no adjustable parameters and all constants were calculated from isotropic theory. The daughter size distribution was derived directly from the breakage rate model.

The current model is a further development of an existing model by Luo & Svendsen (1996), which has been expanded and refined, and where an inherent weakness regarding the break-up rate for small particles and small daughter particle fragments is removed. A new criterion regarding the kinetic energy density of the colliding turbulent eddy causing break-up has been introduced. This new criterion is a novel concept describing the break-up process. The details are thoroughly discussed together with possible further modifications. Based on a new view of the

breakage process a new model has been developed. This new model is consistent in the sense that when the model is used in a population balance model, a steady state distribution between the population classes should be reached, and that the overall dispersed fluid particle size distribution should be independent of the number and distribution of the size classes. This consistent model can be used both in CFD models and for simpler reactor models.

5.2 Review and discussion of existing break-up model

There are at least three possible breakage mechanisms for drops or bubbles in turbulent flow. These are turbulent (deformation) breakage, viscous shear (tearing) breakage and elongation flow breakage in accelerating flow. The model by Luo & Svendsen (1996) is concerned only with the turbulent breakage mechanism which is thought to be the prevailing one in turbulent flow as encountered in multiphase reactors. Viscous shear breakage on the other hand, is a laminar phenomena, and the elongation flow breakage occurs where the continuous flow is accelerated like in the vicinity of impellers, Alopaeus, Koskinen & Keskinen (1999). It is further assumed that the turbulent breakage is binary and the phenomenon is divided into the collision between an eddy and a fluid particle, and the break-up of the particle due to the colliding eddy. The break-up rate can then be written as the product of the collision frequency, ω_B, and a breakage probability, P_B,

$$\Omega_B = \omega_B P_B . \tag{5.1}$$

The following should be noted:

- This equation is an approximation since collisions resulting in break-up should be removed from the class after each event, keeping only particles from collisions that do not result in break-up available for further collisions. Thus, for population classes with decreasing number of particles, Ω_B will be larger than the real event frequency and vice versa. The same consideration also applies for coalescence.
- For the limit of one event the equation is correct.

- For the steady state case the equation is also correct since any particle removed from the class will be replaced with birth occurrences (both break-up and coalescence) from other classes, thus keeping the total amount in the class constant.

Further, equation (5.1) is based on the assumption that the collision frequency and the breakage probability are independent variables. This is a first order model approximation which is adequate when the integration time step is small as higher order terms become negligible. For further reading about stocastic processes, Gikhman & Skorokhod (1980) is recommended.

- Thus in transient cases equation (5.1) may be inaccurate. The error increases with higher relative number of collisions (collisions/particles) and with an increasing event probability as the accuracy reflected by birth and death terms obtained using this model are dependent on the step size choosen for the time integration.
- The error may be decreased by reducing the time step of integration.

The relative change in each class for each time step should thus be monitored, and if the change is considered high (say higher than 25%), the time step should be decreased in order to reduce the error.

5.2.1 The collision frequency

Laidler & Meiser (1982) describes the collision frequency between gas molecules. We can obtain a similar expression for the collision frequency between eddies of size between λ_j and $\lambda_j + d\lambda$ and bubbles (or droplets) of size d_i,

$$\omega_B(d_i, \lambda_j) = \frac{\pi}{4}(d_i + \lambda_j)^2 \bar{u}_{d_i, \lambda_j} n_{d_i} n_{\lambda_j}. \tag{5.2}$$

Here n_{λ_j} is the number of eddies of size class $\lambda_j + d\lambda$ per unit reactor volume, Luo & Svendsen (1996), and $\bar{u}_{d_i, \lambda_j}$ is the average relative velocity between the eddy and the fluid particle. Luo and Svendsen simplified the latter to $\bar{u}_{\lambda_j}$ which is only the turbulent velocity of the eddy. This simplification may not be justified in all cases and should be avoided as a first approach. Equation (5.2) is only a good approximation when the total change in n_{d_i} is not too large. Whereas in situations where this change is significant the time interval should be reduced. This chapter

deals primarily with the break-up probability and the distribution of daughter sizes from this probability. Thus, the collision frequency is not included in the results shown later in this chapter. Prince & Blanch (1990) used an identical formulation for the collision frequency, though they incorrectly used the sum of radiuses rather than the sum of diameters in the squared part of the equation.

The eddy number density is calculated in accordance with the formula given by Luo & Svendsen (1996). They applied a spectral representation of the turbulent energy, $E(k)$, within a wave number interval dk (given by the right hand side of equation (5.3)), combined with a mixed spectral/Lagrangian representation of eddies having the corresponding turbulent kinetic energy in the wave length/eddy size interval between λ_j and $\lambda_j + d\lambda$, in order to derive an expression for $\dot{n}_{\lambda_j}$ (which must be integrated in order to find n_{λ_j}),

$$\dot{n}_{\lambda_j}\rho_L\frac{\pi}{6}\lambda_j^3\frac{\bar{u}_{\lambda_j}^2}{2}d\lambda = E(k)\rho_L(1-\varepsilon_G)(-dk)\,, \tag{5.3}$$

$\left[\frac{1}{m^4}\right][m^3]\left[\frac{m}{s}\right]^2[m] = \left[\frac{m^3}{s^2}\right][\text{-}]\left[\frac{1}{m}\right]$ giving $\left[\frac{m^2}{s^2}\right] = \left[\frac{J}{kg}\right]$ (ρ_L cancels out).

Here $\bar{u}_{\lambda_j} = \beta^{1/2}(\varepsilon\lambda_j)^{1/3}$, $\beta = \frac{8\bar{\beta}}{3\pi}$, $E(k) = \alpha\varepsilon^{2/3}k^{-5/3}$, $k = 2\pi/\lambda_j$, $\alpha = 1.5$ and $\bar{\beta} = 2.41$.

Differentiating $k = 2\pi/\lambda_j$ gives $dk = \frac{-2\pi}{\lambda_j^2}d\lambda$, and inserting this gives

$$\dot{n}_{\lambda_j}\rho_L\frac{\pi}{6}\lambda_j^3\frac{\frac{8\bar{\beta}}{3\pi}\varepsilon^{2/3}\lambda_j^{2/3}}{2}d\lambda = \alpha\varepsilon^{2/3}\left(\frac{2\pi}{\lambda_j}\right)^{-5/3}\rho_L(1-\varepsilon_G)\left(\frac{2\pi}{\lambda_j^2}d\lambda\right). \tag{5.4}$$

Rearranging gives

$$\dot{n}_{\lambda_j}\frac{1}{9}\lambda_j^5\frac{\bar{\beta}}{\pi}\lambda_j^{2/3}d\lambda = \alpha\left(\frac{2\pi}{\lambda_j}\right)^{-5/3}(1-\varepsilon_G)d\lambda\,. \tag{5.5}$$

Dividing by $d\lambda$ on both sides and keeping only $\dot{n}_{\lambda_j}$ on the left hand side gives

$$\dot{n}_{\lambda_j} = \frac{9\pi\alpha\lambda_j^{5/3}(1-\varepsilon_G)}{\lambda_j^5\bar{\beta}\lambda_j^{2/3}(2\pi)^{5/3}} = \frac{9\alpha(1-\varepsilon_G)}{\lambda_j^4\bar{\beta}2^{5/3}\pi^{2/3}} = 0.8226(1-\varepsilon_G)/\lambda_j^4. \qquad (5.6)$$

Thus by using the energy spectrum and assuming isotropic turbulence the eddy density of the interval λ_j and $\lambda_j + d\lambda$ is described as

$$\dot{n}_{\lambda_j} = c_2(1-\varepsilon_G)/\lambda_j^4 \text{ where } c_2 \approx 0.8226. \qquad (5.7)$$

A plot of the eddy density function, see figure 5.1, illustrates how the number of eddies varies as a function of the eddy size, λ_j.

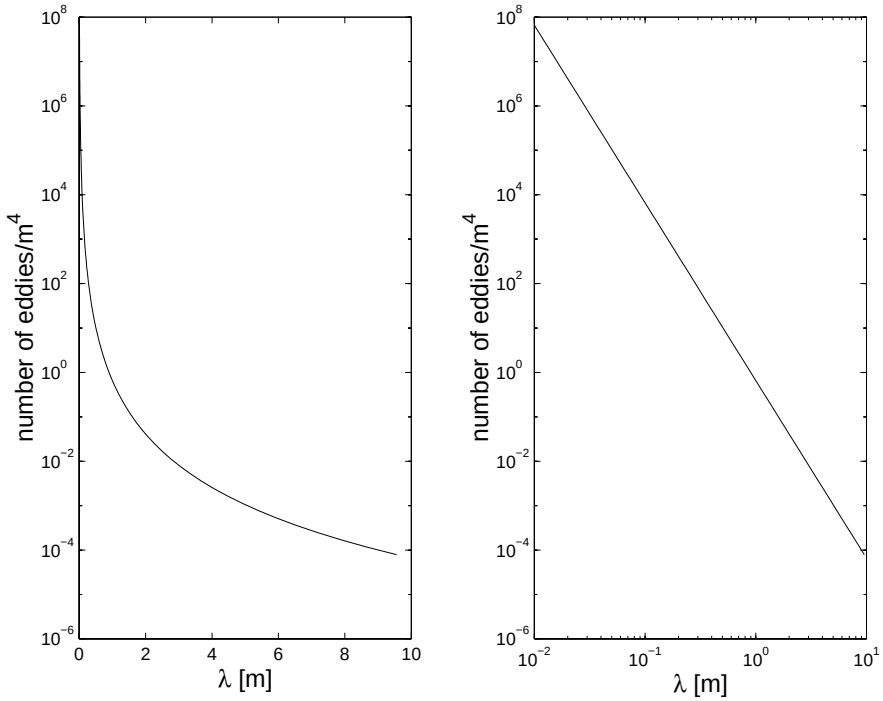

FIGURE 5.1: The number of eddies, see equation (5.7), is plotted as a function of eddy size λ. The left hand figure is log-y and the right hand figure is log-log. A 'random' interval is shown with $\varepsilon_G = 0.2$. The lower (Kolmogorov) limit for eddy size is not included.

As seen from equation (5.7) and from figure 5.1, the number of eddies approaches infinity as the eddy size goes to zero. It must further be noted that isotropic turbulence is assumed, thus limiting the size range. According to equation 1.5.11 in Tennekes & Lumley (1972), the Kolmogorov micro length scale, is given as

$$\eta = (\nu^3/\varepsilon)^{1/4}. \tag{5.8}$$

By using typical values for the air-water system we get

$$\eta = ((1\times10^{-3}/1000)^3/0.25)^{1/4} = 4.5\times10^{-5}\ [m],$$

where $\nu = \left(\frac{\mu_L}{\rho_L}\right)\ [m^2/s]$, $\mu_L = 1\times10^{-3}\ [Pa\cdot s]$ and $\rho_L = 1000\ [kg/m^3]$. A typical value for ε in a bubble column is used, $\varepsilon = 0.25\ [m^2/s^3]$.

5.2.2 The collision outcome

For a collision between an eddy and a fluid particle the outcome can either be break-up or no break-up. For the break-up cases the two daughter particles may have a variety of sizes. This section deals with the criterion for break-up and its relationship to the daughter sizes resulting from the collision.

The first assumption introduced is that the instability created by the collision between an eddy and a fluid particle has a duration much shorter than the time interval between collisions. Thus, the particle will either break up due to the collision or assume normal shape again, i.e. dissipate the previous collision energy, before a new collision takes place. So, in order to model the break-up of fluid particles we only have to model the collision between a single eddy and a fluid particle. Thus, the cases where the dispersed particles are hit by more than one eddy before the original shape is resumed are modelled as multiple separate instances. If the assumption is correct there should be a negligible fraction of such cases.

Risso & Fabre (1998) on the other hand found experimentally that some break-ups are due to series of eddy collisions where the accumulated energy finally result in break-up. They also found other break-ups which were clearly the result of a single eddy. So, only the fundamental case where all the energy from previous collisions are dissipated is modelled and simulated. A possible modification for introducing partial dissipation is discussed later.

The outcome of the collision is dependent upon the turbulent kinetic energy of the colliding eddy. The turbulent kinetic energy probability distribution was by Luo & Svendsen (1996) assumed to be

$$p_e(\chi) = \frac{1}{\bar{e}(\lambda_j)} \exp(-\chi) \text{ where } \chi = e(\lambda_j)/\bar{e}(\lambda_j). \tag{5.9}$$

The new model uses

$$p_e(\chi) = \exp(-\chi) \text{ where } \chi = e(\lambda_j)/\bar{e}(\lambda_j), \tag{5.10}$$

since this gives

$$\int_0^\infty p_e(\chi) d\chi = 1. \tag{5.11}$$

Also equation 15 in Angelidou, Psimopoulos & Jameson (1979), as used by Luo & Svendsen (1996), can be rearranged to equation (5.10).

The mean turbulent kinetic energy of an eddy with size λ_j, $\bar{e}(\lambda_j)$, for the inertial subrange was by Luo & Svendsen (1996) given as

$$\bar{e}(\lambda_j) = \rho_L \frac{\pi}{6} \lambda_j^3 \frac{\bar{u}_\lambda^2}{2} = \frac{\pi\beta}{12} \rho_L \varepsilon^{2/3} \lambda_j^{11/3}, \tag{5.12}$$

where $\beta = 2.05$ is a known constant. It is seen that the shape of the turbulent kinetic energy probability distribution, equation (5.10), is independent of λ_j, i.e. the mean energy is dependent upon λ_j, but the distribution around this mean is not.

It must be noted that $e(\lambda_j)$ is based on a spectral formulation, but it is applied in a Lagrangian interpretation. This leads to conceptual interpretation problems. As an eddy contains both translational and rotational velocity components, $\bar{u}_{\lambda_j}$ in equation (5.12) is then a vector, and the term may be interpreted as the turbulent kinetic energy of an eddy. When it comes to equation (5.2), $\bar{u}_{d_i, \lambda_j}$ is related to both the eddy and the particle velocities. The velocity of a fluid particle is defined by larger eddies in the system since these eddies are (mainly) responsible for the con-

vective movement of the particles. As the eddies are of all length scales we have used $\bar{u}_{\lambda_j}$, the velocity of eddies of the same size as the particles as an approximation of the velocity of the particles, Luo & Svendsen (1996).

A plot of the turbulent kinetic energy distribution around the mean kinetic energy is shown below in figure 5.2. The plot is normalized with the mean value.

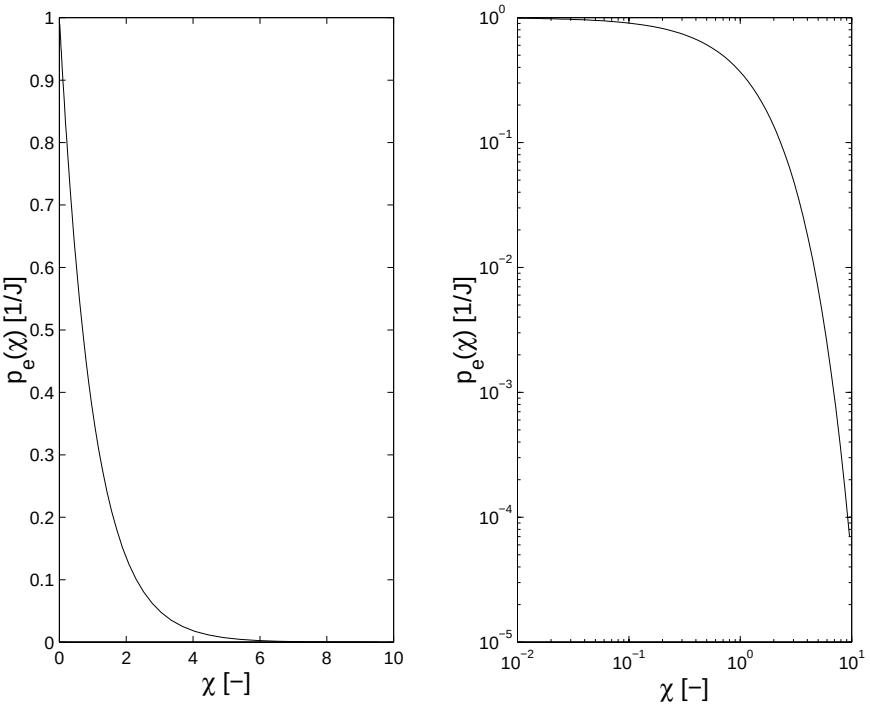

FIGURE 5.2: The turbulent kinetic energy distribution, equation (5.9), of a random eddy size is plotted around the mean turbulent kinetic energy of that size (mean value set to 1). The right hand plot is log-log.

The increase in surface energy due to a break-up can be written as, Luo & Svendsen (1996),

$$e_i(d_i, d_k) = 4\pi(d_j/2)^2\sigma + 4\pi(d_k/2)^2\sigma - 4\pi(d_i/2)^2\sigma \ ,$$

$$e_i(d_i, d_k) = \pi\sigma(d_j^2 + d_k^2 - d_i^2) \ , \qquad (5.13)$$

where d_i in $e_i(d_i, d_k)$ is the parent particle and d_k is the smallest daughter particle. In equation (5.13) it is assumed that the increase in surface energy is due to an increase in the surface area during break-up, see figure 5.3. It is thus assumed that the surface tension itself is not changed when the surface area changes. As a simplification any change in the internal pressure of the bubbles is disregarded. Assuming 1 bar bulk pressure this amounts to an error of about +0.04% in the daughter particles volume for an equal sized break-up of a bubble of radius 1mm. This error increases with decreasing parent bubble size (0.4% for a 0.1mm bubble) and is largest for equal sized breakage. Further, since volume is the radius cubed and surface area is the radius squared, the relative error for the surface area will be less than for the volume.

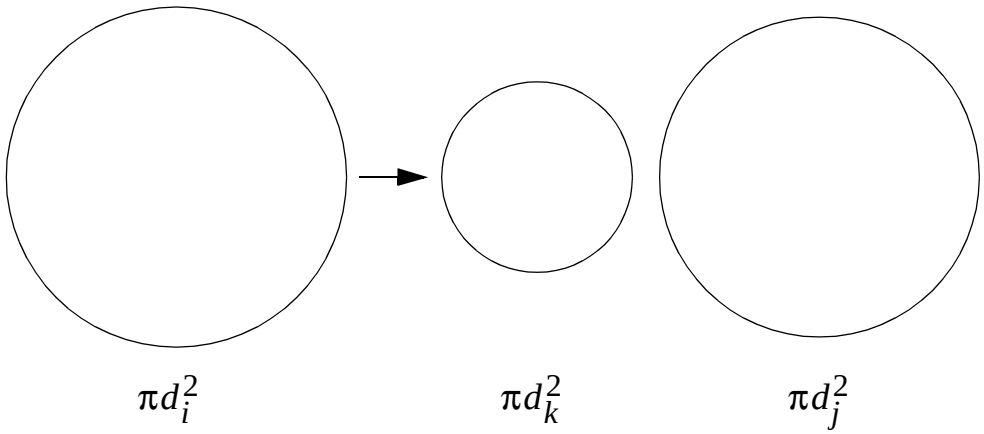

FIGURE 5.3: Break-up shown together with the surface area terms for parent and each daughter particle. Note that the smallest daughter particle is defined with subscript *k*.

By taking into account the volume balance and using the notation of Luo & Svendsen (1996) we get

$$f_{BV,k} = \frac{\upsilon_k}{\upsilon_i} = \frac{d_k^3}{d_i^3} = \frac{d_k^3}{d_j^3 + d_k^3}\ , \tag{5.14}$$

where $f_{BV,k}$ is the volume fraction of the first bubble, in our case the smallest one. The surface area change coefficient is written as

$$c_{f,k} = f_{BV,k}^{2/3} + (1 - f_{BV,k})^{2/3} - 1 \quad , \tag{5.15}$$

and signifies the fractional increase of the surface due to a break-up into two daughter particles. Thus, the change in surface energy may be written as,

$$e_i(d_i, d_k) = c_{f,k}\pi d_i^2\sigma \ . \tag{5.16}$$

By comparing equation (5.13) and equation (5.16) we see that

$$c_{f,k}d_i^2 = d_j^2 + d_k^2 - d_i^2 \ . \tag{5.17}$$

When using the volume balance $d_j^3 + d_k^3 = d_i^3$ we get

$$c_{f,k}d_i^2 = d_k^2 + (d_i^3 - d_k^3)^{2/3} - d_i^2 = [d_k^2/d_i^2 + (1 - d_k^3/d_i^3)^{2/3} - 1]d_i^2 \ . \tag{5.18}$$

By using equation (5.14) it can be seen that the term in brackets in equation (5.18) above equals the expression for $c_{f,k}$ in equation (5.15).

The criterion used by Luo & Svendsen (1996) for breakage of a particle was that when there is enough turbulent kinetic energy in the eddy for the surface increase of the fluid particle breakage is the result, i.e. the criterion was

$$e(\lambda_j) \geq e_i(d_i, d_k) = c_{f,k}\pi d_i^2\sigma \ . \tag{5.19}$$

This means that when an eddy has more turbulent kinetic energy than the increase in energy needed for a particular break-up, the fluid particle will break up into one of the possible fragmentations.

In order to examine equation (5.19) closer we start by plotting the function $e_i(d_i, d_k)$, see figure 5.4. The function is only plotted to about $0.79d_i$, which corresponds to half the volume of the parent particle. For each particle below or equal to half the volume of the parent particle there will be a corresponding particle that accounts for the rest of the parent particle volume. This daughter particle is placed above or at the half volume position, thus the plot is symmetric around half the volume when volume is used as the x-axis. In figure 5.4 we see that if the turbulent kinetic energy, $e(\lambda_j)$, is high enough (upper horizontal line in figure 5.4) the particle can break up into all possible daughter sizes since the curved line representing the increase in surface energy is below the horizontal line which represents this tur-

bulent kinetic energy. This gives $e(\lambda_j) > e_i(d_i, d_k) \rightarrow breakup$ for all possible values of d_k.

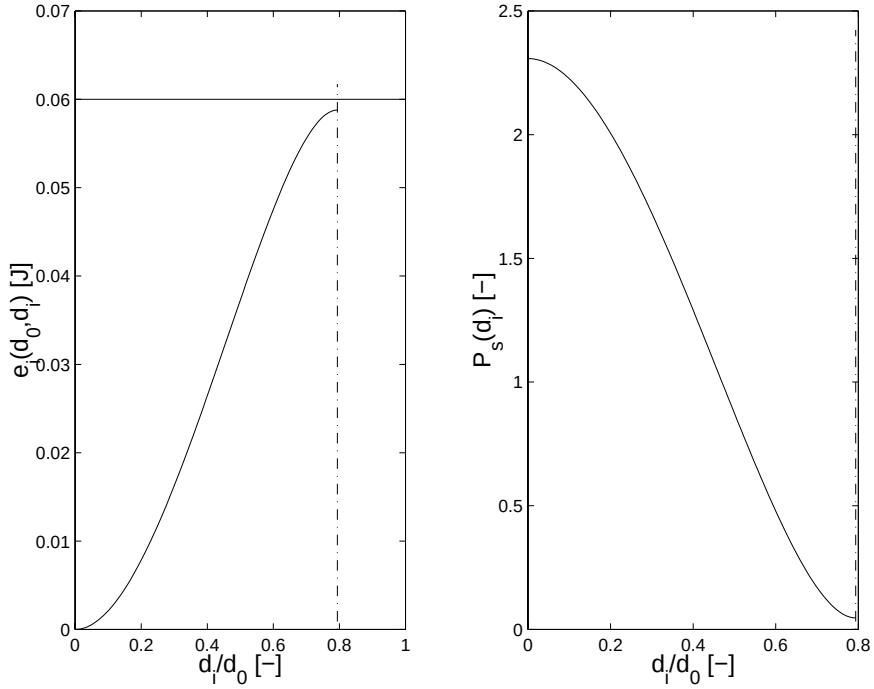

FIGURE 5.4: The left hand figure shows the surface energy, the horizontal line is a randomly choosen value for $e(\lambda_j)$. The right hand figure shows the normalized function (described later in section 5.3.1). The x-axis in both figures is the relative diameter size (daughter diameter divided by parent diameter).

Figure 5.5 below shows an example for a case where $e(\lambda_j) = e_i(d_i, d_k) = 0.04$ $[J]$ limits the range of possible break-up fractions.

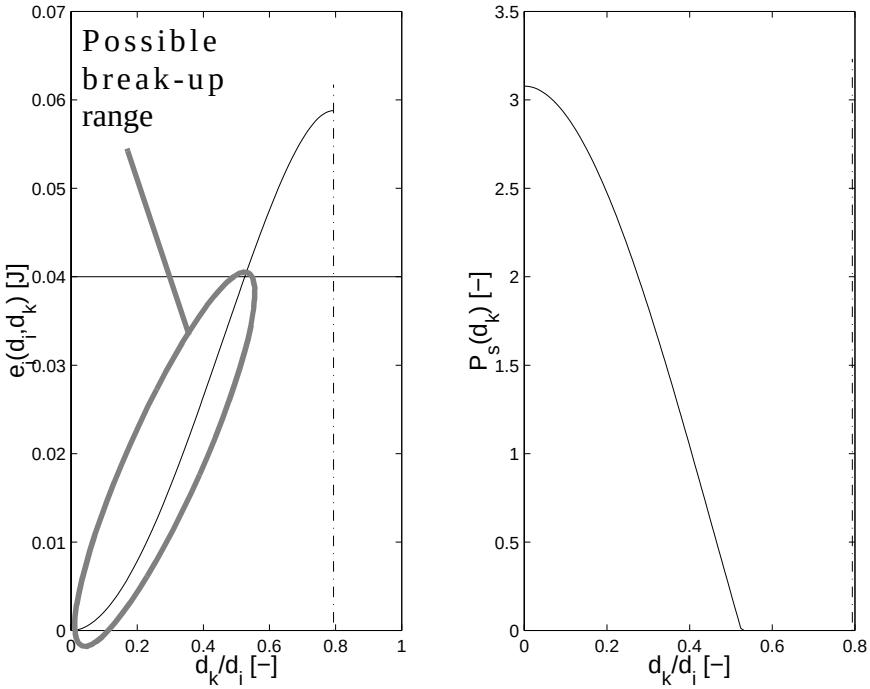

FIGURE 5.5: The left hand figure shows the surface energy with a horizontal line at a randomly chosen value for $e(\lambda_j)$. The daughter sizes that can be created by the value are encircled. The right hand figure shows the normalized function for the encircled part of the left hand figure (described later by eq (5.20) in section 5.3.2). The x-axis in both figures is the relative daughter diameter size (daughter diameter divided by parent diameter).

From figure 5.4 and figure 5.5 it is seen that there will always be a daughter size distribution that requires less energy than what is available in the incoming eddy since the surface energy goes to zero when the smallest daughter particle diameter approaches zero. This means that according to the theory by Luo & Svendsen (1996), all particles will break up when hit by an eddy. With less energy in the eddy we get a more uneven split of the original particle. This is because it is not possible to break up the particles into the most even distributions, see figure 5.5 where sizes larger than the range encircled are not allowed. Taking into account the eddy distribution with an 'infinite' number of small eddies shown in figure 5.1, combined

with figures 5.4 and 5.5 showing that all collisions result in break-up, it can be seen that the model results in an unreasonable high amount in break-up. This is clearly not correct. In practical terms a too large number of break-ups by using this theory would be expected and also the size and number of particle classes would define the break-up rate and resulting size distribution. If smaller classes are added to a case, no matter how small these classes are, particles will occur in these classes and the total break-up rate will increase. Thus there is an inherent inconsistency. In order to remedy this problem a new break-up criterion, the energy density criterion, has been added to the surface energy criterion. This latter criterion has also been modified in the sense that a probability distribution for the daughter fragment classes has been added.

5.3 The modified model

The modified model must both limit break-up downward in size for daughter particles and limit the break-up frequency for the smallest particles. A new criterion is introduced, resulting in such limitations. In order to find the daughter size distribution the existing surface energy criterion is extended. A normalized function has been proposed which together with a similar function for the new criterion gives the daughter size distribution.

5.3.1 The surface energy probability

Figure 5.6 below depicts the two extreme cases of energy utilization when an eddy collides with a fluid particle. The eddy is in this figure shown as concentric circles representing the shear of the eddy towards the surrounding continuous fluid. The turbulence energy can be described by the energy spectrum concept too, thus an eddy can be interpreted in more ways. See for example Alvarez, Alvarez & Hernandez (1994), figure 2, for an alternative interpretation. The maximum energy utilization takes place when the breakage results in two equal-sized particles. This absorbs the most energy due to the highest increase in surface energy, see figure 5.4. Further, this breakage is an extreme case since we assume that exactly all the turbulent kinetic energy of the colliding eddy is used. As shown in figure 5.6, no energy is left for motion of the resulting particles or for a remaining portion of the eddy (which means the eddy dies out). Naturally, this case is not very likely, but we do need a probability distribution for this and other cases which will be addressed below. Note further that an eddy may of course also

have more energy available than what is needed for an equal sized break-up. Such a case is not shown in figure 5.6. The bottom case is the other extreme. It shows a break-up where a very small fluid particle is generated together with a particle of almost the original volume. In addition, the rest of the turbulent kinetic energy of the eddy may be transferred to kinetic motion of the daughter particles, oscillations of the daughter particles (not shown in figure 5.6), and/or it may remain with the eddy. The eddy is in this case depicted as the original eddy, but with a smaller 'kinetic' vector. What happens to this 'drained' eddy after the collision is not important for the particle break-up framework. Further, it is assumed that fluid particles dissipate all collision energy between collisions with an eddy, any transfer of energy to the daughter particles will not be of consequence in future collisions. Note that this is a simplification, see Risso & Fabre (1998).

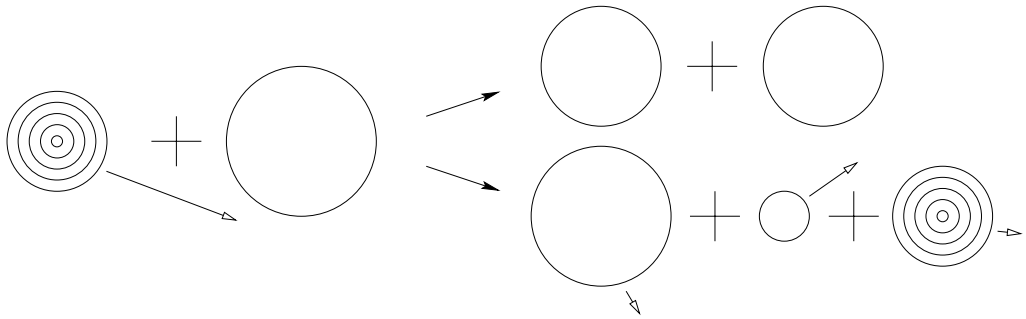

FIGURE 5.6: An eddy colliding with a fluid particle may result in a collision that takes up all the turbulent kinetic energy of the eddy (top right), or surplus energy may leave with the daughter particles and the used eddy (bottom right). The eddy is here drawn by concentric circles which represent the rotational part of the eddy.

We assume that the probability function for break-up due to turbulent kinetic energy in an eddy may be written as a normalized function

$$P_s(d_i, d_k) = \frac{e(\lambda_j) - e_i(d_i, d_k)}{\int_o^{d_{k,max}} (e(\lambda_j) - e_i(d_i, d_k))d(d_k)}, \qquad (5.20)$$

where $d_{k,max}$ is the minimum of the crossover value ($e(\lambda_j) = e_i(d_i, d_k)$), if it exists (see figure 5.5), and if not (see figure 5.4), then the diameter of half the total

volume (approximately $0.79 d_i$). By normalized it is meant that integrating over all possible sizes gives unity. Equation (5.20) is shown in figure 5.4 and in figure 5.5, in the right hand plots, for two 'random' cases. As can be seen from equation (5.20), a break-up that utilizes all the available energy, has a zero probability. The probability increases with the amount of energy not used in the break-up process. This in itself is enough to create a break-up source term in a population balance, but the consistency problem is still not addressed.

5.3.2 The energy density probability

From a physical point of view it makes sense that a particle is split if enough energy is applied. Since this alone is not a sufficient criterion, we need one which takes into account that there is a physical lower limit to the particle size being broken up. As an introduction, Kolmogorov (1949), Hinze (1955) and Bourne & Baldyga (1994) report that the maximum stable fluid particle size can be assumed to be in order of

$$d_{max} \sim O(\sigma^{0.6}\varepsilon^{-0.4}\rho^{-0.6}) . \tag{5.21}$$

Equation (5.21) above is found by balancing the interfacial tension (σ / d_{max}) against the dispersive stress due to inertial, fluctuating motion in the continuous phase, which is given by $\rho\overline{u^2}$. This balance is often expressed as the Weber number

$$We_c = \frac{\rho\overline{u^2} d_{max}}{\sigma} . \tag{5.22}$$

Two assumptions are used, Bourne & Baldyga (1994):

- The viscosity of the dispersed phase is so small that particle deformation is ineffective in opposing dispersion (typically in bubbles).
- The particle size falls in the inertial subrange so that the dispersive stress is inertial and not viscous.

The mean square velocity difference over the maximum particle diameter (d_{max}) is given as, Batchelor (1951)

$$\overline{u^2} \sim (\varepsilon d_{max})^{2/3} . \tag{5.23}$$

Equation (5.21) is thus found by a force balance for the particle. Our idea may be seen as a similarity to the force balance approach, but based on an energy approach. The first criterion involved the total energy available in the eddy and the energy needed for break-up. The second criterion involves the energy density of the colliding eddy and the energy density of the resulting particle fragments. An analogy regarding temperature can be sketched: there is more energy in 100 kg of water at 60 degrees Celsius than in 1 kg of water at 80 degrees, but the water at 60 degrees may not be used to increase the temperature of any amount of water with an initial temperature of 70 degrees as opposed to the 1 kg at 80 degrees.

Thus we arrive at a second criterion:

- The energy density of an eddy must be higher or equal to the energy density of the daughter particles resulting from the break-up.

We thus assume that the energy density in the collision framework can not be increased. The outcome of the collision between an eddy and a fluid particle can only be daughter fragments with the same or lower energy density than the eddy.

The energy density of a particle is here defined as the surface energy divided by the volume of the particle, i.e. the surface energy density, $w_s(d_k)$, for the smallest particle

$$w_s(d_k) = \frac{4\pi(d_k/2)^2\sigma}{\frac{4}{3}\pi(d_k/2)^3} = 6\sigma/d_k \left[\frac{J}{m^3}\right]. \tag{5.24}$$

Similarly we find an analogue eddy energy density, $w_d(\lambda_j)$, to be

$$w_d(\lambda_j) = \frac{e(\lambda_j)}{\frac{4}{3}\pi(\lambda_j/2)^3} \left[\frac{J}{m^3}\right]. \tag{5.25}$$

Here $e(\lambda_j)$ is the turbulent kinetic energy and it must be determined by using the probability function found in equation (5.10). It is seen from equation (5.24) that the smallest daughter particle will have the highest surface energy density. Since the surface energy density is inversely proportional to the diameter of the particle, some lower limit for the size of the daughter particle will exist for each possible break-up case. This lower limit can be found by equating the surface energy density of the smallest daughter particle with the eddy energy density of the colliding eddy,

$$w_s(d_k) = w_d(\lambda_j) \Rightarrow d_{k,\,min} = \sigma\pi\lambda_j^3 / e(\lambda_j) \; . \tag{5.26}$$

- $d_{k,\,min}$ is the lower possible limit. As seen in the results, figures 5.13 to 5.16, we get a distribution of daughter sizes. The average size of the smaller daughter particles may be much larger than any $d_{k,\,min}$ found. Note that $d_{k,\,min}$ is a function of both the eddy size, λ_j, and the turbulent kinetic energy of the eddy, $e(\lambda_j)$.
- d_{max} is defined as the largest stable particle size which means that we should get less break-up of particles smaller than d_{max}. Note though that d_{max} is an approximate value, since We_c varies over an order of magnitude, depending on the flow pattern and structure, Parthasarathy, Jameson & Ahmed (1991).

Thus we can not assume that we will get negligible break-up of particles less than d_{max}, but we should get markedly less break-up of particles smaller than the magnitude set by d_{max}.

An important point is the basis used in equation (5.24) and equation (5.25) for calculating $w_s(d_k)$ and $w_d(\lambda_j)$. We have used a volume basis $[J/m^3]$, whereas another possibility would be to use a mass basis, thus getting $[J/kg]$.

It is easily seen that $w_s(d_k)$ will be much higher for bubbles than for droplets when using a mass basis, to be exact a factor ρ_L/ρ_G higher. Using a mass basis will therefore make it unreasonably much harder to break up bubbles. This large difference will be reduced if one introduced virtual mass when using mass basis.

Looking at the physical system, it may be argued that the energy (or force) supplied to a bubble will to a larger extent move the bubble than a similar energy (or force) would move a droplet. This should make it less likely that the bubble will break up. The argument is flawed since in order to transpose any fluid particle you need to move the continuous fluid occupying its travelling direction, which is the same in both cases. Further, a collision in a turbulent environment is assumed to be on a short time scale, which means that the fluid particle will not be able to move away from the eddy, i.e. the energy will not be used to move the particles in any of the cases above.

A visual analogy will be balloons filled with water or air kept under water. If you hit such balloons quickly, none of them will be able to move much before the collision is over. They will just change shape, or burst, during the collision itself.

Another and probably more important factor is the compressibility of the gas phase. Clearly, a bubble will be better able to withstand break-up due to absorption of eddy energy into potential energy as a compressed state. Thus more of the colliding eddy energy will be available for breaking up the droplet than for breaking up a dimensionally equal bubble. A compressibility factor is not included, which means that the break-up rates we get for bubbles will probably be somewhat high. We have currently not tried to estimate this inherent error, so the simulated values should be looked upon as maximum values. For the droplets on the other hand, the model is more accurate.

Figure 5.7 below shows the particle energy density as a function of the smallest daughter particle size. An arbitrary eddy energy density is shown as the horizontal line in the plot. The left vertical dash-dotted line shows the corresponding minimum daughter particle size, which is found by equating $w_s(d_k)$ to $w_d(\lambda_j)$, equation (5.26). Since the smallest daughter particle has the highest surface energy density only the smallest particle distribution is plotted in the figure, thus the maximum value of the diameter is approximately $0.79d_i$ (half the volume of the parent particle), this value is also dash-dotted.

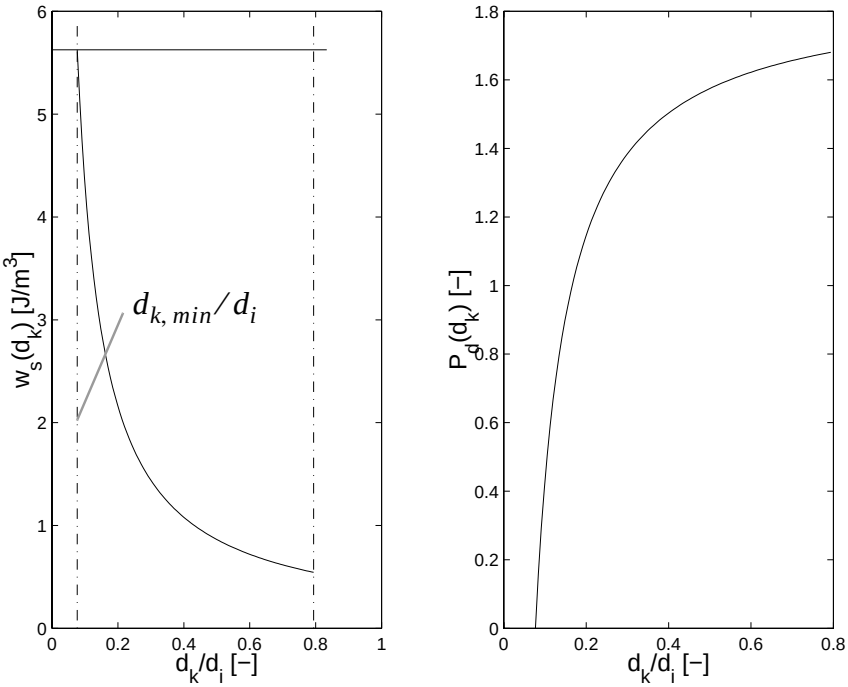

FIGURE 5.7: The left hand figure shows $w_s(d_k)$, equation (5.24), as a function of d_k/d_i (daughter diameter relative to parent diameter). The horizontal line is the arbitrarily choosen $w_d(\lambda_j)$ value, and the left dash-dotted line is the lower critical value for the breakage, $d_{k,min}$. The right hand figure shows the normalized probability function as described by equation (5.27).

The eddy energy density probability function is assumed to be given by a function similar to the surface energy probability, equation (5.20), and is for the smallest daughter particle

$$P_d(d_k) = \frac{w_d(\lambda_j) - 6\sigma/d_k}{\int_{d_{k,min}}^{d_{k,max}} (w_d(\lambda_j) - 6\sigma/d_k)d(d_k)}, \qquad (5.27)$$

where $d_{k,\,max}$ is normally the maximum possible smaller daughter particle size ($\sim 0.79 d_i$). When both criteria are considered together though $0.79 d_i$ may be larger than the possible break-up size. In these cases the maximum possible break-up size should be used, see equation (5.20) and figure 5.5. A zero probability is assigned to the energy density probability function, in the case where the requirements exactly match. The right hand side of figure 5.7 shows an example of the probability function.

As can be seen from figure 5.7 a lower limit for the smallest daughter particle size is established. If this limit is larger than approximately $0.79 d_i$, the parent particle itself can not break up in the current eddy collision. Thus the new model now satisfies both requirements stated initially in section 5.3, which were that there is a minimum size to the smaller daughter particle and that the break-up frequency is limited for small parent particles. This means the breakage model is consistent when equation (5.27) is included in the overall break-up probability, P_B, in equation (5.1).

5.4 Total break-up probability

By combining the surface energy criterion with the energy density criterion, a total probability distribution for the breakage of the parent particle can be established. In this function the probability functions for both separate criteria are combined, which implicitly assumes that the two probability functions are uncorrelated (are independent of each other),

$$P_B = P_s \cdot P_d . \tag{5.28}$$

According to the theory presented in the previous sections there are two criteria limiting the number of break-ups, those and a third criterion normally used Luo & Svendsen (1996), are listed below:

- $d_{k,\,min} \leq d_{i-1}$, this is a reformulation of the energy density criterion, for a particle of class *i* breaking up. The energy density of the eddy must be higher than that of the smallest daughter particle which in turn is at max of same size as the class below. $d_{k,\,min}$ is the minimum size of the smallest daughter particle, equation (5.26), and the size of the class below is d_{i-1}.

- $e_i(d_i, d_{i,\,max}) \leq e(\lambda_j)$, this is the surface energy criterion. The increase in surface area due to break-up can not consume more energy than what is available in the eddy.
- The length scale of the eddy must be comparable to the length scale of the fluid particle. By this we assume that the eddy may at most be of the same order of magnitude as the fluid particle.

According to Luo & Svendsen (1996) and Lee, Erickson & Glasgow (1987) only eddies which have a length scale comparable to the bubble (or droplet) diameter can cause break-up. This criterion is here removed. The assumption was that eddies of a larger scale will just give the fluid particle a translational velocity whereas eddies of similar scale may break up fluid particles. This criterion has been removed in this work. We consider eddies as sub volumes of the continuous fluid that have both rotational and translational motion. When a fluid particle is hit by an eddy it is subjected to a velocity vector gradient (both translational and rotational velocity), see figure 5.8.

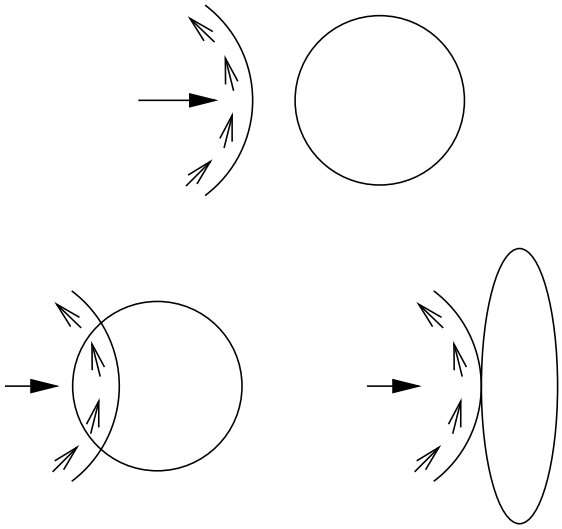

FIGURE 5.8: The upper figure shows an eddy having both rotational and translational velocity about to hit a fluid particle. The lower left figure shows a fluid particle immersed in an eddy, thus experiencing normal and tangential stresses on its surface which may result in break-up. The lower right figure is another possible view of what may happen when they collide. Here we see that the fluid particle is elongated due to the collision with an eddy, which may result in break-up.

As already mentioned, in order for the particle to break up only two properties of the colliding eddy are considered important; the density of the turbulent kinetic energy, $w_d(\lambda_j)$, and the turbulent kinetic energy itself, $e(\lambda_j)$. The density may be visualized as a velocity gradient in and between the eddy and the surrounding bulk phase. Thus a particle will be subjected to this gradient when colliding with an eddy. The length scale of the eddy, will then only affect the break-up indirectly by influencing both the turbulent kinetic energy and the energy density.

To find the number of break-ups, the break-up probability, P_B, must be determined by using both the surface energy and the energy density criteria. Several different situations may occur, as illustrated in figures 5.9 to 5.12. We define a critical energy density (CED), which is the energy density required to break a particle in two equal sized daughter particles. The critical energy level for the energy density criterion may be found by rearranging eq (5.26) to

$$e(\lambda_j)_{CED} = \sigma\pi\lambda_j^3 / d_{k,\,min,\,c}\,, \tag{5.29}$$

where $d_{k,\,min,\,c}$ is the highest possible value for $d_{k,\,min}$ which is for equal sized break-up. This is the lowest energy level that a specific eddy can have if it is to break a given particle. In figure 5.9 the surface energy criterion is given as the solid curve from 0 to 1. The maximum value for equal sized break-up is shown. Now, the critical energy density may be illustrated as the horizontal line given. The ordinate axis is strictly energy, but for a given eddy, with given size, there is a one to one relationship between energy level and energy density. In figure 5.9 the CED lies above the whole surface energy level curve such that if an eddy has an energy level at or above CED, it will also satisfy the surface energy criterion. Thus a breakage will occur if $e(\lambda_j) \geq e(\lambda_j)_{CED}$, and only the energy density criterion affects the break-up probability.

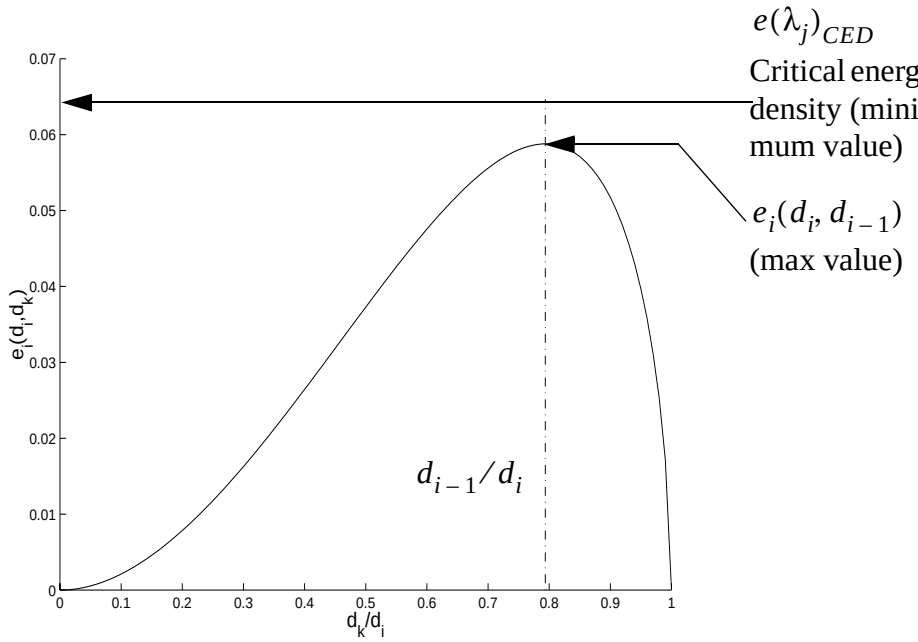

FIGURE 5.9: An example where the maximum value for the surface energy is below the minimum value for the critical energy density (CED) resulting in break-up for all energies that satisfy the energy density criterion.

Figure 5.10 is an example where the CED value is below $e_i(d_i, d_{i-1})$ which is the increase in surface energy needed in order to get two equal sized particles. At an energy level corresponding to the CED the surface energy criterion is not fulfilled. There is not enough turbulent kinetic energy in the eddy for the particle to break up. An increase in the eddy energy, to e.g. $e(\lambda_j)$, is in the figure the same as an upward vertical shift from the horizontal line marked as CED. This increase results in a lower minimum energy density diameter, $d_{k,\,min}$, see eq (5.26), as indicated by a dashed vertical line in the figure. At this energy level the surface energy criterion can at most give a smaller daughter fragment of relative size about 0.33. This position is encircled. However, the energy density criterion demands that the daughter particle must be above $d_{k,\,min}$, and since $d_{k,\,min} > 0.33 d_i$, the two criteria can not be fulfilled simultaneously, giving no break-up of the fluid particle. The range of daughter particle sizes that satisfies the surface energy criterion is shown in the figure as A, and that satisfying the energy density criterion is shown as B.

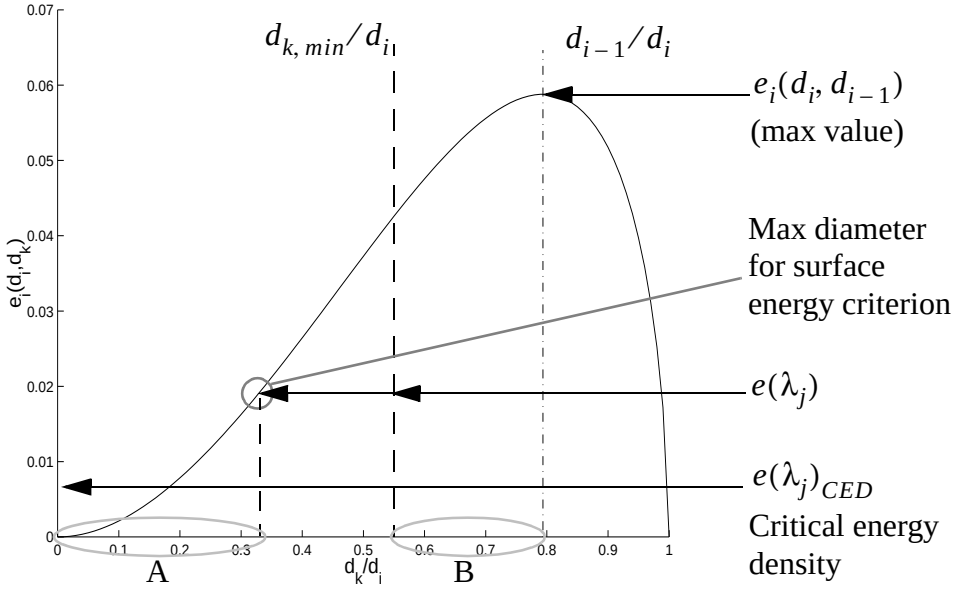

FIGURE 5.10: An example where the turbulent kinetic energy level is above the critical value for the energy density, giving a lower $d_{k,min}$ value (dashed line). At the current energy level the surface energy criterion gives at most a particle of size shown in circle. Both criteria are not both satisfied at the current $e(\lambda_j)$ level for any daughter particle sizes, giving no break-up.

As the energy level $e(\lambda_j)$ increases, the range of fulfilled surface energy criterion, A, increases. At the same time $d_{k,min}$ decreases, i.e. range B increases. Figure (5.11) shows a situation where both criteria are satisfied. At some point the $e(\lambda_j)$ line and the $d_{k,min}$ dashed line will intersect on the curved line for the increase in surface energy. This point may be called the critical break-up point, CBP. This is the minimum energy level for break-up to take place, and it is somewhere between the CED and the maximum surface energy value. Mathematically this point may be found in the following way

$$e(\lambda_j)_{CBP} = e_i(d_i, d_{k,min}) , \tag{5.30}$$

where $e_i(d_i, d_{k,min})$ is found from eq (5.13) by replacing d_k with $d_{k,min}$, and solving numerically for $d_{k,min}$. Thus at the current energy level $e(\lambda_j)_{CBP}$ we get break-up, but only into one specific daughter size fragmentation as that is the only fragmentation that satisfy both the energy density criterion and the surface energy criterion. A smaller daughter size is not allowed by the energy density criterion and a larger daughter size is not allowed by the surface energy criterion.

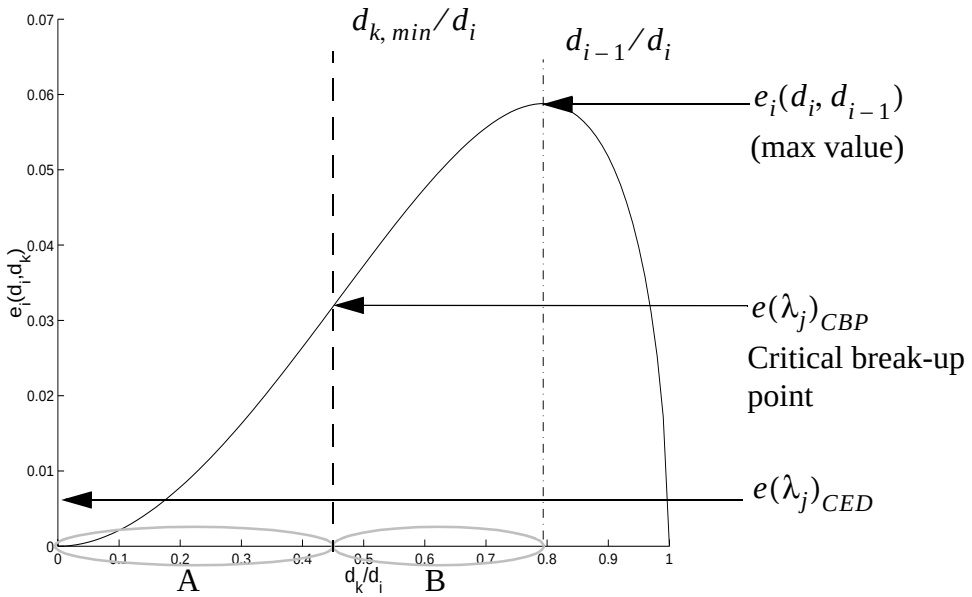

FIGURE 5.11: The critical break-up point (CBP) is found graphically at the intersection between the minimum break-up size, $d_{k,min}$, and the increase in surface energy.

A further increase in the eddy energy level, $e(\lambda_j)$, will result in a wider range of possible break-up sizes. Figure 5.12 shows that an increase in the eddy energy level results in a lower $d_{k,min}$ value and a higher possible value for the surface energy criterion. Thus an overlap between range A and B exists were both criteria are satisfied. The eddy with this specific energy level can result in a specific range of daughter particles, and this range, as seen, does not include equal sized break-up.

Increasing the eddy energy level further will eventually result in the situation shown in figure 5.9 where only the energy density criterion is limiting.

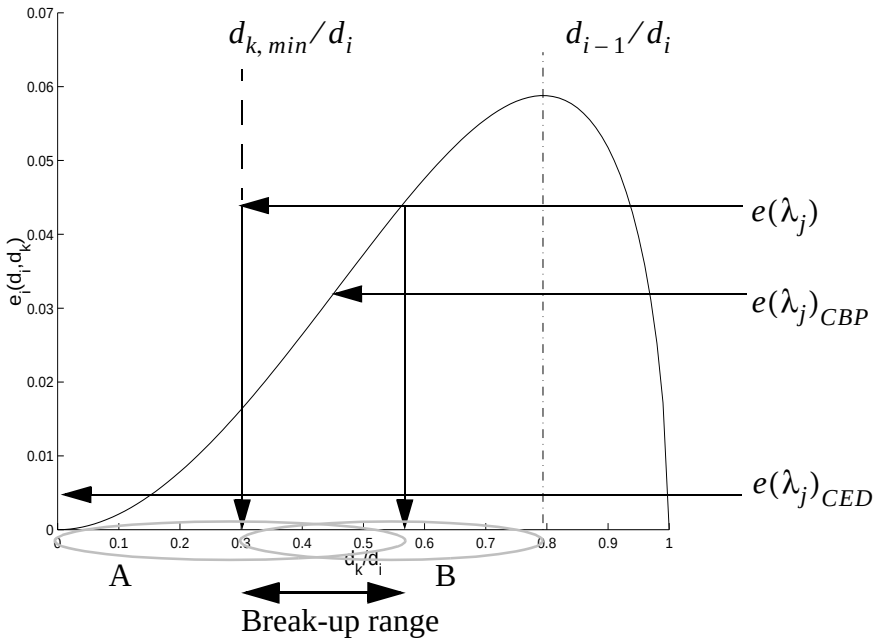

FIGURE 5.12: An eddy energy level above the CBP results in a range of possible break-up sizes. Further increase in the eddy energy level will eventually lead to only the energy density criterion being limiting.

We have now developed a method for deducing $d_{k,min}$ and $e(\lambda_j)_{CBP}$ for each collision. By using eq (5.10) we find $\chi_c = e(\lambda_j)_{CBP}/\bar{e}(\lambda_j)$, which is the critical point for the turbulent kinetic energy probability distribution since $\chi > \chi_c$ results in break-up. By integrating eq (5.10) from χ_c to ∞ we then find the fraction of collisions resulting in break-up,

$$P_B = \int_{\chi_c}^{\infty} \exp(-\chi) d\chi = \exp(-\chi_c). \qquad (5.31)$$

Finally, by using equation (5.1) the number of break-ups is found.

5.5 Daughter size distribution

In this section the daughter size distribution for the parent particle d_i will be developed. So far we have not defined P_B with indexes. We use $P_B(d_i, \lambda_j, e_l, d_k)$ which represent the probability of a particle of size d_i, colliding with eddies of size λ_j, with energy level e_l, breaking up into the smallest daughter fraction d_k.

In order to find the probability of one specific daughter class with given parent particle size and eddy size we sum over the energy levels,

$$P_B(d_i, \lambda_j, d_k) = \sum_l P_B(d_i, \lambda_j, e_l, d_k)\omega(\lambda_j, e_l), \tag{5.32}$$

where $\omega(\lambda_j, e_l)$ is the fraction of eddies of size λ_j having energy level e_l. The sum of these fractions is equal to

$$\sum_l \omega(\lambda_j, e_l) \cong \int_{\chi_c}^{\infty} \exp(-\chi)d\chi = P_B(d_i, \lambda_j). \tag{5.33}$$

This is the break-up fraction found in the previous section. In addition the probability distribution for the daughter classes has been normalized, giving

$$\sum_k P_B(d_i, \lambda_j, e_l, d_k) = 1. \tag{5.34}$$

In the transport equation the population balance source term $\Omega_B(d_i, d_k)$ is needed. We find this by summing up the eddy contributions,

$$\Omega_B(d_i, d_k) = \sum_j P_B(d_i, \lambda_j, d_k)\omega_B(d_i, \lambda_j). \tag{5.35}$$

The above theory is based on the assumption that a large enough number of break-up collisions occur justifying the usage of an averaging method. If the number of break-up collisions is low (without quantifying 'low') another method may be used. This method is described briefly below in a step by step manner.

For each break-up collision do the following:

- Use a Monte Carlo method, Das (1996) and Ramkrishna (1981), to pick the number of collisions resulting in break-up.
- Use a Monte Carlo method to pick an energy level for the eddy so that $e(\lambda) > e(\lambda)_c$ by using the distribution function, equation (5.10), for the energy distribution. Note that it may be faster to redefine the distribution function to encompass values above $e(\lambda)_c$ only.
- Find the daughter size distribution for the $e(\lambda)$ value picked.
- Use a Monte Carlo method again to pick which smallest particle daughter size should be used from the daughter size distribution.
- Generate source terms in the population balance from the randomly choosen daughter sizes.

In this work, however, the averaging method has been used.

5.6 Numerical implementations

This section show how some aspects of the theory are implemented numerically.

5.6.1 Eddy energy

First assume that the energy distribution of the eddies is divided into 50 equal sized classes as a function of χ, and that we use the same distribution for all eddy cases. This gives 50 classes between 0 and 50 (the upper limit should be high enough for all cases). Further assume that $\chi_c = 6.75$, which gives the following relative error for the total integration of eddies resulting in break-up

$$\int_{6}^{50} \exp(-\chi)d\chi \Big/ \int_{6.75}^{\infty} \exp(-\chi)d\chi \;=\; 2.1\,. \tag{5.36}$$

This implies that the answer is 2.1 times too high. Even with 1000 classes the first class may introduce an error in the order of 5%. This shows that the population class distribution for the energy levels of the eddies must be adapted for each case since a general distribution of energy classes introduces an unacceptable high numerical error. It was found from equation (5.36) that the first class is the most critical one and that an even distribution as a function of χ is a poor choice since this gave negligible amounts of eddies in all, but the first very few classes (the smallest χ-value classes).

Both these weaknesses can be removed by dividing the energy levels of eddies into equal sized population classes with regard to the number of eddies, starting at χ_c. By dividing the interval χ_c to $\chi_c + b$ into n classes, the accuracy of the number of eddies included is then

$$\Delta \;=\; \left(\int_{\chi_c}^{\infty} \exp(-\chi)d\chi - \int_{\chi_c}^{(\chi_c + b)} \exp(-\chi)d\chi \right) \Big/ \int_{\chi_c}^{\infty} \exp(-\chi)d\chi\,, \tag{5.37}$$

$$\Delta \;=\; \frac{\exp(-\chi_c) - (\exp(-\chi_c) - \exp(-\chi_c + b))}{\exp(-\chi_c)} \;=\; e^{-b}\,. \tag{5.38}$$

If 99.9% of the eddies causing break-up is included, this gives $\Delta = 0.001$, resulting in $b = 6.91$, as the bandwidth of the energy classes.

As all classes are of the same size, i.e. same $\omega(\lambda_j, e_l)$ size, they may be written as

$$\int_{\chi_k}^{\chi_k + b_k} \exp(-\chi)d\chi \;=\; \exp(-\chi_c) - \exp(-\chi_c - b_k) \;=\; C\,, \tag{5.39}$$

where

$$\int_{\chi_c}^{\chi_c + b} \exp(-\chi) d\chi = \exp(-\chi_c) - \exp(-\chi_c - b) = nC. \tag{5.40}$$

Combining equation (5.39) for the first interval (thus $\chi_k = \chi_c$) and equation (5.40) gives

$$\exp(-\chi_c) - \exp(-\chi_c - b_1) = \frac{\exp(-\chi_c) - \exp(-\chi_c - b)}{n}. \tag{5.41}$$

Solving for b_1 gives

$$b_1 = -\ln\left(1 - \frac{1}{n} + \frac{1}{n}\exp(-b)\right). \tag{5.42}$$

The next interval length is found by setting $n = n - 1$ and $b = b - b_1$, which gives

$$b_2 = -\ln\left(1 - \frac{1}{n-1} + \frac{1}{n-1}\exp(-(b - b_1))\right). \tag{5.43}$$

By similar steps the general equation for the length of each class is found to be

$$b_k = -\ln\left(1 - \frac{1}{n-(k-1)} + \frac{1}{n-(k-1)}\exp\left(-\left(b - \sum_{m=1}^{k-1} b_m\right)\right)\right), \tag{5.44}$$

where $k = 1..n$. Note that the initial value χ_c does not affect the partitioning of the eddy energy classes. This is of importance with regard to computational time. We are implementing a population balance scheme which is fitted to each particular case even though the partitioning, b_k, only has to be calculated once.

5.6.2 Eddy classes

There is a rapidly decreasing number of eddies as the size of the eddies grows. On the other hand we expect a higher fraction of the larger eddies to cause break-up. Based on this, it was decided to use the same eddy class division for all fluid particle classes in order to keep the implementation as simple as possible. Clearly, a class division which is more adaptive to the fluid particle size may be faster and it will also be more accurate with the same number of eddy population classes.

Since the number of break-ups increases with increasing eddy class size, an eddy population class division is derived that gives less and less eddies in each class as the size of the eddies increases. We assign D eddies in the first class, aD eddies to the second class, a^2D eddies to the third class, and so on. This scheme is used both because it gives less and less eddies in each class, and because, as shown below, it is relatively easy to calculate the eddy size range and number of eddies in each class. The number of eddies in each class will be a fraction a of the eddy number of the class below. The total number of eddies can be written as

$$D_{tot} = D + aD + a^2D + ... + a^{m-1}D = \sum_i a^{i-1}D. \tag{5.45}$$

From Barnett & Cronin (1986)

$$D + aD + a^2D + ... + a^{m-1}D = D(a^m - 1)/(a - 1) = D_{tot}. \tag{5.46}$$

Since λ_{min} and λ_{max} are set apriori, D_{tot} is found by integration of equation (5.7). m and a are set in the program which gives us D from equation (5.46). The desired accuracy decides the values used for m and a. It may be difficult to find a good value for a since this depends on m, the total number of classes. Generally a should be low for few classes and approach one when the number of classes is high.

The last step is to find the diameters of each individual interval. For the first interval, see equation (5.7),

$$D = \left[-\frac{k}{\lambda^3}\right]\Bigg|_{\lambda_{min}}^{\lambda_{min}+\lambda_1} = \frac{k}{\lambda_{min}^3} - \frac{k}{(\lambda_{min}+\lambda_1)^3}, \tag{5.47}$$

where $k = c_2(1-\varepsilon_G)/3$. Solving for λ_1 we get

$$\lambda_1 = \left(\frac{k\lambda_{min}^3}{k - D\lambda_{min}^3} \right)^{1/3} - \lambda_{min}, \tag{5.48}$$

which is the size of the first class. The sizes of the other classes are found by updating λ_{min} and the eddy number D in equation (5.48). E.g., for the second class we update λ_{min} to $\lambda_{min} + \lambda_1$ and D to aD, and similar successive updates follow for each class.

5.6.3 Daughter class distribution

The integration of P_B in equation (5.28) between each fluid particle population class is done as follows. Starting with $d_{k,\,min}$, equation (5.28) is integrated by using the Simpson approximation, Edwards & Penney (1986), for each population class ending with the maximum possible size for the break-up. In addition the moment of the interval (the weighted middle) is found, Edwards & Penney (1986), and this is used to split the integral between the lower and upper bounding classes, giving the following equations:

$$k\_\text{fraction} = \left(1 - \left(\frac{W - d_k}{d_{k+1} - d_k}\right)\right) I, \tag{5.49}$$

$$k{+}1\_\text{fraction} = \left(\frac{W - d_k}{d_{k+1} - d_k}\right) I. \tag{5.50}$$

Here W is the weighted middle, and I is the integral between d_k and d_{k+1}. Special care has to be taken if $d_{k,\,min} < d_1$. This case is solved by numerical integration from $d_{k,\,min}$ to d_2 (or $d_{k,\,max}$). If the moment is found to be less than d_1 the entire integral is assigned to the first class. By increasing the energy classes, one will always come to a point where break-up to below the lowest class is possible. Note though that there will be few eddies with such high energies, see figure 5.2.

5.7 Sensitivity analysis

In order to see if the model predictions are physically reasonable a sensitivity analysis has been performed with respect to the following variables: ε (turbulent dissipation rate), ρ_L, ε_G (gas holdup), σ and β (constant from isotropic turbulence theory).

There are two possible cases that must be looked into:

- Break-up is controlled by energy density, see figure 5.9. This situation is more probable for large eddies and for small particles.
- Break-up is controlled by both criteria, see figure 5.11.

For the first case the critical break-up size is equal to the size of the class below,

$$d_{k,\,min,\,c} = d_{i-1}. \tag{5.51}$$

This gives the following critical eddy turbulent kinetic energy for break-up

$$e(\lambda_j)_{CBP} = \pi\sigma\lambda_j^3/d_{i-1}, \tag{5.52}$$

which gives

$$\chi_c = \frac{e(\lambda_j)_{CBP}}{\bar{e}(\lambda_j)} = \frac{\pi\sigma\lambda_j^3/d_{i-1}}{\rho_L\pi\beta\varepsilon^{2/3}\lambda_j^{11/3}/12}. \tag{5.53}$$

Equation (5.53) can be written in the following form

$$\chi_{c0} = k\sigma_0\rho_{L0}^{-1}\beta_0^{-1}\varepsilon_0^{-2/3}. \tag{5.54}$$

For the second case we start by equating the two density equations, see equation (5.26), and get

$$e(\lambda_j) = \pi\sigma\lambda_j^3/d_{k,\,min}. \tag{5.55}$$

Since both criteria are limiting we use equation (5.30), and for the surface energy term we use equation (5.16), which gives

$$[d_{k,\,min}^2/d_k^2 + (1 - d_{k,\,min}^3/d_k^3)^{2/3} - 1]\pi d_k^2\sigma = \pi\sigma\lambda_j^3/d_{k,\,min}. \tag{5.56}$$

Note that $d_{k,\,min}$ is independent of the variables mentioned initially. Thus getting

$$e(\lambda_j)_{CBP} = \pi\sigma\lambda_j^3/d_{k,\,min}. \tag{5.57}$$

A term identical to equation (5.54) is found, but with another constant factor. The influence of each variable can be seen from equation (5.54), giving the following sample sensitivity cases:

$$\sigma = 1.2\sigma_0 \Rightarrow \chi_c = 1.2\chi_{c0},\ \sigma = 0.8\sigma_0 \Rightarrow \chi_c = 0.8\chi_{c0}, \tag{5.58}$$

$$\rho_L = 1.2\rho_{L0} \Rightarrow \chi_c = (5/6)\chi_{c0},\ \rho_L = 0.8\rho_{L0} \Rightarrow \chi_c = 1.25\chi_{c0}, \tag{5.59}$$

$$\varepsilon = 1.2\varepsilon_0 \Rightarrow \chi_c = 0.8855\chi_{c0},\ \varepsilon = 0.8\sigma_0 \Rightarrow \chi_c = 1.1604\chi_{c0}, \tag{5.60}$$

where the change for β is identical with the change for ρ_L. Further, $d_{k,\,min}$ is not changed with any of the variables in both cases and ε_G has no influence. The direction of change is very reasonable. An increase in the surface tension would be expected to give a decrease in break-up as shown by equation (5.58). An increase in break-up from an increase in the eddy dissipation rate is also as expected. The increase in break-up with increased continuous phase density is less intuitive, but is an effect of the eddy dissipation being a constant per unit mass. Thus the volumetric effect will be increased and the break-up ability will also increase with increasing density.

5.8 Results

The simulations were all run for the water/air system with data for the base case as: $\rho_L = 998\ kg/m^3$, $\sigma = 0.0726\ N/m$, $\varepsilon = 0.25\ m^2/s^3$, $\varepsilon_G = 0.12$. The bubbles were divided into 14 classes ranging from 0.375 mm to about 7.5 mm in radius (each class twice the volume of the class below) and the eddies were divided into 80 classes ranging from 0.75 mm to 300 mm with $a = 0.5$. The eddy energy spectrum was split into 20 classes. See section on numerical implementations for details.

In figures 5.13, 5.14, 5.15 and 5.16, examples are shown of probability distributions for break-up into the various daughter classes (left hand side of equation (5.32)). By summing up over all eddy classes multiplied by the collision frequency,

equation (5.35), the break-up rate of particle size d_i into daughter particle size d_k can be found. These in turn, are used in order to determine the total source terms for break-up which are part of the transport equation.

Figure 5.13 shows the probability distribution for collisions between the largest particle class, class 14, and eddies of class 20. The x-axis in the figure gives the diameters of the different resulting daughter sizes. Note that figure 5.13 shows the distribution of the smallest daughter particles. This is why the resulting number in class 14 is zero (each class is twice the volume of the class below and the smallest daughter particle can then at most be of a size equal to the class below). The y-axis gives the break-up probability, see equation (5.28), into each daughter class. The total break-up probability, P_B, for one of the collisions will be the sum of the probabilities for each class. The figure shows that break-up in this example case will tend to give mostly large daughter bubbles, class 12 and 13, but that break-up down to class 8 is significant. The reason for this is that the energy density criterion dominates, and this makes break-up into equal sized or nearly equal sized bubbles most probable.

A sensitivity analysis is also included in figure 5.13. A 20% increase and decrease in the turbulent dissipation, ε, corresponds to a 6.3% increase and 9.2% decrease in the total break-up probability respectively. It is seen from the bottom figure that the relative change in break-up is larger for the smallest daughter classes, but as seen from the top figure the absolute change is higher for the larger daughter size classes. In this case the absolute change is largest for class 11 and 12. The relative change is largest for the small classes because P_B gives a more uneven distribution when break-up is less likely, i.e. for a lower ε value. The direction of change is as expected. Clearly, an increase in the turbulent dissipation rate should cause more break-up, which is what the model predicts. The sensitivity cases for other variables are not shown since these can be directly related to the shown sensitivity case through theoretical considerations.

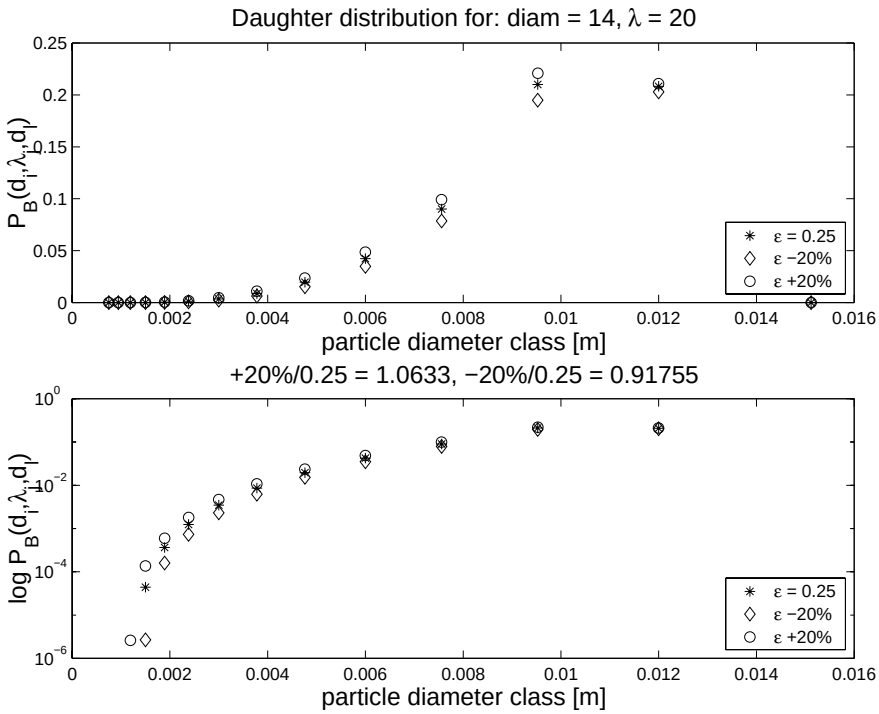

FIGURE 5.13: Break-up probability of daughter classes when particles of class 14 are hit by eddies of class 20. Sensitivity analysis included with decrease and increase in the turbulent energy dissipation, ε.

Figure 5.14 shows the daughter probability distribution for particles of class 10 being broken up by eddies of class 20. The total break-up probability is in this case about half as high as in figure 5.13. This is reasonable because the maximum size of the smallest daughter particle for class 10 is less than for class 14, and will therefore have a higher energy density. The energy density criterion then becomes more stringent. The resulting daughter size probability distribution is also seen to be more narrow in figure 5.14 than in figure 5.13, implying that smaller bubbles will have a larger tendency to break up into even sized bubbles. This can be related to the theory described in figure 5.12. For smaller particles we generally have a more narrow bandwidth of possible break-up sizes. This is because a certain energy level, and thus a given energy density level, will give a certain lower limit for daughter sizes. In terms of possible break-up classes this will set a stricter limit for a small bubble than for a large bubble. The surface energy criterion will in these

cases have little influence on the break-up distribution, resulting in a distribution favouring equal sized break-ups. The change in break-up probability with a change in ε, see header to lower figure 5.14, is higher for class 10 bubbles than for class 14. A 20% increase and decrease in ε corresponds to a 17% increase and 21% decrease in the total break-up probability respectively. Since χ_c is higher in this case, this is expected because the relative change with a change in ε should be larger.

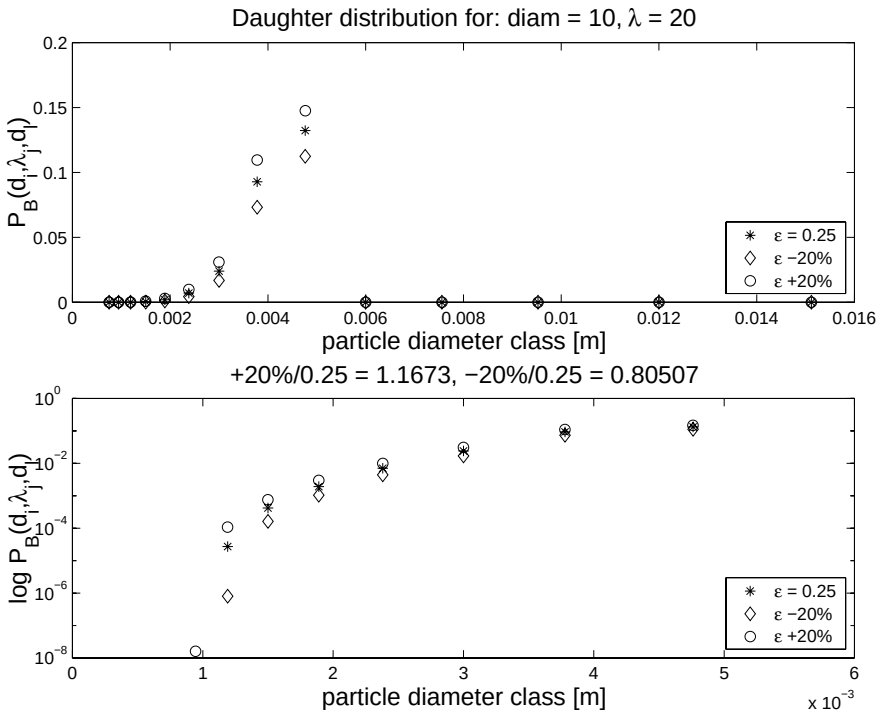

FIGURE 5.14: Break-up probability of daughter classes when particles of class 10 are hit by eddies of class 20. Sensitivity analysis included with decrease and increase in the turbulent energy dissipation, ε.

Figure 5.15, also shows the daughter size probability distribution for the break-up of class 10, but in this case the collisions are with eddy class 10 instead of eddy class 20. The total break-up probability is significantly smaller in this case and the distribution is still more uneven with almost all smaller fractions into daughter classes

8 and 9. This is because the energy level of eddy class 10 is lower than eddy class 20. Since the total break-up probability is lower, the sensitivity towards a change in the turbulent energy dissipation rate, ε, is even larger than the two previous cases.

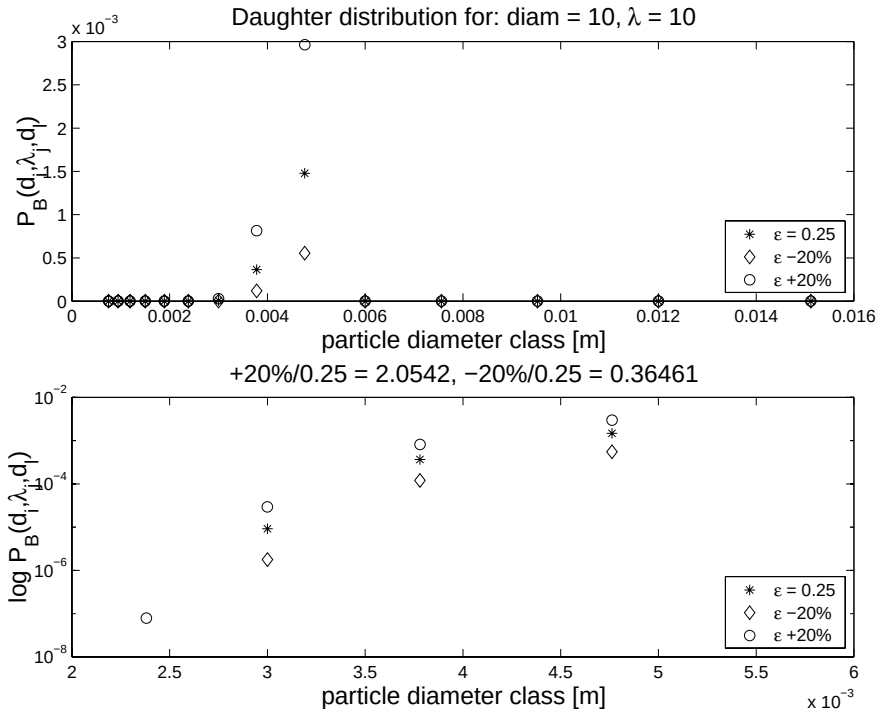

FIGURE 5.15: Break-up probability of daughter classes when particles of class 10 are hit by eddies of class 10. Sensitivity analysis included with decrease and increase in the turbulent energy dissipation, ε.

Figure 5.16 shows the results for collisions between particle size 6 and eddy size 20 and is similar to the previous figures shown. As seen the distribution is now quite narrow. For the break-up of lower classes this trend continues.

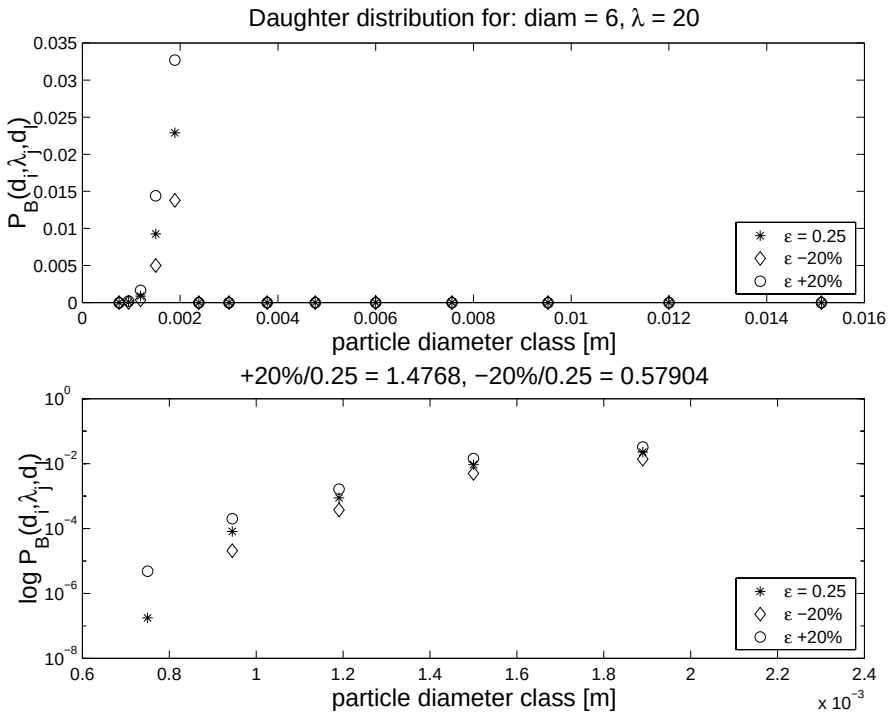

FIGURE 5.16: Break-up probability of daughter classes when particles of class 6 are hit by eddies of class 20. Sensitivity analysis included with decrease and increase in the turbulent energy dissipation, ε.

Figures 5.17, 5.18 and 5.19 show the relative contribution of each eddy class to the total break-up probability for different fluid particles. The total break-up probability for a given particle class is the sum over all eddy classes, thus it is interesting to see which eddy classes contributes most to this sum. As noted in the theory section, the eddy density decreases with increasing eddy size, see equation (5.7) and figure 5.1. It is also seen that large eddy sizes generally give a higher break-up probability than smaller eddy sizes, compare figures 5.14 and 5.15. The relative importance of each eddy class is of course also dependent on the size of the classes themselves.

As seen from figure 5.17, for bubble class 14, eddies of size below about 0.3 relative to the particle diameter contribute insignificantly to the bubble break-up. Note that the maximum frequency is for an eddy approximately equal to the bubble size. However, eddies with sizes larger than the bubble contribute significantly to

the break-up. Thus, the assumption that the size of the eddy must be of the same order of magnitude or less than the particle seems not to hold for bubbles of size 14 (radius 7.5 mm). If we assume P_B ~ constant we get for relatively large eddies that $\Omega_B \sim C'\lambda_j^2 n_{\lambda_j} \sim C/\lambda_j$. Thus the upper boundary for the eddy length scale, λ, should be the boundary of the inertial subrange since $E(k) \to 0$ above this limit, see Tennekes & Lumley (1972). In order to improve the accuracy of the calculation of the total break-up rate for bubble class 14 more eddy classes in the relative range between 0.3 and 2 should be included. The y-axis gives the number of particles broken up during one time unit (which was 1 second). For the simulations we uses initially 1000 particles in each class. The total break-up rate, given in the bottom figure, is much higher than this value. This simply means that the time increment used when solving the population balances must be much lower than 1 second. Ideally this time increment should be so low that the change in the class becomes much lower than the total number of particles in the class. As mentioned before, steady state between the classes is a situation which make it possible to use larger time increments.

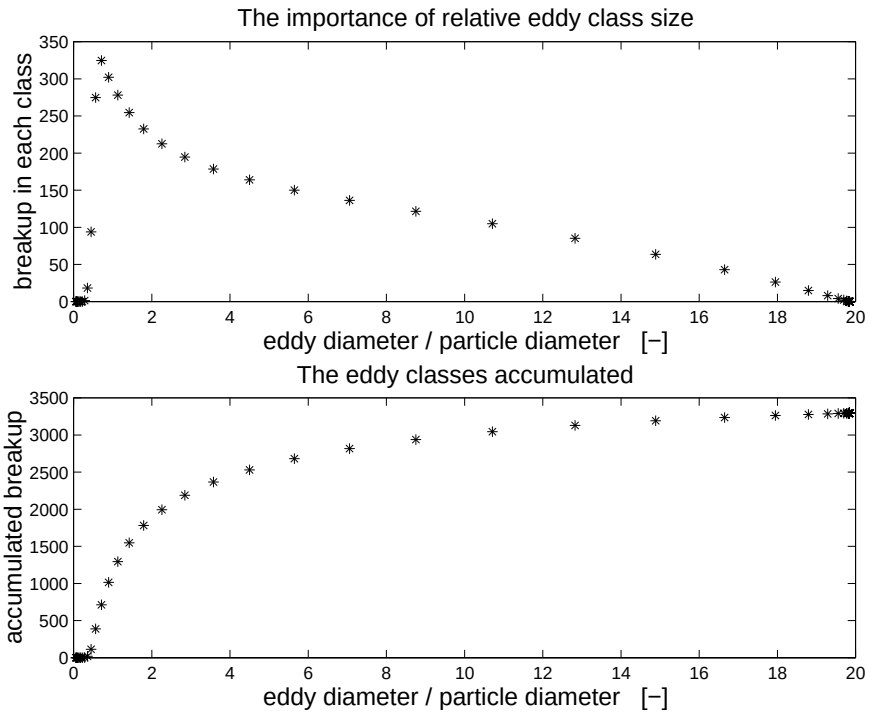

FIGURE 5.17: The relative importance of each eddy class in breaking up particles of class 14 is shown in the top figure and the accumulated break-up is shown below. Each eddy class has 50% of the number of eddies in the class below. The y-axis is a measure of the number of break-ups in one time unit.

Figure 5.18 shows the importance of the individual eddy classes in breaking up bubbles of class 10. The total break-up rate of class 10 is seen to be about 4-5 times smaller than that of class 14. For this bubble size class it is seen that the larger eddy classes become more important than for class 14. This is because the energy density criterion, as mentioned before, becomes more stringent for smaller particles and because the energy density increases with eddy size.

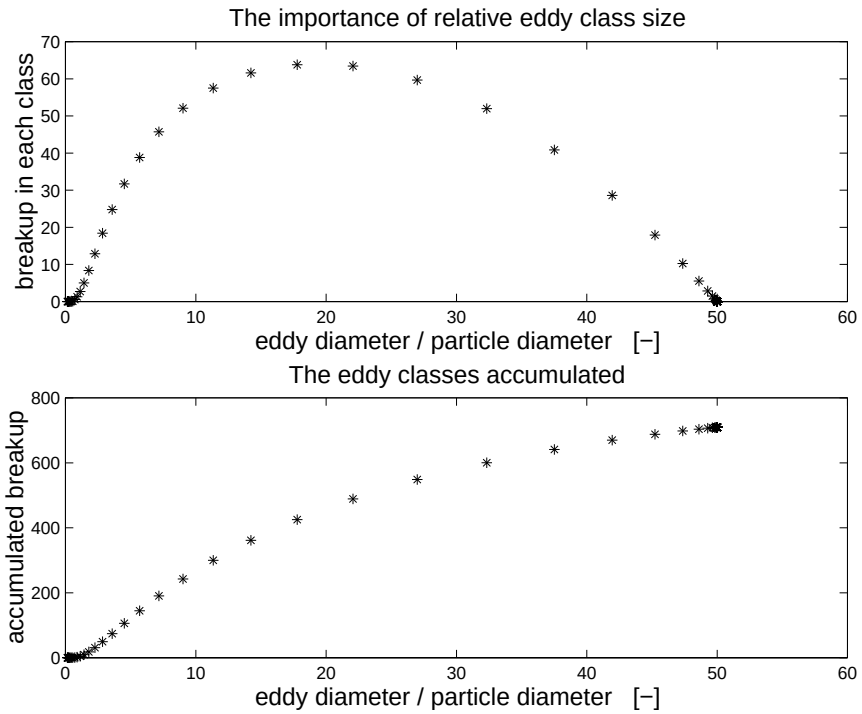

FIGURE 5.18: The relative importance of each eddy class in breaking up particles of class 10 is shown in the top figure and the accumulated break-up is shown below. Each eddy class has 50% of the number of eddies in the class below. The y-axis is a measure of the number of break-ups in one time unit.

Figure 5.19 shows a similar plot for the break-up of bubbles of class 6. Eddies with relative size about 8 and above cause break-up. For this case it is not a good approximation to assume that eddies less than the fluid particle cause break-up. In this case the total break-up rate is about 140 which is about 25 times less than the break-up rate for particle class 14.

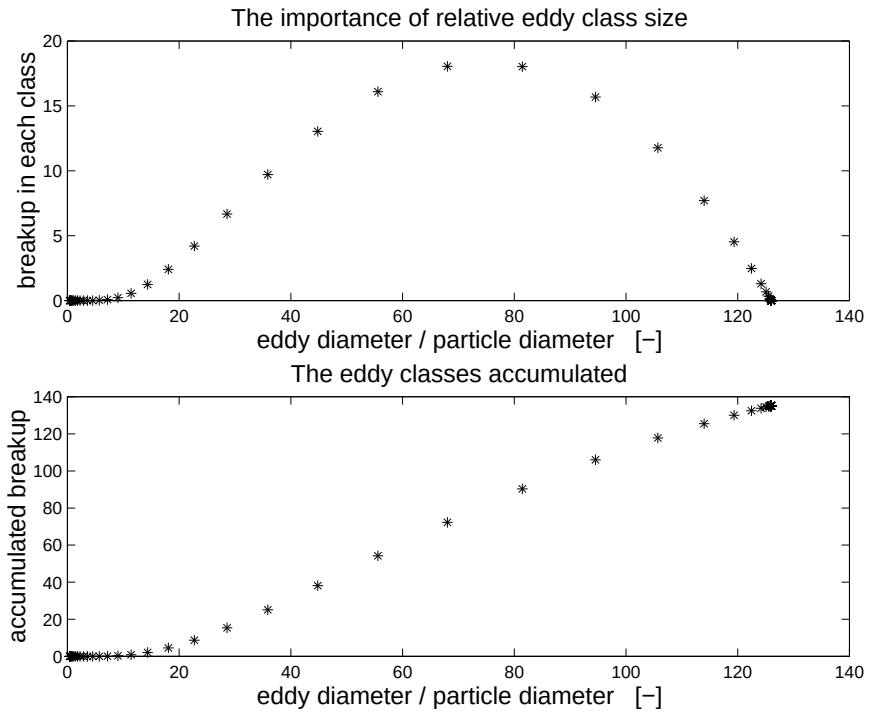

FIGURE 5.19: The relative importance of each eddy class in breaking up particles of class 6 is shown in the top figure and the accumulated break-up is shown below. Each eddy class has 50% of the number of eddies in the class below. The y-axis is a measure of the number of break-ups in one time unit.

Figure 5.20 shows χ_c for all combinations of particle classes and eddy classes. The upper plot is the one resulting from using both the energy density criterion and the surface energy criterion. The bottom plot is from using only the energy density criterion. From the upper plot we se that we get low χ_c values (same as a high probability for break-up) when we have large eddy classes. For small eddies the surface energy criterion becomes important and a combination of both criteria is needed. For small particle classes the density criterion dominates and we have high χ_c values. The values pass a minimum and we get higher values again as the particle classes increase due to the surface energy criterion.

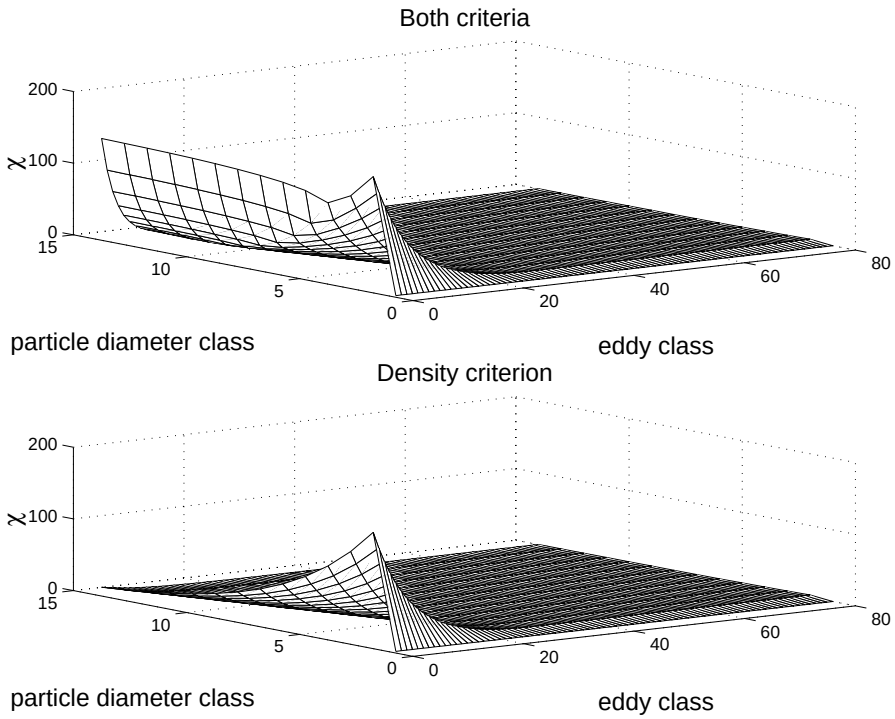

FIGURE 5.20: The χ_c values (giving the break-up probability) when both the energy density criterion and the surface energy criterion are used, are shown in the top figure. Similar values for only the energy density criterion are shown in the bottom figure. The values are shown for all combinations of particle classes and eddy classes.

Where this latter criterion is also of importance is shown in figure 5.21 where values for the energy density criterion minus values for both criteria are shown. Thus negative χ values indicate that the surface energy criterion is of importance. This area is circled in the figure. As expected this area is generally larger as the fluid particles grow in size and also more important when eddies are small in size, since small eddies have less energy available than eddies which are large in size. Further, it is for rather few combinations of eddies and particles that the surface energy criterion affects the break-up probability. Also, its effect on the daughter size distribution will be diminishing with increasing eddy size classes, P_s in equation (5.20), and equation (5.28), since we get a more and more equal distribution for P_s as the

total energy level $e(\lambda)$ increases above the level needed for an equal daughter size division. The impact of the surface energy criterion is on the other hand quite large in the region of small eddy classes. A change of 2.3 in χ is the same as an order of magnitude change in the total break-up probability.

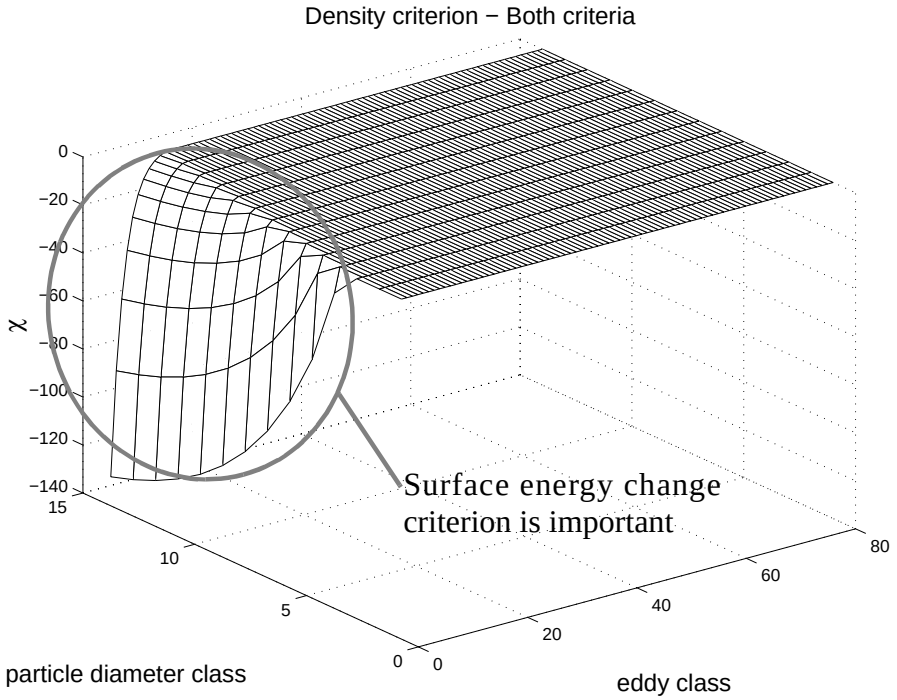

FIGURE 5.21: Relative χ_c values, values for the energy density criterion minus values for both criteria together, are shown. Values below zero means that the combination of criteria is limiting the break-up, this area is circled in the figure. The values are shown for all combinations of particle classes and eddy classes.

Hesketh, Etchells & Russel (1991) observed breakages which they defined as two types of breakage. The first kind, and most prevalent, was for particles to undergo large scale deformation resulting in a wide range of daughter sizes. The second kind was defined as a tearing mechanism giving a local deformation of one end of a fluid particle producing a daughter fragment of essentially the same volume and a second daughter fragment which was less than 0.5% of the original volume. The

first breakage type can in our model framework be a large eddy hitting a fluid particle. Such eddies generally break up particles to daughter fragments which cover a wide range of sizes, see figure 5.13. The second type can be seen as a small eddy with a high turbulent kinetic energy level hitting a fluid particle. As seen from figure 5.21 such an eddy will generally be limited by the surface energy criterion. Thus daughter fragments from such collisions are expected to be of unequal or highly unequal size.

5.9 Possible model refinements

Several possible improvements to the developed model are listed below, and the consequences are discussed.

5.9.1 Activation energy

As an analogy to the chemical reaction activation energy one may assume that such an approach is also applicable for the collision between an eddy and a fluid particle. Physically this intermediate step may be seen as a deformed parent particle with a larger surface area than the sum of both daughter particles, see figure 5.22 below.

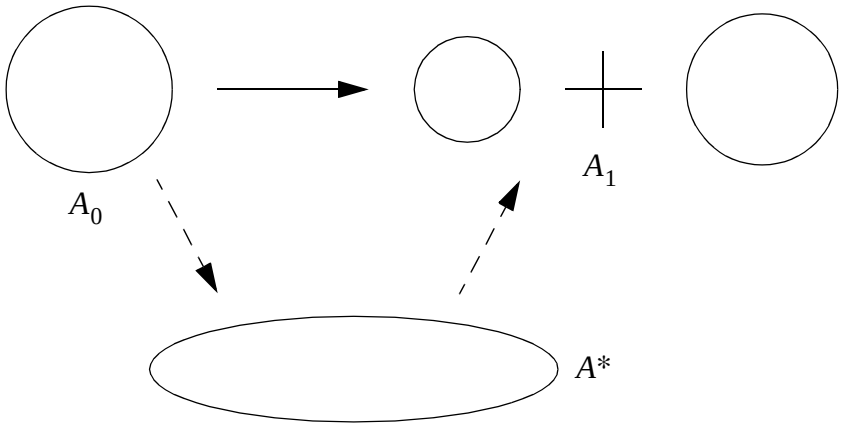

FIGURE 5.22: Breakage of a fluid particle into two daughter particles is shown as a direct path and through an activated state (dashed arrows). It is assumed that $A^* > A_1 > A_0$, which means the activated state has a larger surface area than the sum of the two daughter particles.

Since the activated state require more energy than the daughter particles combined this state will define the energy requirement for the break-up process. The following condition for the surface energy criterion giving break-up can then be written as

$$e(\lambda_j) \geq e_i^*(d_i, d_k) \,, \tag{5.61}$$

where $e_i^*(d_i, d_k)$ is the energy requirement for the activated state. Similarly, for the energy density criterion there may be a need for a surplus energy density in order to create a daughter fragmentation. Thus, the new lower limit for daughter size will be (refer to equation (5.26))

$$w_s(d_k) \;=\; k_{ae} \cdot w_d(\lambda_j) \Rightarrow d_{k,\,min} \;=\; \sigma\pi\lambda_j^3 / (e(\lambda_j) k_{ae}) \,, \tag{5.62}$$

where k_{ae} represent the surplus of energy density needed. This factor may not be a constant for the different fragmentations. Including these considerations will limit the break-up rate and will also change the daughter size distribution between

the daughter classes since P_s and/or P_d in equation (5.28) will be more unevenly distributed.

5.9.2 Surface energy criterion

The surface energy criterion defines that break-up can not require more energy than what is available in the eddy. This criterion may have to be changed when the eddy is much larger than the fluid particle. If the diameter of the eddy is say 10 times the diameter of the particle, it is rather unlikely that the particle can absorb all the energy of the eddy. Absorbing all the turbulent kinetic energy may be looked upon as a maximum surface energy limit for the model and the simulations. A minimum could be that the particle only absorbs turbulent kinetic energy corresponding to its size compared to the eddy. Thus when the eddy, υ_e, is larger in diameter than the fluid particle, υ_p, we get

$$e(\lambda_j) \geq e_i(d_i, d_k) \cdot (\upsilon_e / \upsilon_p) \ . \tag{5.63}$$

The inclusion of this criterion will result in a different daughter size distribution since P_s will be changed. The distribution will become more uneven favouring uneven sized break-up (one large and one small particle). If only this modification is included the break-up rate will not be changed since this criterion is less important than the energy density criterion (this has been tested in simulations). This may be seen from figure 5.21, showing that the energy density criterion is most important for large eddy classes. Only for large particles and small eddies will the surface energy criterion be important. In these cases equation (5.63) is not used since the particle is larger in diameter than the eddy. Thus, the modification in equation (5.63) will not affect the break-up rate, but it will change the daughter size distribution through changing P_s.

5.9.3 Inertial subrange of turbulence

The model assumes we are operating in the inertial subrange of turbulence in the column. According to Tennekes & Lumley (1972), figure 8.8, the $-5/3$ power law used for the turbulent energy, $E(k)$, will be reduced dramatically (toward 0) at the lower boundary of *k* of the inertial subrange. Thus, a better approximation of the lower end for *k* in the inertial subrange will reduce the rate of break-up.

Even with the current approximation for the lower end of the inertial subrange (meaning for larger eddies since $k = 2\pi/\lambda$), the turbulent energy is overestimated, thus giving an overestimation of the break-up rate. This can be seen from the fact that $E(k) \rightarrow 0 \Rightarrow \varepsilon \rightarrow 0$, see after equation (5.3). Combined with figures 5.13 to 5.16, showing a decrease in break-up probability with decreasing turbulent energy dissipation rate, ε, it is found that an overestimation in the turbulent energy is the same as an overestimation in the break-up probability. The break-up rate is also overestimated since the collision frequency also decreases with decreasing turbulent energy dissipation rate, see the $\bar{u}_{d_i, \lambda_j}$ term in equation (5.2).

5.9.4 Fluid particle rest state

According to Risso & Fabre (1998) energy may be accumulated through successive collisions, finally resulting in break-up. This can most easily be approximated by assigning an energy rest state which is above zero as assumed in this paper. Equation (5.19) could thus be replaced by

$$e(\lambda_j) - E(\lambda_j)_0 \geq e_i(d_i, d_k) \ , \tag{5.64}$$

where $E(\lambda_j)_0$ is the energy level in the rest state for fluid particle λ_j. $E(\lambda_j)_0$ can by caused by numerous collisions with small eddies resulting in low amplitude oscillations. It can also be caused by other flow phenomena which are superimposed on the turbulent flow, Risso & Fabre (1998). From figure 5.21 it is seen that this refinement will result in more break-up when small eddies collide with fluid particles.

5.9.5 Number of daughter fragments

As noted by Chatzi & Lee (1987), Prince, Walters & Blanch (1989), Risso & Fabre (1998) and others, fluid particles may break into more than two fragments. This may be due to the same eddy breaking up the parent particle and then successive daughter particles. This is currently not included in the model, but can be implemented relatively easily. However, more likely this will have a negligible impact on the result. More likely the complex dynamics of a break-up sometimes result in a number of daughter fragments which can not be explained by the theory given in this chapter (very small fragments having too high energy densities). Such frag-

mentations probably have to be explained through dynamic CFD simulations on the micro scale where single fluid particle - turbulent eddy collisions are simulated.

5.9.6 Collision frequency

The formula for collision frequency used, equation (5.2), is based on collisions between gas molecules. For large eddies covering a significant fraction of the column diameter this formula is probably a coarse estimate of the actual number of collisions.

5.9.7 Entropy

The second law of thermodynamics states that the entropy tends toward a maximum. We have a tentative theory that the change in entropy is zero for the critical case where the energy density criterion is exactly met, and that an increase in the energy density would result in a decrease in the entropy. This remains to be proven.

5.10 Conclusions

A new break-up model has been developed that takes into account a statistical approach to the energy level and energy density of colliding eddies. It further introduces a new particle break-up criterion based on the requirement that no increase in energy density can occur as a result of the collision and break-up. It is found that the new energy density criterion is more important in finding the break-up rate for large eddies colliding with fluid particles than the surface energy criterion. For small eddies the surface energy criterion is important and the break-up rate is severely limited because of the combination of both criteria.

The daughter size distribution follows directly from the model assumptions. The distribution varies with fluid particle size, eddy size and energy level, and system variables. However, generally most of the smaller daughter particles are found in the particle size classes just below the class breaking up. The spread of daughter particle sizes is larger for large particles and large eddies than for smaller particles and smaller eddies.

It is shown that the importance of the relative eddy size (to the particle size) varies with the colliding particle size. Larger relative eddy sizes are generally more

important as the particle size decreases and eddies of magnitude an order or larger than the particles are important for break-up into smaller particle classes.

The new model needs to be tested and validated with experimental data. In order to do this the module must be implemented in a CFD model, and is directly applicable for that.

Notation

A^*	surface area of activated state, m^2
A_0	surface area of parent particle, m^2
A_1	surface area of daughter particles, m^2
a	number fraction for one class of eddies divided by the number of eddies in the class below, see equation (5.45), -
b	bandwidth of eddy energy, see equation (5.37), -
b_1, b_2	first and second bandwidth size of an energy class, see equations (5.42) and (5.43), -
b_k, b_m	bandwidth size of an energy class, see equation (5.44), -
C	size of energy integration for one class, see equation (5.39), -
C	constant in estimation of Ω_B, -
C'	constant in estimation of Ω_B, -
c_2	constant, defined in equation (5.7), -
$c_{f,k}$	coefficient for increase of surface area, see equation (5.15), -
D	number of eddies in first eddy class, see equation (5.47), $1/m^3$
D_{tot}	total number of eddies, see equation (5.45), $1/m^3$
d_1, d_2	diameter of daughter particle, m
d_i	diameter of parent particle, m

d_{i-1} maximum diameter of smallest daughter particle when particle of diameter d_i breaks up, *m*

d_j diameter of largest daughter particle, *m*

d_k, d_{k+1} diameter of daughter classes *k* and $k + 1$, *m*

$d_{k,\,min}$ lower limit of diameter due to energy density criterion, see equation (5.26), *m*

$d_{k,\,min,\,c}$ critical lower limit of diameter due to energy density criterion, see equation (5.26), *m*

$d_{k,\,max}$ minimum crossover diameter, see definition after equation (5.20), *m*

d_{max} maximum stable particle size in a stirred vessel, see equation (5.21), *m*

$E(k)$ energy spectrum function of turbulence, m^3/s^2

$E(\lambda_j)_0$ energy level at rest state for fluid particle, *J*

$e(\lambda)$ energy level of eddy of size λ, *J*

$\bar{e}(\lambda)$ average energy level of eddy of size λ, see equation (5.12), *J*

$e(\lambda)_{CBP}$ critical energy for break-up, see equation (5.30), *J*

$e(\lambda)_{CED}$ critical energy for break-up, see equation (5.29), *J*

$e_i(d_i, d_k)$ increase in surface energy when particle with diameter d_i breaks up into particle with diameter d_k and complementary particle, *J*

$e_i^*(d_i, d_k)$ increase in surface energy for activated state when particle with diameter d_i breaks up into particle with diameter d_k and complementary particle, *J*

$f_{BV,\,k}$ breakage volume fraction, index *k* defines the size of the daughter fragment, see equation (5.14), -

I integral between two daughter diameter classes, see equation (5.49)

k wave number of eddies in turbulence, $1/m$

k constant defined after equation (5.47)

k class number variable, see equation (5.44)

k_{ae} surplus fraction of energy density needed, see equation (5.62), -

k_fraction see equation *(5.49)*

k+1_fraction see equation *(5.50)*

n number of eddy energy classes, see equation (5.40), -

n_{d_i} number of particles of size d_i per unit reactor volume, $1/m^3$

$\dot{n}_{\lambda_j}$ number of eddies of size λ_j to $\lambda_j + d\lambda$ per unit reactor volume, $1/m^4$

n_{λ_j} number of eddies in size group λ_j to $\lambda_j + d\lambda$ per unit reactor volume, $1/m^3$

m number of eddy classes, -

P_B break-up probability, -

$P_B(d_i, \lambda_j, d_k)$ break-up probability of particle d_i colliding with eddy size λ_j, giving daughter size d_k, -

$P_B(d_i, \lambda_j, e_l, d_k)$ break-up probability of particle d_i colliding with eddy size λ_j, with energy level e_l, giving daughter size d_k, -

$P_d(d_k)$ normalized probability function for break-up due to energy density, see equation (5.27), -

$P_s(d_i, d_k)$ normalized probability function for break-up due to turbulent kinetic energy, see equation (5.20), -

$p_e(\chi)$ turbulent kinetic energy probability distribution function, equation (5.9), -

$\overline{u^2}$	fluctuating squared velocity in continuous phase, see equation (5.23), m^2/s^2
$\bar{u}_i$	particle class velocity, m/s
$\bar{u}_{\lambda_j}$	eddy velocity, m/s
$\bar{u}_{d_i,\lambda_j}$	relative velocity between particle of size d_i and eddy of size λ_j, m/s
W	weighted middle of integral between two diameters, see equation (5.49), m
We_c	Weber number, see equation (5.22), -
$w_d(\lambda_j)$	energy density of an eddy, see equation (5.25), J/m^3
$w_s(d_i)$	energy density of a particle, see equation (5.24), J/m^3
α	universal constant in turbulence, $\alpha = 1.5$, used by Luo & Svendsen (1996), -
$\bar{\beta}$	universal constant in turbulence, Luo & Svendsen (1996), -
β	constant defined after equation (5.3), -
β_0	constant, reference state defined after equation (5.3), see equation (5.54), -
Δ	defined as accuracy, see equation (5.37), -
ε	turbulent energy dissipation rate, m^2/s^3
ε_0	reference state of turbulent energy dissipation rate, see equation (5.54), m^2/s^3
ε_G	void fraction, -
η	Kolmogorov micro length scale, equation (5.8), m

ϑ_e volume of eddy, m^3

ϑ_i volume of parent particle for break-up, largest parent particle for coalescence, m^3

ϑ_k volume of smallest daughter particle for break-up, m^3

ϑ_p volume of particle, m^3

λ, λ_j diameter of eddy, m

λ_1 length size of first eddy class, see equation (5.48), m

λ_{min} minimum size of lamda used, m

λ_{max} maximum size of lamda used, m

ρ, ρ_L continuous phase density, kg/m^3

ρ_G gas phase density, kg/m^3

ρ_i dispersed class i density, kg/m^3

ρ_{L0} reference state of continuous phase density, see equation (5.54), kg/m^3

μ_L viscosity of continuous phase, after equation (5.8), $Pa \cdot s$

ν continuous kinematic viscosity, equation (5.8), m^2/s

σ surface tension, N/m

σ_0 reference state of surface tension, see equation (5.54), N/m

χ dimension less energy in energy distribution function, see equation (5.10), -

χ_c dimension less critical break-up energy, -

χ_{c0} reference state of dimension less critical break-up energy, see equation (5.54), -

χ_k dimension less critical break-up energy, -

Ω_B break-up rate, $1/(m^3 s)$

$\Omega_B(d_i, d_k)$ break-up rate of particle with diameter d_i into daughter particle with diameter d_k, $1/(m^3 s)$

ω_B collision frequency, $1/(m^3 s)$

$\omega_B(d_i, \lambda_j)$ collision frequency between particle of size d_i and eddy of size λ_j, $1/(m^3 s)$

$\omega(\lambda_j, e_l)$ fraction of eddy of size λ_j with energy level e_l, -

References

Alopaeus, V., Koskinen, J. & Keskinen, K.I. (1999). Simulation of the population balances for liquid-liquid systems in a nonideal stirred tank. Part 1 Description and qualitative validation of the model. *Chemical Engineering Science*, **54**, 5887-.

Alvarez, J., Alvarez, J. & Hernandez, M. (1994). A population balance approach for the description of particle size distribution in suspension polymerization reactors. *Chemical Engineering Science*, **49**, 99-.

Angelidou, C., Psimopoulos, M. & Jameson, G.J. (1979). Size distribution functions of dispersions. *Chemical Engineering Science*, **34**, 671-.

Barnett, S. & Cronin, T.M. (1986). Mathematical formulae for engineering and science students, 4th ed., Longman Scientific & Technical, Bradford University Press, UK.

Batchelor, G.K. (1951). Pressure fluctuations in isotropic turbulence, *Proc Camb Phil Soc*, **47**, 359-.

Bourne, J.R. & Baldyga, J. (1994). Drop breakup in the viscous subrange: a source of possible confusion. *Chemical Engineering Science*, **49**, No 7, 1077-.

Chatzi, E. & Lee, J.M. (1987). Analysis of interactions for liquid-liquid dispersion in agitated vessels. *Ind. Chem. Engng. Res.*, **26**, No 11, 2263-.

Das, P.K. (1996). Monte Carlo simulation of drop breakage on the basis of drop volume. *Computers chem. Engng*, **20**, No 3, 307-.

Edwards, C.H. Jr. & Penney, D.E. (1986). Calculus and Analytic Geometry, 2nd ed., Prentice-Hall International (UK) Limited, London, UK, 292- & 338-.

Gikhman, I.I. & Skorokhod, A.V. (1980). The theory of stocastic processes, Springer-Verlag, Berlin.

Hesketh, R.P., Etchells, A.W. & Russell, T.W.F. (1991). Experimental observations of bubble breakage in turbulent flow. *Ind. Eng. Chem. Res.*, **30**, 835-.

Hinze, J.O. (1955). Fundamentals of the hydrodynamic mechanism of splitting in dispersion processes. *A.I.Ch.E. Journal*, **1**, No 3, 289-.

Kolmogorov, A.N. (1949). Disintegration of drops in turbulent flows. *Dokl. Akad. Nauk. SSSR*, **66**, 825-.

Laidler, K.J. & Meiser, J.H. (1982). Physical Chemistry, The Benjamin/Cummings Publishing Company, Inc., Menlo Park, California, USA, 19-.

Lee, C.-H., Erickson, L.E. & Glasgow, L.A. (1987). Bubble breakup and coalescence in turbulent gas-liquid dispersions. *Chem. Eng. Comm.*, **59**, 65-.

Luo, H. & Svendsen, H.F. (1996). Theoretical model for drop and bubble breakup in turbulent dispersions. *AIChE Journal*, **42**, No. 5, 1225-.

Parthasarathy, R., Jameson, G.J. & Ahmed, N. (1991). Bubble breakup in stirred vessels- Predicting the sauter mean diameter. *Trans IChemE*, **69**, Part A.

Prince, M.J. & Blanch, H.W. (1990). Bubble Coalescence and Break-Up in Air-Sparged Bubble Columns. *AIChE Journal*, **36**, No. 10, 1485-.

Ramkrishna, D. (1981). Analysis of population balances - IV, the precise connection between Monte Carlo simulations and population balances. *Chem. Engng Sci.*, **36**, 1203-.

Risso, F. & Fabre, J. (1998). Oscillations and breakup of a bubble immersed in a turbulent field. *J. Fluid Mech.*, **372**, 323-.

Tennekes, H. & Lumley, J.L. (1972). A First Course in Turbulence, 11th ed., The MIT Press, Cambridge.

CHAPTER 6

Modeling of the dispersed phase size distribution in a bubble column

This chapter is a modified version of the paper 'Modeling of the dispersed phase size distributions in bubble columns' accepted for publication in Industrial & Engineering Chemistry Research by Hagesaether, Jakobsen & Svendsen. The aim of this chapter is to verify the model developed in chapter 5 by use of CFD and compare the results with experimental data. Details for the implementation of the break-up rate and details for the source term formulations are given in appendix A.

6.1 Introduction

The potential of computational fluid dynamics (CFD) for describing the dynamics of bubble column reactors has been described in several recent publications, and multi-fluid models have been found to represent a trade-off between accuracy and computational efforts for practical applications. However, even though the bubble coalescence and break-up phenomena observed in this type of reactors have a determining influence on the bubble size distribution and thus the interfacial heat, mass and momentum transfer fluxes, the chemical and physical mechanisms involved are still not satisfactorily understood. To improve on the predictive capabilities of these models, more accurate constitutive equations are needed, describing the coalescing and break-up processes.

In our model development we have chosen to apply a modular approach. At this stage we focus on the inclusion of elaborate models for bubble coalescence and break-up phenomena, while the flow formulation is more simplified. To analyze the important mechanisms involved, a population balance model is developed with emphasis on the source and sink term formulations describing the birth and death rates as given by Hagesaether, Jakobsen & Svendsen (2000). The model is developed such as to facilitate the direct future inclusion into a more sophisticated flow calculation, a full multi-fluid model.

The current break-up model is based on the work of Luo & Svendsen (1996), but further expanded and refined by Hagesaether, Jakobsen & Svendsen (2001) to remove an inherent weakness regarding the break-up rate for small particles and small daughter particle fragments. The main purpose of this work is to validate the extended break-up model, as given in chapter 5.

For model validation, the results from both the basic model and the extended model version are compared to experimental data obtained in our own laboratory for bubble size and volume fraction distributions. The extended model results are found to be encouraging as the break-up rate is greatly reduced when the dispersed fluid particles are reduced in size, and the size distribution is in good agreement with the corresponding experimental data. The coalescence model used is basically the same as the one used by Luo (1993), although the collision rate formula was modified when used with the current break-up model.

The results obtained indicate that, for predictive purposes, the population balance model approach may substantially improve on the empirically based analysis in use today. Combined with multi fluid CFD evaluations, it appears that this approach may have inherent capabilities calculating the bubble-bubble and bubble-liquid interactions in a more reliable manner providing improved predictions of the interfacial contact area and thus the heat-, mass- and momentum transfer fluxes.

6.2 The model

The continuity equation for the dispersed phase is given by:

$$\frac{\partial}{\partial t}(\rho\alpha) + \nabla \cdot (\rho \vec{u} \alpha) = 0 \quad [kg/(m^3 s)]. \tag{6.1}$$

The dispersed gas phase is divided into a number of subclasses according to particle mass size, giving one transport equation for the mass of each particle class. The dispersed phase volume fraction and the mass averaged gas velocity are defined as:

$$\alpha = \sum_i n_i \frac{\pi}{6} d_i^3 \text{ and } \vec{u} = \sum_i (n_i \vec{u}_i \rho \vartheta_i) / \sum_i (n_i \rho \vartheta_i) . \tag{6.2}$$

The following transport or balance equation for each bubble size class can be obtained adopting the well-known population balance concept:

$$\frac{\partial}{\partial t}(\rho n_i) + \nabla \cdot (\rho \vec{u}_i n_i) = \rho [B_B - D_B + B_C - D_C]_i \ [kg/(m^6 s)] . \tag{6.3}$$

In this approach the individual bubble classes are assumed to have their own velocities, and the density of the gas phase may be calculated according to a suitable equation of state. It is assumed that the gas density is constant.

In order to apply the population balance on the discrete particle size distributions observed in bubble columns, the continuous particle size distribution function is represented by a finite number of size classes, each discrete particle class representing a subrange of the size distribution function.

In accordance with Hounslow, Ryall & Marshall (1988), the prescribed bubble classes are chosen in such a way that the bubble volume (or mass) in class, *i+1*, is twice the volume (or mass) of the class below, *i*,

$$\vartheta_{i+1} = 2\vartheta_i . \tag{6.4}$$

This is convenient as it simplifies the particle size redistribution budget calculations needed to account for the bubble break-up and coalescence processes.

We emphasize that the population balance model formulation used here is based on mass and is thus of general nature whereas the implementation is volume based. However, in small columns where the compressibility of the gas phase is unimportant, the bubble density may be assumed constant as done in this paper. To relax this limitation, only a minor modification is needed. The discretization of the particle size distribution should be based on mass rather than volume. This change is easily implemented and the result is that particles which rise in the column will not change class due to changes in pressure. The parameterizations developed for the sink and source terms are already applicable to variable density flows.

The redistribution scheme adopted requires both the mass and number balances to be fulfilled. Considering particles of a specific size resulting from a break-up or coalescence process, indicated by index, *j*, each being characterized by a mass lying between two of the prescribed population classes, e.g. *i* and *i+1*, the mass balance yields:

$$n_j m_j = n_i m_i + n_{i+1} m_{i+1}. \tag{6.5}$$

The mass of these particles, $n_j m_j$, is redistributed between the two population classes characterized by the masses, m_i, and m_{i+1}. The resulting particle number densities, n_i and n_{i+1}, are not necessarily integer values, but must comply with the corresponding number balance:

$$n_j = n_i + n_{i+1}. \tag{6.6}$$

The number of particles is thus conserved. Combining (6.5) and (6.6) gives:

$$m_j = \left(\frac{n_i}{n_j}\right) m_i + \left(\frac{n_j - n_i}{n_j}\right) m_{i+1}, \tag{6.7}$$

which uniquely defines the redistribution process as n_i is the only unknown.

An alternative to this redistribution scheme could be to require the mass and area balances to be conserved, intending to provide better estimates for the mass transfer fluxes. This procedure is, however, not used as an error in the number balance will be propagated by the source term calculations, as the break-up mechanisms are a function of the number density of $O(n)$, while coalescence mechanisms are a function of the number density of $O(n^2)$. An error in the number balance will thus introduce an error of unknown magnitude in the area balance.

As stated above, the source terms determine the parameterizations of the underlying breakage- and coalescence mechanisms. First, we consider the break-up parameterizations, discussing how to adjust the resulting daughter size to the prescribed population size discretization scheme. Two versions of the breakage model are considered here, the model of Luo & Svendsen (1996) and an extension of this model developed by Hagesaether *et al.* (2001). These parameterizations are based on principles of molecular collision and isotropic turbulence and they contain no adjustable model parameters as all constants are derived from isotropic turbulence

theory. The daughter particle size distribution is derived from the breakage rate parameterizations. The extended parameterization given by Hagesaether *et al*. (2001) requires two criteria fulfilled in order to obtain particle break-up. The first criterion was also used by Luo & Svendsen (1996). It states that the energy of the colliding eddy must be equal to, or larger than the particle surface energy increase due to break-up into a particular daughter size configuration. The second criterion introduced by Hagesaether *et al.* (2001) states that the energy density of the daughter particles must be equal to or less than the energy density of the colliding eddy. This latter criterion limits the possibility of break-up in a more realistic manner, as the first criterion allows all fluid particles to be broken when hit by eddies. Further, a criterion stating that the eddy must be less in size than the bubble in order for a break-up to be possible, has been removed.

A detailed description of the basic break-up modeling framework was provided by Luo & Svendsen (1996). This model, and details for numerical implementation of it (not given by Luo & Svendsen (1996), are found in appendix A. Therefore, only a brief description of the extended particle break-up parameterization scheme will be given here, along with some minor updates on the particle collision frequency parameterization adopted calculating the coalescence rate. For the coalescence a detailed description is given by Luo (1993).

As discussed by Luo & Svendsen (1996), the break-up parameterization used is based on the assumption that bubbles break-up into two daughter bubbles only. In line with previous work, we also assume that the density of the gas phase is constant. For such binary break-up processes, the parent particle volume, ϑ_i, is distributed into two daughter particles of volumes, ϑ_j and ϑ_k, in accordance with the following volume balance:

$$\vartheta_i \rightarrow \vartheta_j + \vartheta_k, \tag{6.8}$$

where the volume of daughter particle *k*, ϑ_k, is smaller or equal to the volume of daughter particle *j*, ϑ_j. In the model we have set the volume of the smaller daughter particle, ϑ_k, to one of the population class sizes less than ϑ_i. The volume of daughter particle *j*, ϑ_j, must be equal to the prescribed population size class ϑ_{i-1} or larger, and thus split between size class *i* and *i-1*. This may not have been the case if we had used a factor lower than 2 in the population class discretization scheme,

see (6.4). The daughter volume, ϑ_j, is divided into the population classes $(i-1)$ and i, according to a modified version of (6.7):

$$\vartheta_j = x_{i,k}\vartheta_{i-1} + (1-x_{i,k})\vartheta_i . \tag{6.9}$$

In addition, we express the volume of the daughter size class, ϑ_j, as a function of the neighboring population particle sizes in terms of the volume of population class 1,

$$\vartheta_j = \vartheta_i - \vartheta_k = 2^{(i-1)}\vartheta_1 - 2^{(k-1)}\vartheta_1 . \tag{6.10}$$

Combining (6.4), (6.9) and (6.10) gives

$$x_{i,k} = 2^{1+k-i},\ k<i , \tag{6.11}$$

where $x_{i,k}$ is the number fraction in class $i-1$ and $(1-x_{i,k})$ is the number fraction in population class i. Thus, break-up of a parent particle gives the following volume distribution in the population classes:

$$\vartheta_i = \vartheta_k + x_{i,k}\vartheta_{i-1} + (1-x_{i,k})\vartheta_i . \tag{6.12}$$

This means that the break-up processes give rise to a whole particle in volume class (k) below the class (i) being broken up, and one equal or larger particle which is divided in a number fraction within the class below the one breaking up, i.e. $(i-1)$, and a number fraction in the same class as the one being broken up (i).

The break-up parameterization consists of two parts, the product of the break-up probability and the collision frequency. Summarizing over the possible eddy sizes yields (as in chapter 5 the terms are defined by diameters, which can be interchanged with identical volume or mass class divisions),

$$\Omega_B(d_i, d_k) = \sum_j P_B(d_i, \lambda_j, d_k)\omega_B(d_i, \lambda_j) . \tag{6.13}$$

The collision frequency between eddies of size between λ_j and $\lambda_j + d\lambda$ and bubbles of diameter size d_i, is given as a sum of a turbulent collision and a buoyancy collision frequency contribution:

$$\omega_B(d_i, \lambda_j) = \omega_{B,t}(d_i, \lambda_j) + \omega_{B,b}(d_i, \lambda_j). \tag{6.14}$$

The turbulent collision is given by Luo & Svendsen (1996):

$$\omega_{B,t}(d_i, \lambda_j) = \frac{\pi}{4}(d_i + \lambda_j)^2 \bar{u}_{d_i, \lambda_j} n_{d_i} n_{\lambda_j}. \tag{6.15}$$

The relative velocity between the colliding bubble and turbulent eddy is expressed as:

$$\bar{u}_{d_i, \lambda_j} = (\bar{u}_{d_i}^2 + \bar{u}_{\lambda_j}^2)^{1/2}, \tag{6.16}$$

with the turbulent velocity:

$$\bar{u}_{\lambda_j} = \beta^{1/2}(\varepsilon\lambda_j)^{1/3}, \tag{6.17}$$

where β is a constant. Equation (6.17) is also used to find the turbulent velocity of the bubbles replacing the eddy length scale λ_j, with the bubble diameter d_i (Luo & Svendsen, 1996).

The buoyancy term used is based on Prince & Blanch (1990):

$$\omega_{B,b}(d_i, \lambda_j) = \frac{\pi}{4}(d_i + \lambda_j)^2 u_{a,d_i} n_{d_i} n_{\lambda_j}. \tag{6.18}$$

The relative bubble rise velocity has been approximated by the axial bubble velocity calculated from experimental data, thus assuming no eddy movement due to buoyancy effects.

The probability for obtaining one specific daughter class, as a result of a break-up of a given parent particle size, d_i, colliding with a given eddy size, λ_j, is given as the sum over the different eddy energy levels, e_l:

$$P_B(d_i, \lambda_j, d_k) = \sum_l P_B(d_i, \lambda_j, e_l, d_k)\omega(d_i, \lambda_j, e_l), \tag{6.19}$$

where $\omega(d_i, \lambda_j, e_l)$ is the fraction of eddies of size λ_j having energy level e_l. It is assumed that the turbulent kinetic energy probability distribution is

$$p_e(\chi) = \exp(-\chi), \text{ where } \chi = e(\lambda_j)/\bar{e}(\lambda_j). \tag{6.20}$$

The mean turbulent kinetic energy of an eddy with size λ_j, $\bar{e}(\lambda_j)$, was by Luo & Svendsen (1996) given as

$$\bar{e}(\lambda_j) = \frac{\pi\beta}{12}\rho_L\varepsilon^{2/3}\lambda_j^{11/3}. \tag{6.21}$$

The sum over all, *l*, fractions is equal to

$$\sum_l \omega(d_i, \lambda_j, e_l) \cong \int_{\chi_c}^{\infty} \exp(-\chi)d\chi = \exp(-\chi_c) = P_B(d_i, \lambda_j), \tag{6.22}$$

where $\chi_c = \dfrac{12\sigma}{\rho_L\beta\varepsilon^{2/3}\lambda_j^{2/3}d_{i-1}}$ for the most common situations where the energy density is the only limiting break-up criterion. When adding the eddy energy density criterion, we get $\chi_c = \dfrac{12\sigma}{\rho_L\beta\varepsilon^{2/3}\lambda_j^{2/3}d_{k,\,min}}$, where $d_{k,\,min} = \sigma\pi\lambda_j^3/e(\lambda_j)$. $P_B(d_i, \lambda_j)$ is the probability for breaking up a bubble of diameter d_i when hit by a turbulent eddy of diameter λ_j.

The sum of the daughter class probability distribution yields:

$$\sum_k P_B(d_i, \lambda_j, e_l, d_k) = 1. \tag{6.23}$$

The probability distribution, $P_B(d_i, \lambda_j, e_l, d_k)$, can be expressed in terms of a normalized product of two functions related to the two break-up criteria. The two functions are assumed to be independent, giving:

$$P_B(d_i, \lambda_j, e_l, d_k) = \overline{F_s F_d}. \tag{6.24}$$

The function related to break-up due to the turbulent kinetic energy of an eddy (the surface criterion) may be written as (non-normalized version of $P_s(d_i, d_k)$ in chapter 5)

$$F_s(d_i, d_k) = max\left[e(\lambda_j) - \pi\sigma d_i^2 \left[\frac{d_k^2}{d_i^2} + \left(1 - \frac{d_k^3}{d_i^3} \right)^{2/3} - 1 \right], 0 \right], \qquad (6.25)$$

where the first term on the right hand side is the turbulent kinetic energy of the eddy. The function related to break-up due to the energy density causing breakage into a smallest daughter volume size, ϑ_k, (the energy density criterion) may be written as (non-normalized version of $P_d(d_k)$ in chapter 5)

$$F_d(d_k) = max\left[\frac{e(\lambda_j)}{\frac{4}{3}\pi(\lambda_j/2)^3} - 6\sigma/d_k, 0 \right]. \qquad (6.26)$$

The continuous function (6.24) is integrated numerically between each population balance class, and the moment (weighted average) is also found. The integral is then split by using the weighted average between the lower and upper limiting classes giving the $P_B(d_i, \lambda_j, e_l, d_k)$ values, see Hagesaether *et al.* (2001).

Secondly, we consider the coalescence parameterizations and discuss how to adjust the resulting, or merged, particle size to the prescribed population size discretization scheme. In the simple case when two particles of equal volume coalesce, the resulting particle will be of one class higher than the two colliding particles. Thus,

$$\vartheta_i + \vartheta_i \rightarrow \vartheta_{i+1}. \qquad (6.27)$$

Note that this is only true if we use the factor 2 between the volume (or mass) classes, see (6.4). When two unequal sized particles collide, the coalesced particles will be of a size larger than the largest colliding particle, but smaller than the class above the largest particle. Thus, for such a collision the resulting particle will always be placed in the same class as the largest particle and the class above it. When using a factor lower than 2 between the classes, see (6.4), this may not be the case. If we assume *i* to be the largest of the two particles colliding, we get by using (6.7), converting to volume, and using (6.4):

$$\vartheta_i + \vartheta_j = x_{i,j}\vartheta_i + (1 - x_{i,j})\vartheta_{i+1} = (x_{i,j}2^{i-1} + (1 - x_{i,j})2^i)\vartheta_1 . \quad (6.28)$$

We may also express the two colliding particles as multiples of the class 1 size,

$$\vartheta_i + \vartheta_j = (2^{i-1} + 2^{j-1})\vartheta_1 . \quad (6.29)$$

Combining (6.28) and (6.29) gives:

$$x_{i,j} = 1 - 2^{j-i} , \; i \geq j , \quad (6.30)$$

where $x_{i,j}$ is the number fraction in class *i* and $(1 - x_{i,j})$ is the number fraction in class *i+1*.

The coalescence rate is also a product of two parts, the coalescence probability and the collision frequency:

$$\Omega_C(d_i, d_j) = P_C(d_i, d_j) \cdot \omega_C(d_i, d_j) , \quad (6.31)$$

where the collision rate, Saffman & Turner (1956), may be written as

$$\omega_C(d_i, d_j) = \frac{\pi}{4}(d_i + d_j)^2 n_{d_i} n_{d_j} \bar{u}_{d_i, d_j} \text{ with } \bar{u}_{d_i, d_j} = (\bar{u}^2_{d_i} + \bar{u}^2_{d_j})^{1/2} . \quad (6.32)$$

In the extended model the collision rate is expressed as the sum of contributions of two different physical mechanisms:

$$\omega_C(d_i, d_j) = \omega_{C,t}(d_i, d_j) + \omega_{C,b}(d_i, d_j) , \quad (6.33)$$

which are the turbulent collision frequency (as in (6.32)) and the buoyancy collision frequency, respectively. The latter is based on Prince & Blanch (1990):

$$\omega_{C,b}(d_i, d_j) = \frac{\pi}{4}(d_i + d_j)^2 \left| u_{a,d_i} - u_{a,d_j} \right| n_{d_i} n_{d_j} . \quad (6.34)$$

Again the measured axial bubble velocities have been used.

The coalescence efficiency is given as $P_C = \exp(-t_c / t_i)$ by Coulaloglou & Tavlarides (1977). Luo (1993) found the coalescence and interaction time scales and expressed the probability as

$$P_C(d_i, d_j) = \exp\left\{-C_1 \frac{[0.75(1+\xi_{ij}^2)(1+\xi_{ij}^3)]^{0.5}}{(\rho_G/\rho_L+\gamma)^{1/2}(1+\xi_{ij})^3} We_{ij}^{1/2}\right\}, \text{ where}$$

$$We_{ij} = \rho_L d_i \bar{u}^2_{d_i, d_j}/\sigma. \tag{6.35}$$

The breakage model (6.14) and the coalescence model (6.31) give the source terms in (6.3). The source terms may be written, assuming no break-up of the smallest class, $(i = 1)$, and no coalescence in the largest class, $(i = N)$, as:

$$B_B(i) = \sum_{k=i+1, i\neq N}^{N} \Omega_B(d_k, d_i) + \sum_{k=1, i\neq N}^{i} x_{i+1,k}\Omega_B(d_{i+1}, d_k) + \sum_{k=1, i\neq 1}^{i-1} (1-x_{i,k})\Omega_B(d_i, d_k)$$

$$i = 1 \,..\, \mathrm{N}, \tag{6.36}$$

corresponding to the three terms on the right hand side in (6.12), respectively.

$$D_B(i) = \sum_{k=1}^{i-1} \Omega_B(d_i, d_k),\ i = 2 \,..\, \mathrm{N}, \tag{6.37}$$

corresponding to the left hand side term in (6.12).

$$B_C(i) = \sum_{j=1, i\neq N}^{i-1} x_{i,j}\Omega_C(d_i, d_j) + \sum_{j=1}^{i-1} (1-x_{i-1,j})\Omega_C(d_{i-1}, d_j),\ i = 2 \,..\, \mathrm{N}, \tag{6.38}$$

corresponding to the terms on the right hand side in (6.28), respectively.

$$D_C(i) = \sum_{j=1}^{N-1} \Omega_C(d_i, d_j) + \Omega_C(d_i, d_i), \; i = 1 \,..\, \text{N-1}, \tag{6.39}$$

similarly corresponding to the terms on the left hand side in (6.28). The source terms are further explained in appendix A.

6.3 Numerical methods

The time discretization of the basic balance equations is performed by use of the fractional time step method that has become very popular in geophysical sciences, e.g. Berge & Jakobsen (1998). The fractional step concept is more a generic approach than a particular method. It is essentially an approximate factorization of the various numerical operators determining the transport equation. It is also possible to split the convective and diffusive terms further into their components in the various coordinate directions. Strang (1968) pointed out that the accuracy of such splitting methods depends both on the accuracy of the numerical solution methods applied to the individual operators in the equations, and on the accuracy of the time splitting procedure itself. By performing the intermediate time integrations in a prescribed order, the splitting method itself can be shown to be second order accurate in time. Therefore, when the individual operators applied are second order (or higher order) in time, the total time integration procedure will be second order accurate.

The various transport, source and sink terms in the balance equations have accordingly been split into separate numerical operators that are successively solved by intermediate time integrations. The convective terms are calculated by use of an explicit second order method in space, a conservative Total Variation Diminishing (TVD) scheme. The TVD scheme applied was constructed by combining the central difference scheme and the classical upwind scheme by adopting the ‘smoothness monitor’ of van Leer (1974) and the Superbee limiter of Roe (1986), see also Sweby (1984) and Le Veque (1990). An Euler explicit advancement is applied for the individual source terms. This approach is by definition modular, and the balance equations can easily be implemented in any consistent CFD code.

6.4 Model validation

For model validation the simulations were run for the air/water system with data: ρ_L = 998 kg/m^3, σ = 0.0726 N/m, ε = 0.25 m^2/s^3 and α_G = 0.025. The superficial gas velocity was 2 cm/s and the water was stagnant. The bubbles were divided into 14 classes ranging from 0.75 *mm* to about 1.5 *cm* in diameter (each class twice the volume (or mass) of the class below). The column used was 4.3 *m* high with an inner diameter of 0.288 *m*. The bubble size and the axial velocity were measured with a five point conductivity probe at two axial levels in the column (Buchholz, Zakrzewski & Schugerl, 1981). We have here used measured data obtained at the centre of the column at axial levels 0.3 *m* and 2.0 *m* above the distribution plate in the bottom of the column.

The number of particles given in table 6.1 and 6.2, characteristic for each volume averaged particle size, are time averaged over an interval of about 10 minutes.

Table 6.1 on page 163 gives the measured number values and bubble diameters at the position 0.3 *m* above the inlet. The measured data that were originally divided into 24 discrete particle classes by the data interpretation procedures, have been adjusted to the 14 prescribed population particle classes used in the simulations in accordance with equation (6.7).

TABLE 6.1: First two columns give the numbers of particles measured and their sizes measured respectively. The last two columns give the numbers and sizes used in the simulation. The experimental data was measured at 0.3 *m* above the gas inlet in the centre of the column.

measured number	measured bubble diameter	adjusted number	adjusted bubble diameter
300	0.82	208	0.750
424	1.26	92	0.945
429	1.77	345	1.19
490	2.26	232	1.50
468	2.76	418	1.89
393	3.25	555	2.38
287	3.73	570	3.00
171	4.21	480	3.78
91	4.74	208	4.76

TABLE 6.1: First two columns give the numbers of particles measured and their sizes measured respectively. The last two columns give the numbers and sizes used in the simulation. The experimental data was measured at 0.3 *m* above the gas inlet in the centre of the column.

measured number	measured bubble diameter	adjusted number	adjusted bubble diameter
66	5.25	77	6.00
37	5.70	28	7.56
21	6.24	12.1	9.52
12	6.79	5.84	12.00
11	7.18	1.37	15.12
5	7.78		
5	8.12		
5	8.63		
4	9.19		
2	9.65		
4	10.74		
3	11.58		
1	12.88		
1	13.18		
1	14.61		

Table 6.2 on page 165 gives the corresponding data at the position 2.0 *m* above the inlet, as well as the measured axial velocities. The axial velocities based on volume (or mass) were transformed to the population classes used, requiring that the resulting particle velocities were consistent with the measured mass flux. The axial velocities measured at 2.0 *m* above the inlet were used as fixed rise velocities for the individual population classes through the column. Similar data were also meas-

ured at 0.3 *m* above the inlet, but we have as a first approach used the data from 2.0 *m* above the inlet only.

TABLE 6.2: First three columns give the numbers of particles measured, their sizes measured and their axial velocity measured respectively. The last three columns give the numbers, sizes and axial velocities used in the simulation. The experimental data was measured at 2.0 *m* above the gas inlet in the centre of the column.

measured number	measured bubble diameter	measured axial velocity	adjusted number	adjusted bubble diameter	adjusted axial velocity
405	0.82	0.25	343	0.750	0.25
670	1.28	0.33	62	0.945	0.25
739	1.76	0.40	605	1.19	0.33
814	2.26	0.45	489	1.50	0.39
760	2.76	0.50	714	1.89	0.43
585	3.24	0.53	890	2.38	0.48
400	3.73	0.54	926	3.00	0.52
246	4.25	0.57	563	3.78	0.55
133	4.73	0.60	255	4.76	0.61
80	5.22	0.62	93	6.00	0.63
59	5.72	0.68	18.8	7.56	0.62
37	6.24	0.61	4.76	9.52	0.70
8	6.64	0.61	1.33	12.00	0.86
12	7.27	0.62	0.53	15.12	1.37
7	7.69	0.52			
3	8.17	0.79			
2	8.91	0.74			
2	9.78	0.86			
2	9.56	0.49			
1	12.22	0.58			
1	14.42	1.37			

Compressibility effects are not accounted for by the model, thus the simulations do not take into account the volumetric increase in bubble size as the pressure decreases toward the top of the column. Therefore, the data measured at level 2.0 *m* above the inlet have been adjusted, subtracting the volume effect due to the pres-

sure change, in accordance with the ideal gas law. The experimental diameter classes are thus multiplied with $(P_{2.0}/P_{0.3})^{1/3} \sim 0.96$.

The measured number data must fulfill the global volume balance over the calculation domain,

$$Q = u_s A, \tag{6.40}$$

where u_s is the superficial gas velocity and A is the column cross section. For each population class the corresponding balance is,

$$Q_i = n_i \vartheta_i u_{a,\,d_i} A, \tag{6.41}$$

where $u_{a,\,d_i}$ is the axial velocity for bubble class *i*. Combining (6.40) and (6.41) gives

$$u_s = \sum_i n_i \vartheta_i u_{a,\,d_i}. \tag{6.42}$$

The measured data at 0.3 *m*, must be converted into inlet number densities, assuming a linear relationship gives

$$n_i = x\tilde{n}_i, \tag{6.43}$$

where $\tilde{n}_i$ is the measured number values (given in tables 6.1 and 6.2). Combining (6.42) and (6.43), solving for x and inserting for x in (6.43) gives

$$n_i = (\tilde{n}_i u_s)/\sum_i (\tilde{n}_i \vartheta_i u_{a,\,d_i}). \tag{6.44}$$

The data have thus been normalized to be consistent with the volume (or mass) flux at the inlet.

The average gas phase velocity is calculated from the following formula

$$u_{average} = \sum_i (u_i n_i \vartheta_i)/\sum_i (n_i \vartheta_i). \tag{6.45}$$

6.5 Multi-fluid modeling

The present one-dimensional model, having a constant turbulent dissipation rate, can easily be extended to two- and three-dimensional cases where the dissipation fields are non-constant by adding transport equations for turbulent quantities like the turbulent energy dissipation rate (e.g., a $k-\varepsilon$ model). That is, the full two-fluid model equations have to be solved.

In the churn-turbulent flow regime there are up to four different flow regions; descending flow, vortical-spiral flow, fast bubble flow and central plume, see Chen, Reese & Fan (1994). Furthermore, shapes and velocities for the dispersed phase will vary in the various regions, and in addition to turbulent break-up, turbulent collisions and buoyancy driven collisions between bubbles, dense flow mechanisms should also be included. Among these mechanisms are the swarming effects in the fast bubble flow regime. The present model can be used describing industrial bubble columns operating in the churn-turbulent flow regime, introducing drag and Sauter mean particle diameter variables to account for shape effects. The shape of the fluid particles varies significantly within the wider size distribution. This significantly influences the interfacial drag, heat- and mass-transfer fluxes. An alternative is to extend the model using shape factors.

When using a multi-fluid model proper boundary conditions are needed, e.g. for phasic velocities, volume fractions and bubble size, as discussed by Jakobsen (1993). Normally it is assumed that the gas does not wet the wall indicating that the gas volume fraction there is zero. By using the time-after volume averaging procedure the diffusive mass flux through the wall is set to zero by adopting the boundary condition that the normal volume fraction gradient is equal to zero. This is clearly not a physical condition and mass weighted velocity variables should therefore be used, as discussed by Jakobsen (2001). The particle size distribution obtained just above the distribution plate is very difficult to determine. The current practice is to assume physically reasonable and uniform bubble size and shape distributions, and an approximate gas volume fraction (and thus a given phasic velocity or visa versa). A proper analysis on micro scale determining the Lagrangian particle distribution should be used developing proper relations for the inlet boundary value of the gas volume fraction and particle size distribution. Introductory analyses was performed by Grevskott (1997). However, the flow pattern is usually not very sensitive to inlet boundary conditions, whereas the interfacial heat and mass transfer fluxes can be notably affected. This dependents on the break-up and coalescence rates. At high rates the dynamic equilibrium will be

reached close to the inlet boundary, and the transfer fluxes will in this case be insignificantly affected by the chosen inlet gas phase size distribution. At the outlet, the normal gradients are usually set to zero both for the gas volume fraction and the number densities. The radial velocity component is also set to zero. This approach is questionable as the physical flow pattern is turbulent and recirculating zones exists in this part of the column. Further, the pressure is normally specified at the outlet. An alternative to the pressure boundary condition is to specify that the axial velocity gradient is zero at the outlet, but this often reduces the convergence rate considerably.

6.6 Results and discussion

The basic population model used here is the same as the one used by Hagesaether *et al.* (2000). An extended version of the parameterization scheme for particle breakage developed by Hagesaether *et al.* (2001) combined with a modification of the particle-particle collision frequency relation given by Prince & Blanch (1990) have also been investigated.

In all simulations the local and global mass and bubble number budgets were calculated by integrating the convective fluxes in and out of the boundaries, and the death and birth rates within the calculation domain. The discrepancies in all balances were found to be of order close to the machine number representation.

The behavior of the population model using two different versions of the break-up parameterization scheme, applied to a bubble column is discussed in the following, using the system data given in the previous section. The bubble rise velocities for the various classes were taken as the experimentally measured axial velocities at 2.0 *m* above the inlet of the bubble column. This means that the liquid velocity profile was indirectly taken into account. The integration time step used in the calculations was generally 0.001 seconds with the *extended break-up model* included, and 0.005 seconds with the *basic model* of Luo (1993) and Luo & Svendsen (1996). The total simulation time was set to 100 seconds, which was more than enough to obtain steady state conditions. If a larger time step was used with the extended break-up model, the model gave rise to oscillations in the resulting profiles for some of the classes. In space, 32 axial grid cells were used for the calculation domain between 0.3 *m* and 2.0 *m* above the column inlet.

Figure 6.1 shows the bubble distribution for the basic model as log(n) versus the height of the bubble column. In general, it can be seen that the bubble number den-

sity at position 2.0 *m* increases slowly towards population class 9. After class 9, the bubble density decreases with bubble size. Based on physical observations, it is expected that the lowest and the highest population classes will contain very few bubbles if the prescribed bubble mass (or volume) range is wide enough. If this is not the case, the assumption of no break-up of the lowest class and no coalescence of the highest class will influence the results and the prescribed size range has to be extended.

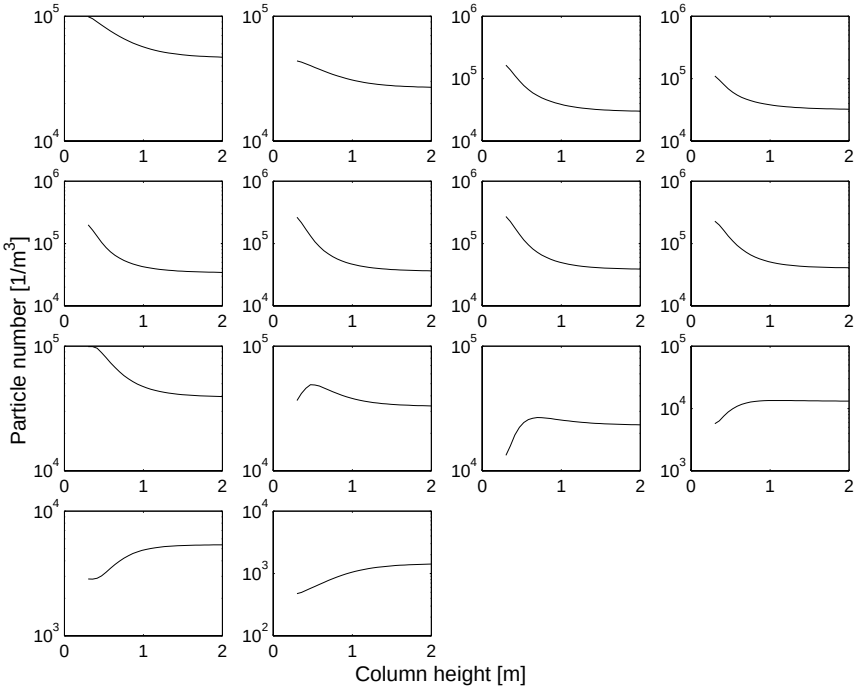

FIGURE 6.1: Steady state distribution between the two experimental measuring points in the bubble column. The 14 bubble classes, ranging from 0.75 *mm* to about 1.5 *cm* in diameter, are shown by rows from top left. Model for break-up, Luo & Svendsen (1996), and coalescence, Luo (1993).

For the basic break-up model by Luo & Svendsen (1996), the predicted particle density distribution is given in figure 6.1. The requirement that the prescribed range of population classes should not affect the simulated results was then evaluated by including 3 additional population classes being smaller than the previous

class 1, in a second simulation. The model results from the second simulation, figure 6.2, show that the mass of gas is further distributed to the lower population classes. Thus the model predictions are not independent of the prescribed population class range. The number densities in the extra classes are about the same as in the original population classes. Another test, not shown in this work, includes 12 extra classes below class 1. This test also showed a very gradual decrease of the number densities as the classes got smaller. The smallest additional class had about 10% of the number density of class 1 in the basic setup. Examining the measured data we find a sharp decrease in the number densities for bubble size classes smaller than about 0.5-1 *mm*. It should, however, be noted that the measuring technique applied has an inherent lower limit of about 0.5-1 *mm* for detecting bubbles. It may therefore have been smaller bubbles in the column, but the observed trend that there is a marked decrease in the number densities for very small bubbles is believed to be physically realistic.

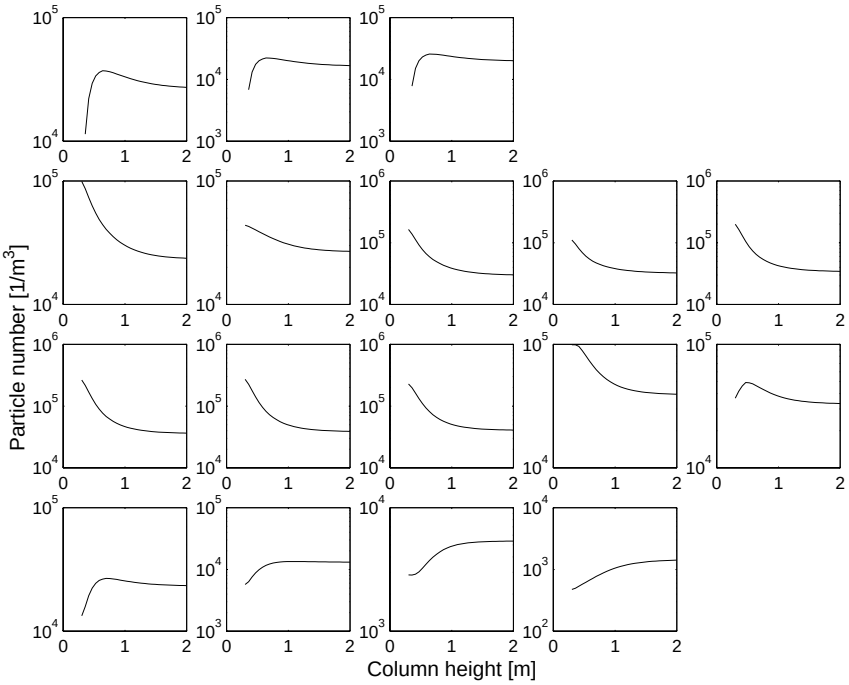

FIGURE 6.2: Steady state distribution between the two experimental measuring points in the bubble column. The 17 bubble classes, ranging from 0.375 *mm* to about 1.5 *cm* in diameter, are shown by rows from top left. The first row contains 3 extra classes which are added below the experimentally measured bubble sizes. Model for break-up, Luo & Svendsen (1996), and coalescence, Luo (1993).

The magnitude of the source terms determining the birth and death rates due to bubble coalescence and break-up are shown in figure 6.3, as predicted by the basic model. A general trend that the magnitude of the terms decrease from the entrance boundary at 0.3 *m* above the column inlet towards the outlet boundary at 2.0 *m* above the column inlet, is observed. The magnitude of the source terms due to coalescence are initially relatively large with a maximum for class 9, but the magnitude decreases rapidly within a region of about 0.6 *m*. This is consistent with the results shown in figure 6.1, indicating that steady state for the bubble distribution is nearly reached after about 0.6 *m* above the inlet boundary. Comparing the corresponding profiles from figures 6.1 and 6.2, it can be seen that the particle density

profiles are hardly influenced by the population classes added in the second simulation. Only the first class seem to have been significantly altered by the addition of the 3 extra classes.

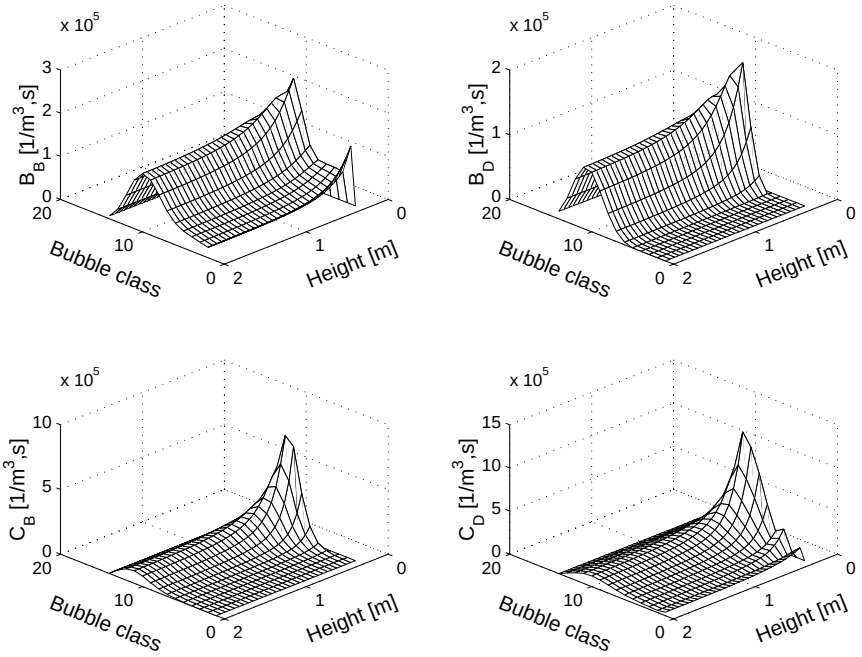

FIGURE 6.3: Steady state values of the source terms, B_B, B_D, C_B and C_D, in the transport equation (6.3). Model for break-up, Luo & Svendsen (1996), and coalescence, Luo (1993).

The results obtained by the basic model are not independent of the prescribed population class range in regard to the total number density of bubbles. Though, as each class is twice the volume of the class below the volume (or mass) distribution is changed insignificantly with the addition of more classes at the lower end of the population class distribution.

Figure 6.4 shows a comparison of the corresponding experimental and the basic model simulated accumulated mass profiles for the gas phase, normalized by the total amount of bubble mass found experimentally at 2.0 *m*. It is seen that there is

a much higher fraction of smaller bubbles found in the experimental data. The simulated total volume is about 72% of the experimental one. The deviation is related to the inaccurate predictions of the bubble size distribution. The larger bubbles have a higher terminal velocity relative to the smaller ones, indicating that a higher fraction of larger bubbles will give rise to lower gas hold-up.

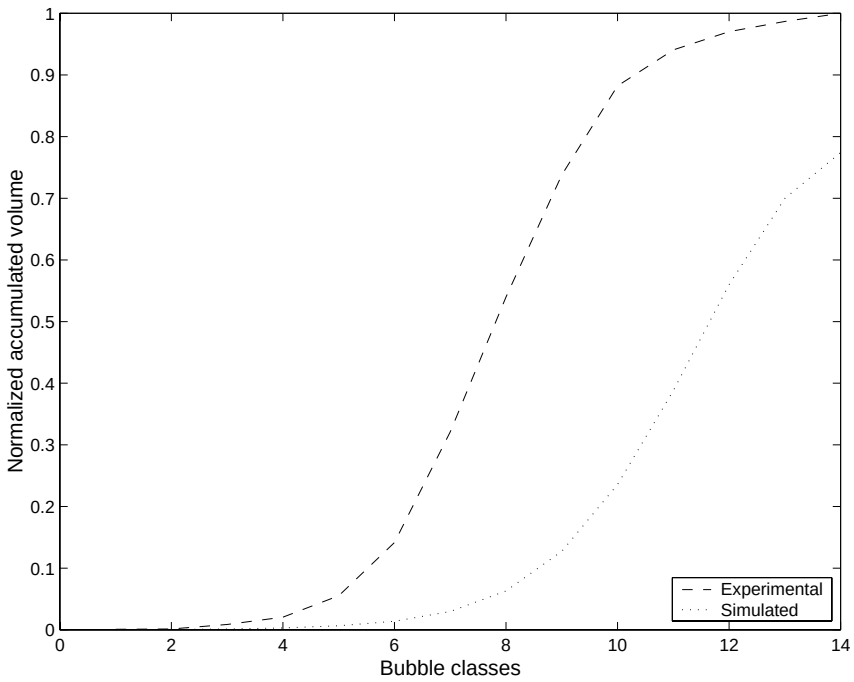

FIGURE 6.4: Accumulated mass (or volume) as a function of bubble class at 2.0 *m* height in the bubble column. Both experimentally measured values and simulated values are shown. Model for break-up, Luo & Svendsen (1996), and coalescence, Luo (1993).

To improve on the model predictions for the bubble size distribution, the model changes suggested by Hagesaether *et al*. (2001) have been implemented as well as the modified formulation of the particle-particle collision frequency of Prince & Blanch (1990). The results obtained based on the extended model are presented in figure 6.5.

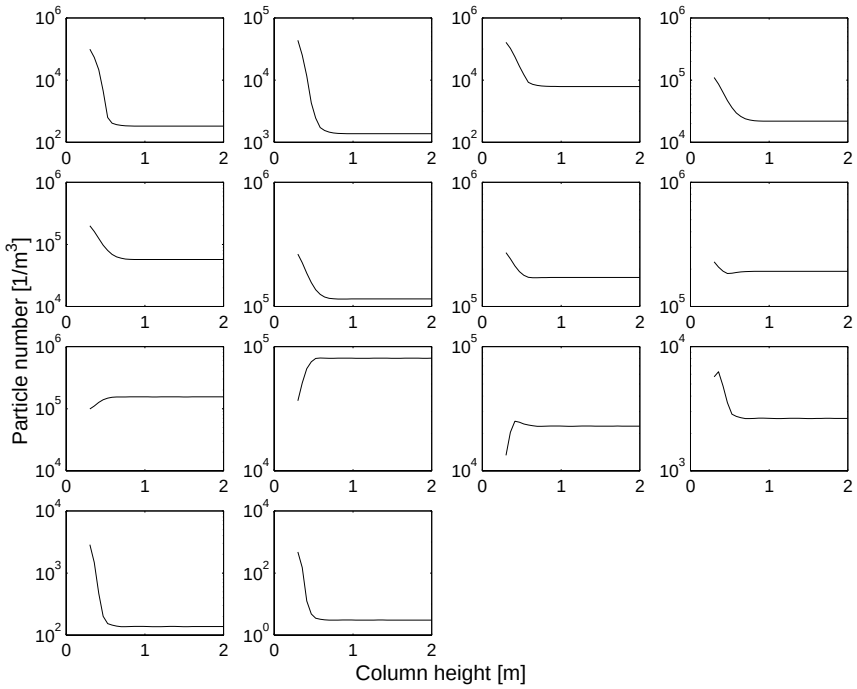

FIGURE 6.5: Steady state distribution between the two experimental measuring points in the bubble column. The 14 bubble classes, ranging from 0.75 *mm* to 1.5 *cm* in diameter, are shown by rows from top left. Break-up model by Hagesaether *et al.* (2001) and coalescence model by Luo (1993).

These profiles correspond to the results shown in figure 6.1. Comparing the results presented in the two figures, it can be seen that the extended model version predicts a stabilization of the size distribution of bubbles within a shorter zone after the entrance to the calculation domain. This indicates that the source terms are larger in the extended parameterization. After about 0.3 *m* above the simulation inlet, about 0.6 *m* height in the reactor, steady state is reached for the bubble number density distribution. For the smallest population classes the number densities predicted by the extended parameterization deviates more compared to the experimental data than the results predicted by the model by Luo (1993), but the results predicted by the extended model are in better agreement with the experimental data for the size classes in the middle of the population class range.

The results from adding 3 population classes at the lower end of the population class range for the extended model version are given in figure 6.6.

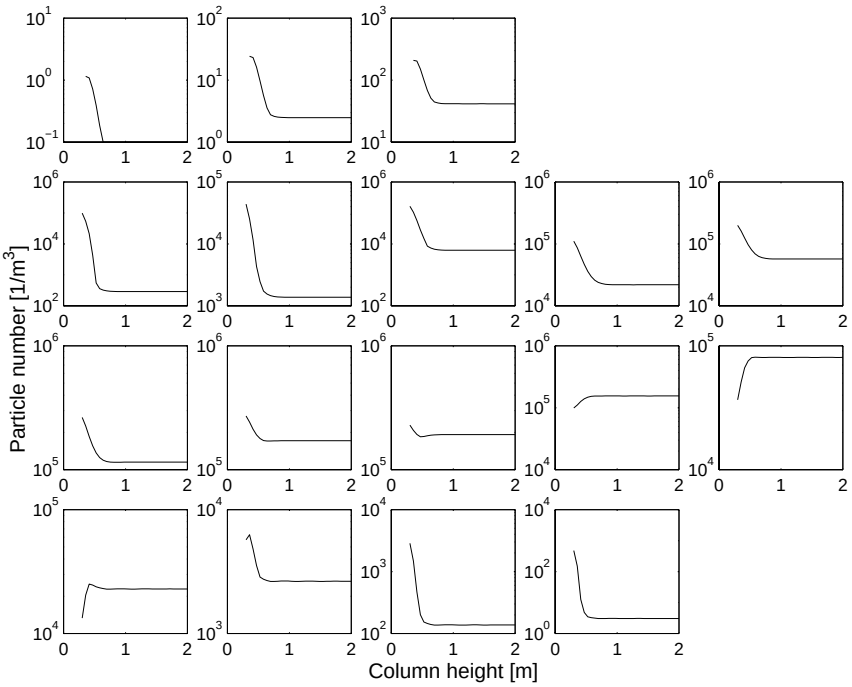

FIGURE 6.6: Steady state distribution between the two experimental measuring points in the bubble column. The 17 bubble classes, ranging from 0.375 *mm* to 1.5 *cm* in diameter, are shown by rows from top left. The first row contains 3 extra classes which are added below the experimentally measured bubble sizes. Break-up model by Hagesaether *et al*. (2001) and coalescence model by Luo (1993).

As expected, contrary to the results predicted by the original model the extended model predicts profiles having a sharp drop in the bubble number density toward the lower classes. The trend observed in these profiles is a result of the energy density criterion in the bubble break-up parameterization scheme stating that a daughter bubble can at most have an energy density equal to the colliding eddy. Thus, the extended model is based on an inherent assumption that for each colliding eddy there is a minimum size limit for the bubble that can break-up and that there is a

minimum size for the smallest daughter size fragment being generated in the break-up process.

Figure 6.7, which is the analogue to figure 6.3, shows the source terms based on the extended parameterization scheme. The break-up terms predicted by this model version are much larger than the corresponding ones predicted by the previous model. This is due to the removal of a break-up criterion used by Luo & Svendsen (1996), stating that the eddy must be equal or smaller than the colliding bubble in order to induce break-up, as discussed by Hagesaether *et al*. (2001).

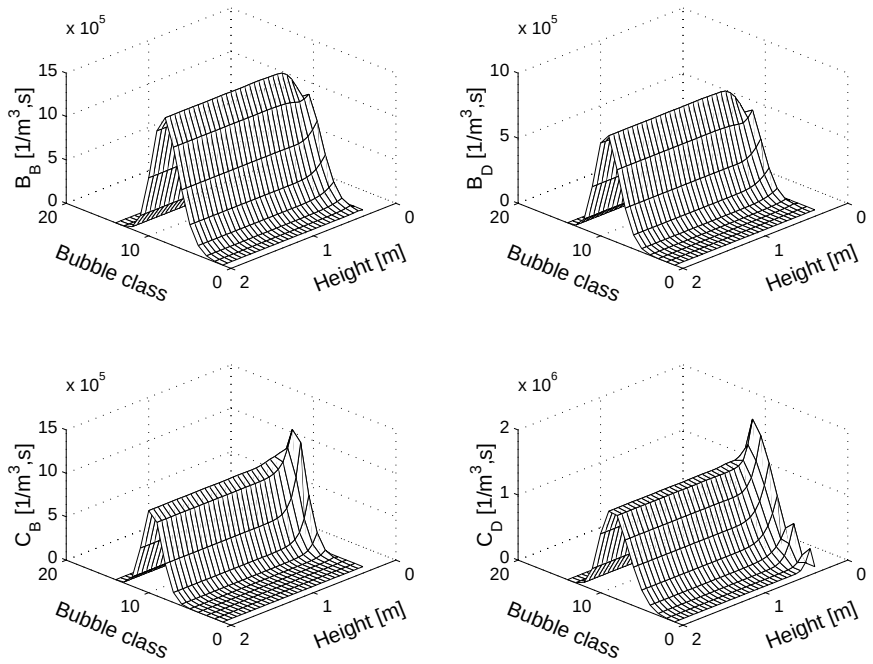

FIGURE 6.7: Steady state values of the source terms, B_B, B_D, C_B and C_D, in the transport equation (6.3). Break-up model by Hagesaether *et al.* (2001) and coalescence model by Luo (1993).

The accumulated mass (or volume) predicted by the extended model at steady state for the bubble distribution, is shown in figure 6.8. Comparing the results presented in figures 6.4 and 6.8, it is seen that the extended model predictions are in much better agreement with the experimental data than what was obtained by the former

model. As seen from the figure, there are too few particles in the smaller classes whereas a better fit is obtained for the population classes in the middle of the population size range. The predicted volume fraction is now increased to about 96% of the experimentally measured one, without introducing any additional model parameters. The extended model formulation thus seems to provide better estimated for the interfacial heat-, mass-, and momentum transfer fluxes, compared to the previous one (Luo (1993) and Luo & svendsen (1996)).

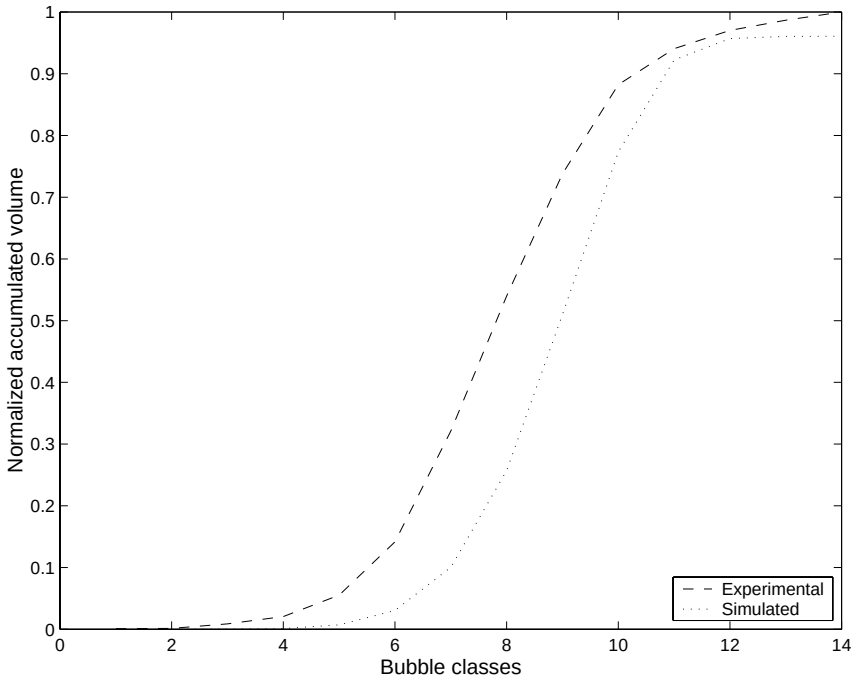

FIGURE 6.8: Accumulated mass (or volume) as a function of bubble class at 2.0 *m* height in the bubble column. Both experimentally measured values and simulated values are shown. Break-up model by Hagesaether *et al*. (2001) and coalescence model by Luo (1993).

Another test was performed in order to check if the break-up parameterization scheme solely could be the reason for the low number density in the smaller population classes. The coalescence model was in this test turned off for the lowest 5 classes. This modification resulted in number density predictions well above the

experimental levels for these classes, as shown in figure 6.9. It thus seems that the coalescence model predicts too high coalescence probabilities for collisions within the smallest bubble classes.

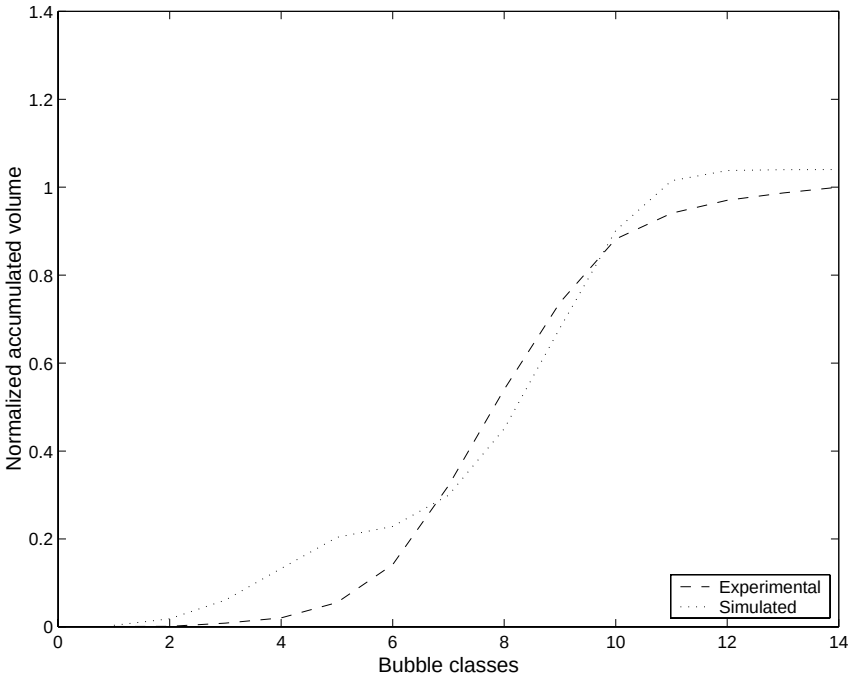

FIGURE 6.9: Accumulated mass (or volume) as a function of bubble class at 2.0 *m* height in the bubble column. Both experimentally measured values and simulated values are shown. Break-up model by Hagesaether *et al*. (2001) and coalescence model by Luo (1993). The coalescence terms are set to zero for the first 5 classes.

For all models considered the turbulent energy dissipation rate was set as a model parameter fixed at a prescribed value, which was estimated based on the experimental conditions. It is though known that the energy dissipation in a bubble column varies as a function of axial position, e.g. Grevskott, Sannaes, Dudukovic, Hjarbo & Svendsen (1996). As a parameter sensitivity analysis, the turbulent energy dissipation rate was changed from 0.25 m^2/s^3 to 0.40 m^2/s^3, and the results obtained with the modified parameter value are shown in figure 6.10. It can be seen from the figure that the void fraction for the simulation becomes approx-

imately the same as the experimental one. In this simulation there are still too few bubbles in the lowest population classes, but the agreement with experimental data is better.

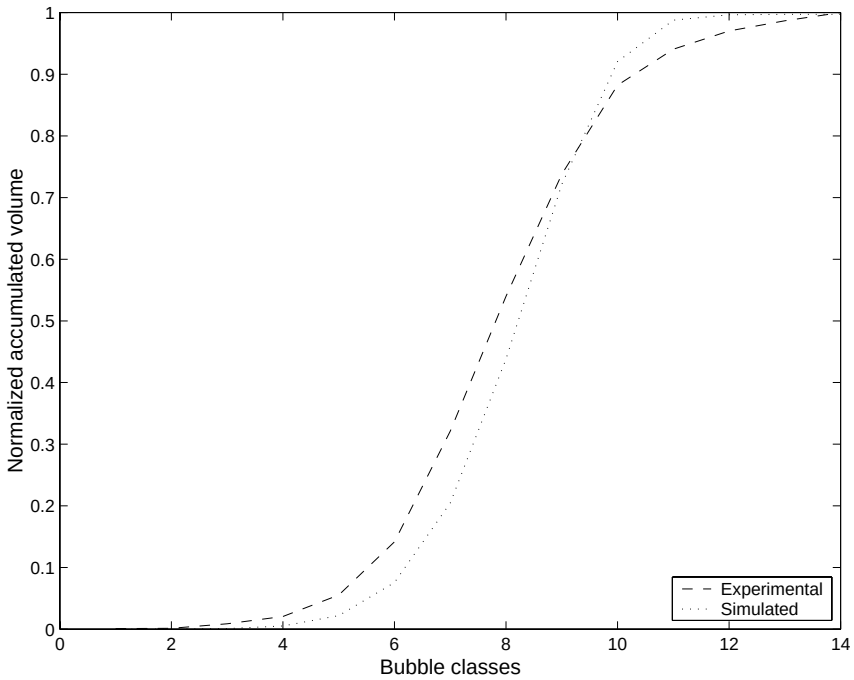

FIGURE 6.10: Accumulated mass (or volume) as a function of bubble class at 2.0 *m* height in the bubble column. Both experimentally measured values and simulated values are shown. Break-up model by Hagesaether *et al*. (2001) and coalescence model by Luo (1993). The eddy dissipation rate was changed to 0.40 m^2/s^3 (default was 0.25 m^2/s^3).

In a few recent papers, Jakobsen (2001), Krishna, Urseanu, van Baten & Ellenberger (1999a), Krishna, Urseanu, van Baten & Ellenberger (1999b), Krishna, van Baten & Urseanu (2000) and Krishna, van Baten & Urseanu (2001), the interaction between the interfacial drag and the dispersed phase distribution has been discussed. For relatively high gas void fraction flows, drag correlations based on empirical single bubble data have been found unable to predict gas velocity profiles with reasonable accuracy compared to experimental data. This has been

related to the inherent limitation that none of these drag relations do explicitly take into account the hydrodynamic bubble-liquid and bubble-bubble interaction effects. Krishna *et al*. (1999a) studied the rise velocity of a swarm of large gas bubbles in liquid by use of a multi-fluid model, empirically dividing the bubble distribution into two size classes. The small bubbles were empirically set to be in the size range of 3 to 6 *mm*, whereas the large bubbles were typically in the range of 20-80 *mm*. The CFD model predictions reported were in very good agreement with experimental data, but the model suffers from the need of empirical data for determining the bubble size distribution. In this context, our modeling approach provides a better modeling framework improving the theoretical analyzes, as it reduces the need for empirical data on the phase distribution phenomena. An analysis was performed on the capabilities of the present model for predicting a reasonable bubble number average gas phase velocity. Based on the experimental data at 2.0 *m* above the column inlet, a number averaged gas phase velocity of 0.58 *m/s* was obtained. The corresponding gas velocity calculated based on the results provided by the models of Luo (1993) and Luo & Svendsen (1996) was 0.74 *m/s*, whereas the extended model of Hagesaether *et al*. (2001) predicted a number averaged gas phase velocity of 0.60 *m/s* in good agreement with the experimental data. With the latter modeling approach it seems possible to improve the predictions of the bubble number distributions enabling better estimates on the interfacial transfer fluxes for heat-, mass- and momentum within CFD codes. However, the current break-up and coalescence parameterizations are designed for the homogeneous bubbly flow regime only. In order to extend the model to the churn turbulent flow regime, we need to account for flow regime transition mechanisms and regime specific effects such as bubble swarms. Computational time requirements is also an important issue. One simulation solving the population balance model with 14 size classes took approximately 2 hours on a SGI Origin 3800 supercomputer (on one processor). Combining the dynamic population balance model with a consistent CFD model will require large computational resources, indicating that these simulations will benefit substantially from parallelization and performance optimization of the model. Therefore, research continue in order to develop further extensions and improve the implementation of this or similar population balance model formulations within CFD codes (e.g. as is currently performed within commercial codes like CFX (Lo, 1999) and FLUENT (Sanyal, 2001)).

6.7 Conclusions

A population balance model containing coalescence and break-up parameterizations have been used to simulate the bubble size distribution within a bubble column operating in the homogeneous flow regime. The population model with two different versions of the break-up parameterization scheme, and two different coalescence rate functions, one for each break-up parameterization, have been evaluated. The models have been implemented into an in-house code and validated against experimental number distributions and particle axial velocities data.

Comparing the results obtained by the two model versions against experimental data, indicate that the extended model provides an improved description of the bubble size distribution, hold-up and thus also the volume averaged gas phase velocity.

Further validation against experimental data are needed in order to evaluate the capability of the model to predict reasonable size distributions for a variety of chemical systems and operating conditions. Furthermore, the quantitative responses due to pertubations in the coalescence rate for some of the population size classes indicate that further work may be needed on the underlying model for the coalescence parameterization in particular.

Notation

A	cross sectional area of the bubble column, m^2
B_B	birth break-up, $1/(m^3 s)$
B_C	birth coalescence, $1/(m^3 s)$
C_1	constant, $C_1 = 1$, -
D_B	death break-up, $1/(m^3 s)$
D_C	death coalescence, $1/(m^3 s)$
d_i, d_j, d_k	bubble (class) diameter, m
$d_{k,min}$	minimum daughter break-up size, m

e_l eddy energy level, J

$e(\lambda_j)$ energy in eddy of diameter size λ_j, J

$\bar{e}(\lambda_j)$ average energy level in eddy of diameter size λ_j, J

$F_s(d_i, d_k)$ function for break-up of particle d_i into smallest daughter fragment d_k due to turbulent kinetic energy in the eddy (the surface criterion), J

$F_d(d_k)$ function for break-up due to energy density into smallest daughter fragment d_k (the energy density criterion), J/m^3

$\overline{F_s F_d}$ normalized function giving the daughter size distribution, -

m_i mass of one particle in population class i, kg

m_j mass of one particle in some size class j, kg

N total number of population classes, -

n_i number density of size i, $1/m^3$

n_{d_i} number density of particles in class i, $1/m^3$

n_{λ_j} number density of eddies in diameter class λ_j, $1/m^3$

n_j number density in some size class j, $1/m^3$

$\tilde{n}_i$ number value measured experimentally

P pressure, Pa

$P_B(d_i, \lambda_j)$ break-up probability of bubble with diameter d_i being hit by eddy of size λ_j, -

$P_B(d_i, \lambda_j, d_k)$ break-up probability of a bubble with diameter d_i being hit by an eddy of size λ_j breaking up into smallest daughter fragment d_k, -

$P_B(d_i, \lambda_j, e_l, d_k)$ break-up probability of a bubble with diameter d_i being hit by

	an eddy of size λ_j with energy level e_l breaking up into a smallest daughter diameter fragment d_k, -
$P_C(d_i, d_j)$	coalescence efficiency between two bubbles of diameters d_i and d_j, -
$p_e(\chi)$	kinetic energy distribution of eddies in turbulence, -
Q	gas volume flow into the bubble column, m^3/s
Q_i	gas volume flow into the bubble column for population class *i*, m^3/s
t	time, s
t_c	coalescence time, s
t_i	coalescence interaction time, s
$\vec{u}$	velocity vector, m/s
$\vec{u}_i$	velocity vector for bubble class *i*, m/s
$\bar{u}_{d_i, d_j}$	relative velocity between bubbles of diameter sizes d_i and d_j, m/s
$\bar{u}_{d_i, \lambda_j}$	relative velocity between a bubble of diameter size d_i and an eddy of diameter size λ_j, m/s
u_{a, d_i}, u_{a, d_i}	axial velocity of bubbles in diameter classes *i* and *j*, m/s
$u_{average}$	average gas velocity in column, m/s
u_i	bubble class velocity, m/s
u_s	superficial gas velocity, m/s
$\bar{u}_{d_i}$, $\bar{u}_{d_j}$	turbulent velocity of bubbles in diameter classes *i* and *j*, m/s
$\bar{u}_{\lambda_j}$	turbulent velocity for an eddy of diameter size λ_j, m/s
We_{ij}	Weber number, -

x	transformation function for conversion of measured bubble numbers into inlet number concentrations
$x_{i,j}$	number fraction for coalescence between volume class ϑ_i and volume class ϑ_j, -
$x_{i,k}$	number fraction for break-up of volume ϑ_i into smallest volume class ϑ_k, -
α	volume fraction, -
α_G	void fraction, -
β	constant, $\beta = 2.0457$, -
γ	added mass parameter, $\gamma = 0.5$, -
ε	eddy dissipation, m^2/s^3
ϑ_1	volume of the first population class, m^3
$\vartheta_i, \vartheta_j, \vartheta_k$	volume of population classes *i, j* and *k*, m^3
ϑ_j	volume of a fluid particle of size *j*, m^3
λ_j	eddy diameter class *j*, *m*
ξ_{ij}	bubble size fraction, $\xi_{ij} = \vartheta_i/\vartheta_j$, -
ρ	density, kg/m^3
ρ_G	gas density, kg/m^3
ρ_L	liquid density, kg/m^3
σ	surface tension, N/m
χ	kinetic energy fraction for eddy in turbulence, $\chi = e(\lambda_j)/\bar{e}(\lambda_j)$, -
χ_c	critical breakage energy fraction, -

$\Omega_B(d_i, d_k)$ break-up rate of class with diameter d_i into smallest daughter class with diameter d_k, $1/(m^3 s)$

$\Omega_C(d_i, d_j)$ coalescence rate between two bubbles of diameters d_i and d_j, $1/(m^3 s)$

$\omega(d_i, \lambda_j, e_l)$ fraction of eddies of diameter size λ_j having energy level e_l, -

$\omega_B(d_i, \lambda_j)$ collision frequency between bubble and eddy, $1/(m^3 s)$

$\omega_{B,b}(d_i, \lambda_j)$ buoyancy collision frequency between bubble and eddy, $1/(m^3 s)$

$\omega_{B,t}(d_i, \lambda_j)$ turbulent collision frequency between bubble and eddy, $1/(m^3 s)$

$\omega_C(d_i, d_j)$ coalescence collision rate between two bubbles of diameters d_i and d_j, $1/(m^3 s)$

$\omega_{C,b}(d_i, d_j)$ buoyancy coalescence collision rate between two bubbles of diameters d_i and d_j, $1/(m^3 s)$

$\omega_{C,t}(d_i, d_j)$ turbulent coalescence collision rate between two bubbles of diameters d_i and d_j, $1/(m^3 s)$

Indexes used:

i population balance size
i parent break-up bubble
i largest coalescence parent bubble
j largest break-up fragment
j smallest coalescence parent bubble
j random size bubble between classes *i* and *i+1*
k daughter size classes
k smallest break-up fragment
l eddy energy classes

References

Berge, E. & Jakobsen, H.A. (1998). A Regional Scale Multi-layer Model for the Calculation of Long-Term Transport and Deposition of Air Pollution in Europe. *Tellus*, **50**, 205-223.

Buchholz, R., Zakrzewski, W. & Schugerl, K. (1981). Techniques for determining the properties of bubbles in bubble columns. *Int. Chem. Eng.*, **21**, 180-187.

Chen, R.C., Reese, J. & Fan, L.-S. (1994). Flow structure in a three-dimensional bubble column and three-phase fluidized bed. *AIChE Journal*, **40**, No. 7, 1093-1104.

Coulaloglou, C.A. & Tavlarides, L.L. (1977). Description of interaction processes in agitated liquid-liquid dispersions. *Chem. Eng. Sci.*, **32**, 1289-1297.

Grevskott, S. (1997). Studies on modelling of bubble driven flows in chemical reactors. Dr.Ing. Thesis, The Norwegian Institute of Technology, Trondheim.

Grevskott, S., Sannaes, B.H., Dudukovic, M.P., Hjarbo, K.W. & Svendsen, H.F. (1996). Liquid Circulation, Bubble Size Distribution, and Solids Movement in Two- and Three-Phased Bubble Columns. *Chem. Eng. Sci.*, **51**, No. 10, 1703-1713.

Hagesaether, L., Jakobsen, H.A. & Svendsen, H.F. (2000). A coalescence and breakup module for implementation in CFD-codes. *Computer-Aided Chemical Engineering*, Elsevier Science, **8**, 367-372.

Hagesaether, L., Jakobsen, H.A. & Svendsen, H.F. (2001). A model for turbulent binary breakup of dispersed fluid particles. Accepted for publication in *Chem. Eng. Sci.*

Hounslow, M.J., Ryall, R.L. & Marshall, V.R. (1988). A Discretized Population Balance for Nucleation, Growth, and Aggregation. *AIChE Journal*, **34**, No. 11, 1821-1832.

Jakobsen, H.A. (1993). On the modelling and simulation of bubble column reactors using a two-fluid model. Dr.Ing. Thesis, The Norwegian Institute of Technology, Trondheim.

Jakobsen, H.A. (2001). Phase distribution phenomena in two-phase bubble column reactors. *Chem. Eng. Sci.*, **56**, 1049-1056.

Krishna, R., Urseanu, M.I., van Baten, J.M. & Ellenberger, J. (1999a). Rise velocity of a swarm of large gas bubbles in liquids. *Chem. Eng. Sci.*, **54**, 171-183.

Krishna, R., Urseanu, M.I., van Baten, J.M. & Ellenberger, J. (1999b). Influence of scale on the hydrodynamics of bubble columns operating in the churn-turbulent regime: experiments vs. Eulerian simulations. *Chem. Eng. Sci.*, **54**, 4903-4911.

Krishna, R., van Baten, J.M. & Urseanu, M.I. (2000). Three-Phase Eulerian simulation of bubble column reactors operating in the churn-turbulent regime: a scale up strategy. *Chem. Eng. Sci.*, **55**, 3275-3286.

Krishna, R., van Baten, J.M. & Urseanu, M.I. (2001). Scale Effects on the Hydrodynamics of Bubble Columns Operating in the Homogeneous Flow Regime. *Chem. Eng. Technol.*, **24** (5), 451-458.

Le Veque, R.J. (1990). Numerical Methods for Conservative Laws. Chapter 16, Birkhauser Verlag, Basel.

Lo, S. (1999). Application of population balance to CFD modelling of bubbly flows via the MUSIG model. CFX Technology, UK, Presented at GLS'99 in Delft, Netherlands.

Luo, H. & Svendsen, H.F. (1996). Theoretical model for drop and bubble breakup in turbulent dispersions. *AIChE Journal*, **42**, 1225-1233.

Luo, H. (1993). Coalescence, breakup and liquid circulation in bubble column reactors. Dr.Ing. Thesis, The Norwegian Institute of Technology, Trondheim.

Prince, M.J. & Blanch, H.W. (1990). Bubble Coalescence and Break-Up in Air-Sparged Bubble Columns. *AIChE Journal*, **36**, 1485-1499.

Roe, P.L. (1986). Characteristic-Based Schemes for the Euler Equations. *Ann. Rev. Fluid Mech.*, **18**, 337-365.

Saffman, P.G. & Turner, J.S. (1956). On collision of drops in turbulent clouds. *J. Fluid Mech.*, **1**, 16-30.

Sanyal, J. (2001). A Break-up and Coalescence Model for Dispersed Gas-Liquid Flows. Presented at the Fluent User's Group Meeting, Manchester, NH, USA.

Strang, G. (1968). On the Construction and Comparison of Difference Schemes. *SIAM J. Numer. Anal.*, **5**, No. 3, 506-517.

Svendsen, H.F. & Luo, H. (1996). Modeling of Approach Prosesses for Equal and Unequal sized Fluid Particles. *Can. J. Chem. Eng.*, **74,** 321-330.

Sweby, P.K. (1984). High Resolution Schemes Using Flux Limiters for Hyperbolic Conservation Laws. *SIAM J. Numer. Anal.*, **21**, No. 5, 995-1011.

van Leer, B. (1974). Towards the Ultimate Conservation Difference Scheme II. Monotonicity and Conservation Combined in a Second Order Scheme. *J. Comp. Phys.*, **14**, 361-370.

CHAPTER 7

Conclusions and recommendations for further work

7.1 General overview

The overall goal of this thesis was to improve upon the understanding of the break-up and coalescence phenomena by extending earlier models made at the department for these phenomena. The earlier break-up model was found to be dependent upon the population balance size distribution used, and no limit for the lower break-up size nor the amount of break-up existed. All these consistency problems have been removed by the inclusion of an additional break-up criterion. The coalescence model was limited to only giving the maximum collision interface radius during the collision between two fluid particles. The new model predicts both the collision radius and the film thickness as a function of time. The idea behind the binary coalescence term formulation was to use a Lagrangian momentum balance model to determine coalescence efficiency and then transform data from this micro-scale model into a coalescence model formulation suited for inclusion into a macro-scale CFD-program. A force balance model has been developed, but no clear coalescence criterion was found. Both break-up models and the existing coalescence model have been implemented into a 'CFD-code'. Simulations with the models have been compared to experimental data from our laboratory, giving a comparison between the two break-up models.

7.2 General conclusions

A review of population balance models has been written, with focus on the coalescence probability. Details for film drainage, dimpling of the film, non-ideal systems, force balances and non-ideal collisions are given. Some experimental data for the coalescence process are also reviewed. A Lagrangian momentum balance model was envisioned for coalescence probability calculations, thus giving the general layout and focus of the review.

Collision model:

A general collision model was developed accounting for the following mechanisms:

- different sized fluid particles
- exact volume formulations (new)
- damped oscillations of the particles (new)
- oscillation phase angle at contact (new)
- energy loss through dissipation (new)
- film drainage (new)

A force balance is solved for each individual particle, and the interaction between the fluid particle collision and the film drainage is calculated and used to find the shape of the particles. The film contact area and the force balance dictate the film drainage. The outputs of the model are the collision interface area and the film thickness, in addition to the length variables of each fluid particle. Generally it is found that collisions that end in rebound have a tendency to contain thicker films than collisions that coalesce, but no reliable coalescence criterion was found. The simulation of the collision interface radius and the contact time were in most cases in good agreement with experimental data.

Break-up model:

An improved fluid particle break-up model was developed. This model includes a new criterion requiring the energy density of the daughter particles generated to be less or equal to the energy density of the eddy, generating the break-up. This criterion limits the degree of break-up through limiting the lower possible size of

daughter particles. The model calculates a probability distribution for the daughter sizes, and equal sized daughter particles are favoured in most cases due to the energy density criterion which limits the rate of break-up in most cases. The other criterion, the surface energy criterion, states that the increase in surface energy due to the break-up must be less or equal to the energy available from the colliding eddy. This criterion favours unequal breakage and is most limiting when small fluid particles and small eddies collide. A criterion used in earlier models requiring eddies to be smaller in size than the fluid particle in the collision, has been removed. The theory predicts that eddies of larger sizes are important for the rate of break-up and thus also for the daughter size distribution probability.

Population balance:

Underlying algebraic models for the sink and source terms for break-up and coalescence, initially containing integral terms, have been formulated into algebraic approximations for use in a population balance. Through these terms, two different break-up models and a coalescence model have been implemented into an in-house 'CFD code'. The simulation results from the implementation were compared with experimental data from a bubble column in our laboratory. When comparing the accumulated mass for the gas phase given as a function of the bubble sizes, the new model give a closer fit to the experimental data. There are generally too few bubbles in the smallest classes, but an evaluation of the coalescence terms for these classes shows that this may as well be a result of too much coalescence as too little break-up. Overall the comparison is good. Increasing the turbulent eddy dissipation parameter results in an even closer fit to the experimental data and shows that the turbulent eddy dissipation is an important variable in the system, as expected.

7.3 Recommendations for further work

The force balance model needs to be extended, as additional mechanisms seem to be relevant. The most important ones are off centre collisions and the contact angle at collision. Currently only collisions that are head on and along the same axis are considered. For the contact angle one may use only the head-on component as an approximation, but this leaves out the physical mechanism of one fluid particle rolling off another one. This may also be the case if the collision is not

perfectly head-on. Further, a flat interface is assumed. This may be a good assumption in most relevant cases, but for verification one should solve for the film thickness as a function of the radius of the contact area.

The original scope of the model was to find a coalescence criterion. In order to try to find a coalescence criterion which is valid for all situations listed above, the surface shape for the whole particles should be solved. One should also solve for the film thickness at all contact points, and for the flow in the fluid particles themselves. In this way one may not only evaluate if the two fluid particles coalesce (if a coalescence criterion is found), but also if the coalescence is stable or not. In addition, one may be able to find some criterion for the tearing up of fluid particles, which sometimes happens when particles collide. Such simulations as described above would require much more computational time than a simple force balance, but as the force balance model itself already is too complicated for direct inclusion into a CFD-code, one may as well try to solve the collision process completely. This should probably be done in a customized CFD code.

Additional and more detailed experimental data for the collision process between two fluid particles are needed to validate the present coalescence model and future extensions. The following variables should be measured, for example by use of a high speed digital camera:

- contact area
- film thickness for the contact area
- overall particle shape (and the mass centre positions)
- flow inside the dispersed particles
- flow in the draining film
- the (induced) oscillation of the fluid particles
- the pressure field in the contact area

The impact of the following variables or phenomena should be validated:

- impact velocity
- impact angle
- impact position (off centre collisions)
- phase angles
- sizes of fluid particles
- density

- viscosity
- surface tension
- mass transfer
- heat transfer

All these variables and phenomena are likely to influence the coalescence probability and should thus be included when gathering data for the collision process.

The break-up model in the current state only applies to turbulent flow (with buoyancy included). Obviously, modifications for other flow phenomena (or combinations of flow phenomena) should be included in order to make the model more general. Further, only binary breakage is included. There are break-up processes that lead to more than two daughter particles. Such processes should be included in a more general model. For the break-up model that is applicable in a turbulent environment there are also some improvements or possible improvements that should be looked into. Most noteworthy is the assumption that prior collisions do not affect the break-up probability. This is a simplification that for low levels of turbulence has been shown to be incorrect. A possible suggestion for this is included in the thesis. Another possible improvement is the inclusion of an activated state that the fluid particle must go through in order to break up. As indicated in the thesis such an activated state would require more surface energy than both the parent particle and the combined daughter particles, thus this state should further limit the amount of break-up in some cases (when the surface energy limits the break-up rate). Further, since large eddies are shown to be important, the turbulence structure outside the inertial range should be better described.

The current version of the population balance and the source terms are limited to each class being twice the mass (or volume) of the class below. The code should be made more flexible by allowing any class division. This is more of an implementation problem as the governing equations are already given. Lastly, the CFD model used has so far only been formulated and implemented in one spatial dimension only, the model should be extended to 2D/3D.

APPENDIX A

Population balances

The primary function of this appendix is to show in detail how to calculate the source terms for break-up for the model by Luo (1993), and how the birth and death terms for break-up and coalescence are found.

A.1 Finding the population balance like equation

In order to solve a population balance model for say the different dispersed gas particle sizes in a bubble column one need to couple the population balance to the flow model for the continuous phase. Starting with the continuity equation for the dispersed phase:

$$\frac{\partial}{\partial t}(\rho\alpha) + \nabla \cdot (\rho \bar{u}\alpha) = 0 \ [kg/(m^3 s)], \tag{A.1}$$

and using the following definition for the volume fraction

$$\alpha = \sum_i n_i \frac{\pi}{6} \overline{d_{v,i}}^3 \left[\frac{\text{\# bubbles} \cdot \text{volume per average bubble}}{\text{control volume}} \right] = [-], \tag{A.2}$$

together with a Favre averaged velocity,

$$\bar{u} = \sum_i (n_i \bar{u}_i \rho \vartheta_i) / \sum_i (n_i \rho \vartheta_i), \tag{A.3}$$

this gives in analogy to population balances a transport equation for each class

$$\frac{\partial}{\partial t}\left(\rho_i n_i \overline{d_{v,i}^3} \frac{\pi}{6}\right) + \nabla \cdot \left(\rho_i \bar{u}_i n_i \overline{d_{v,i}^3} \frac{\pi}{6}\right) = S' \ [kg/(m^3 s)]. \tag{A.4}$$

In eq (A.4) above one have the source and sink terms given as S' on the right hand side. Without mass transfer between classes S' is equal to zero. From population balances one has that

$$S = [B_B - D_B + B_C - D_C] \ [1/(m^3 s)], \tag{A.5}$$

which gives

$$S' = S \vartheta_i \rho_i. \tag{A.6}$$

Combining eq (A.4) and eq (A.6) gives

$$\frac{\partial}{\partial t}(\rho_i n_i) + \nabla \cdot (\rho_i \bar{u}_i n_i) = \rho_i [B_B - D_B + B_C - D_C] \ [kg/(m^6 s)], \tag{A.7}$$

which is the equation that has to be solved together with the flow equations for the continuous phase.

A.2 Split into classes

A population balance model divides the dispersed phase into different classes according to some criteria. In this case we divide by mass, or volume since we approximate the same density in all population classes. We choose to divide the dispersed phase into classes that are exactly twice as large as the class below. This means that we split the dispersed phase which got an assumed continuous size distribution into a finite number of classes with discrete size. How to treat sizes that fall between the discrete sizes available is shown below.

When choosing that each class is twice the volume of the class below we get

$$\vartheta_2 = 2\vartheta_1, \ \vartheta_3 = 2\vartheta_2, \ldots \tag{A.8}$$

which gives

$$\vartheta_i = 2^{(i-1)}\vartheta_1 . \tag{A.9}$$

Note that the factor two between each class is not arbitrarily chosen. It will be shown later that a factor lower than two complicates the allocation of particles into classes when coalescence or break-up occurs. Further a factor higher than two will decrease the accuracy of the simulations while at the same time decrease computation time. We choose to maximize the accuracy as this is not a commercial code where computational speed needs to be optimized.

A given particle of random size must be assigned to one or more classes. When using this kind of population balance the particle is assigned to the two closest classes. The following formula is used

$$\vartheta = y\vartheta_1 = x\vartheta_i + (1-x)\vartheta_{i+1} = x2^{(i-1)}\vartheta_1 + (1-x)2^i\vartheta_1 , \tag{A.10}$$

where ϑ is the particle of random size, y is the multiplication factor to the minimum class size, x is the fraction assigned to class i and $(1-x)$ is assigned to class $(i+1)$. Notice that the number balance of particles is not changed in this operation. One particle is divided into two classes but the two classes add up to one particle and the volume balance is still satisfied. Both the number and the volume balance are kept for any class division, not just for the factor two scaling chosen in eq (A.9). Eq (A.10) is one equation with two unknowns, x and i, but is limited to $x \in [0, 1]$ which gives only one possible positive integer value for i when $x \in (0,1)$.

A.3 Break-up

Limitations in the population balance are that the smallest particle class may not be broken up and that no daughter fragment may be smaller than the smallest particle class. Further, only break-up into two daughter particles is considered. The break-up model is taken from Luo (1993) and Luo & Svendsen (1996), and is based on the arrival of turbulent eddies to the surface of the fluid particles. This brings about an increase in the surface energy through deformation, and if the increase is high enough fragmentation occurs. The model is given as

$$\overline{\Omega}_B(\vartheta_i, \vartheta_i f_{BV}) = c_3(1-\varepsilon_G)n_i\left(\frac{\varepsilon}{d_i^2}\right)^{1/3}\int_{\xi_{min}}^{1}\frac{(1+\xi)^2 e^{-\chi_C}}{\xi^{11/3}}d\xi, \qquad (A.11)$$

where

$$\chi_C = \frac{12c_f\xi^{-11/3}}{We_i},\ We_i = \rho_L d_i\overline{u_i}^2/\sigma \text{ and } c_f = f_{BV}^{2/3} + (1-f_{BV})^{2/3} - 1. \qquad (A.12)$$

For the mean turbulent velocity, $\overline{u_i}^2$, Luo uses

$$\overline{u_i} = \left(\frac{8\overline{u^2}}{3\pi}\right)^{1/2} = \left(\frac{8\bar{\beta}}{3\pi}\right)^{1/2}(\varepsilon d_i)^{1/3} = \beta^{1/2}(\varepsilon d_i)^{1/3}, \qquad (A.13)$$

where the theoretical value for $\bar{\beta}$ is 2.41 and the measured value is 2.0, Luo (1993).

The integration in eq (A.11) is not straight forward, numerically one need to use the incomplete gamma function and the gamma function to solve the integral. How to get from the integral part of eq (A.11) to a numerical implementation of it is shown below. Starting with writing out the integral part of eq (A.11) we get

$$\Omega' = \int_{\xi_{min}}^{1}\frac{(1+\xi)^2\exp\left(-\dfrac{12c_f\sigma}{\rho_L d_i(\beta^{1/2}(\varepsilon\lambda)^{1/3})^2\xi^{11/3}}\right)}{\xi^{11/3}}d\xi. \qquad (A.14)$$

The constants in the exponential part of eq (A.14) may be written as

$$\gamma' = \frac{12c_f\sigma}{\rho_L d_i\beta\varepsilon^{2/3}}, \qquad (A.15)$$

giving

$$\Omega' = \int_{\xi_{min}}^{1}\frac{(1+\xi)^2\exp\left(-\dfrac{\gamma'}{\lambda^{2/3}\xi^{11/3}}\right)}{\xi^{11/3}}d\xi. \qquad (A.16)$$

Since $\xi = \lambda / d_i$ eq (A.16) may be written as

$$\Omega' = \int_{\xi_{min}}^{1} \frac{(1+\xi)^2 \exp\left(-\frac{\gamma}{\xi^{13/3}}\right)}{\xi^{11/3}} d\xi \text{, where } \gamma = \frac{\gamma'}{d_i^{2/3}}. \tag{A.17}$$

The next step is to change the integration variable. By using $t = \gamma / \xi^{13/3}$, the derivative, which is $dt = -(13/3)(\gamma/\xi^{16/3})d\xi$, and the change of limits $\xi_{min} \sim 0 \Rightarrow t \to \infty$ and $\xi = 1 \Rightarrow t = \gamma$ we get

$$\Omega' = \int_{\infty}^{\gamma} \frac{(1+\xi)^2 e^{-t}}{\xi^{11/3}} \left(-\frac{3}{13}\xi^{16/3}\right) dt. \tag{A.18}$$

Simplifying and using that $\xi = (\gamma/t)^{3/13}$ gives

$$\Omega' = \frac{3}{13\gamma} \int_{\gamma}^{\infty} \left(1 + 2\left(\frac{\gamma}{t}\right)^{3/13} + \left(\frac{\gamma}{t}\right)^{6/13}\right)\left(\left(\frac{\gamma}{t}\right)^{3/13}\right)^{5/3} e^{-t} dt. \tag{A.19}$$

Further simplification gives

$$\Omega' = \frac{3}{13\gamma} \int_{\gamma}^{\infty} \left(\left(\frac{\gamma}{t}\right)^{5/13} + 2\left(\frac{\gamma}{t}\right)^{8/13} + \left(\frac{\gamma}{t}\right)^{11/13}\right) e^{-t} dt, \tag{A.20}$$

where each of the three integration parts may be solved with an incomplete gamma function and a gamma function both which are defined and solved in chapter 6 of Numerical Recipes, Press, Teukolsky, Vetterling & Flannery (1992). The gamma function is defined by the integral

$$\Gamma(z) = \int_{0}^{\infty} t^{z-1} e^{-t} dt, \tag{A.21}$$

and the incomplete gamma function is defined by

$$P(a,x) \equiv \frac{\gamma(a,x)}{\Gamma(a)} \equiv \frac{1}{\Gamma(a)}\int_0^x t^{a-1}e^{-t}dt\,,\ (a>0)\,. \tag{A.22}$$

The compliment of $P(a,x)$ is also confusingly called an incomplete gamma function and it is defined as

$$Q(a,x) \equiv 1 - P(a,x) \equiv \frac{\Gamma(a,x)}{\Gamma(a)} \equiv \frac{1}{\Gamma(a)}\int_x^\infty t^{a-1}e^{-t}dt\,,\ (a>0)\,. \tag{A.23}$$

Thus, the first term in (A.20) is written as

$$\Omega_1' = \frac{3}{13\gamma}\gamma^{5/13}Q\left(\frac{8}{13},\gamma\right)\Gamma\left(\frac{8}{13}\right). \tag{A.24}$$

Note that Numerical Recipes returns the natural logarithmic value of $\Gamma(a)$, thus the implementation of eq (A.24) in FORTRAN should be

$$\Omega_1' = \frac{3}{13}\gamma^{-8/13}gammq\left(\frac{8}{13},\gamma\right)\exp\left(gammln\left(\frac{8}{13}\right)\right), \tag{A.25}$$

the 2nd and 3rd term of eq (A.20) are similarly implemented. Note that the approximation $\xi_{min} \sim 0$ has been used. It is quite possible to solve the equation without this approximation, though it requires a few more gamma terms to be solved.

By using eq (A.25) it is possible to solve eq (A.11), but $\overline{\Omega}_B(\vartheta_i, \vartheta_i f_{BV})$ is only the chance of one particular fluid particle, ϑ_i, breaking up into another, $\vartheta_i f_{BV}$, and a corresponding daughter particle. Obviously the total breakage of ϑ_i may be written as the integral

$$\Omega_B(i) = \frac{1}{2}\int_0^1 \overline{\Omega}_B(\vartheta_i, \vartheta_i f_{BV})df_{BV} = \int_0^{1/2} \overline{\Omega}_B(\vartheta_i, \vartheta_i f_{BV})df_{BV}, \tag{A.26}$$

where the factor 1/2 in front of the first integral is to avoid counting each fragment twice. Due to symmetry only half of the interval need to be integrated as in the second integral in eq (A.26). Eq (A.26) may also be written as

$$\Omega_B(i) = \sum_{f_{BV}} \overline{\Omega}_B(\vartheta_i, \vartheta_i f_{BV}) \Delta f_{BV}, \tag{A.27}$$

as the $\overline{\Omega}_B(\vartheta_i, \vartheta_i f_{BV})$ values are found numerically it may seem like a good idea to use these values in order to find $\Omega_B(i)$. For $i = 1$ .. N classes the values of f_{BV} will be $f_{BV} = 0.5/i^2 = 0.5, 0.25, 0.125, 0.0625, \ldots$. These values are ill posed for the summation in eq (A.27). With few values, low N, the accuracy will obviously not be high enough. When N is large most of the f_{BV} values will be very low, i.e. ill posed for finding the summation in eq (A.27).

In our FORTRAN code we find $\Omega_B(i)$ by choosing M equidistant points between 0 and 0.5. For $M = 10$ this gives 10 values from 0.025 to 0.475. Thus

$$\Omega_B(i) = \sum_{j=1}^{10} \overline{\Omega}_B(\vartheta_i, \vartheta_i f_{BV}) \cdot 0.05 . \tag{A.28}$$

We want to transfer the continuous breakage into the discrete points ϑ_i. This is done by normalizing the discrete points to the total breakage rate, i.e. using

$$\Omega_B(\vartheta_i, \vartheta_i f_{BV}) = \frac{\overline{\Omega}_B(\vartheta_i, \vartheta_i f_{BV})}{\int_0^{1/2} \overline{\Omega}_B(\vartheta_i, \vartheta_i f_{BV}) df_{BV}} \Omega_B(i), \tag{A.29}$$

where $\overline{\Omega}_B(\vartheta_i, \vartheta_i f_{BV})$ and $\int_0^{1/2} \overline{\Omega}_B(\vartheta_i, \vartheta_i f_{BV}) df_{BV}$ are from eq (A.26) and $\Omega_B(i)$ is from eq (A.28). By using $\Omega_B(\vartheta_i, \vartheta_i f_{BV})$, also written as $\Omega_B(\vartheta_i, \vartheta_j)$, we are now able to express the breakage source terms algebraically.

A.4 Coalescence

A limitation in the population balance is that the largest particle class may not coalescence with any classes. We further limit the model to two particle coalescence. The model used is taken from Luo (1993), and is a combination of a collision frequency and a collision probability,

$$\Omega_C(\vartheta_i, \vartheta_j) = \omega_C(\vartheta_i, \vartheta_j) P_C(\vartheta_i, \vartheta_j). \tag{A.30}$$

The coalescence probability is expressed as

$$P_C(\vartheta_i, \vartheta_j) = \exp\left\{-c_1 \frac{[0.75(1+\xi_{ij}^2)(1+\xi_{ij}^3)]^{1/2}}{(\rho_G/\rho_L+\gamma)^{1/2}(1+\xi_{ij})^3} We_{ij}^{1/2}\right\}, \tag{A.31}$$

where

$$We_{ij} = \rho_L d_i \overline{u_{ij}}^2/\sigma \text{ and } \overline{u_{ij}} = (\overline{u_i}^2 + \overline{u_j}^2)^{1/2}. \tag{A.32}$$

The coalescence collision rate is written as

$$\omega_C(\vartheta_i, \vartheta_j) = (\pi/4)(d_i + d_j)^2 n_i n_j \overline{u_{ij}}, \tag{A.33}$$

and is based on kinetic gas theory, i.e. collisions between gas molecules.

A.5 Break-up in population balance

When assuming that all break ups are binary, the break-up may be written as

$$\vartheta_i \rightarrow \vartheta_j + \vartheta_k, \tag{A.34}$$

where ϑ_k is smaller or equal to ϑ_j in size. In the models used we assume that ϑ_k is of a size identical to a particle class smaller than the particle which is split (ϑ_i). ϑ_j must thus be of size ϑ_{i-1} or larger, which may not be the case if we had used a factor lower than 2 for the population class division. ϑ_j is divided into class $(i-1)$ and class i the following way

$$\vartheta_j = x_{i,k}\vartheta_{i-1} + (1 - x_{i,k})\vartheta_i \tag{A.35}$$

In addition we express the volume as a function of the two other particles and use the base volume, i.e. volume of class 1.

$$\vartheta_j = y\vartheta_1 = \vartheta_i - \vartheta_k = 2^{(i-1)}\vartheta_1 - 2^{(k-1)}\vartheta_1 \tag{A.36}$$

Combining eq (A.9), eq (A.35) and eq (A.36) gives

$$x_{i,k} = 2^{1+k-i},\ k < i \tag{A.37}$$

where $x_{i,k}$ is the fraction in class $i-1$ and $(1-x_{i,k})$ is the fraction in class i. Thus a break-up of a particle gives the following

$$\vartheta_i \rightarrow \vartheta_k + x_{i,k}\vartheta_{i-1} + (1-x_{i,k})\vartheta_i \tag{A.38}$$

A test case with $N = 4$ gives the following break-up terms (simplified form used, $\Omega_B(\vartheta_i, \vartheta_k)$ written as $\Omega(i,k)$):

$\Omega(4,3)$, $\Omega(4,2)$, $\Omega(4,1)$, $\Omega(3,2)$, $\Omega(3,1)$, $\Omega(2,1)$.

Note that size 1 does not break up and that we naturally get fewer break-up possibilities as the particles get smaller.

Each of the terms above must be assigned to different classes:

$\Omega(4,3) \rightarrow \Omega(4,3)$ in class 3, $x_{4,3}\Omega(4,3)$ in 3 and $(1\text{-}x_{4,3})\Omega(4,3)$ in 4,

$\Omega(4,2) \rightarrow \Omega(4,2)$ in class 2, $x_{4,2}\Omega(4,2)$ in 3 and $(1\text{-}x_{4,2})\Omega(4,2)$ in 4,

$\Omega(4,1) \rightarrow \Omega(4,1)$ in class 1, $x_{4,1}\Omega(4,1)$ in 3 and $(1\text{-}x_{4,1})\Omega(4,1)$ in 4,

$\Omega(3,2) \rightarrow \Omega(3,2)$ in class 2, $x_{3,2}\Omega(3,2)$ in 2 and $(1\text{-}x_{3,2})\Omega(3,2)$ in 3,

$\Omega(3,1) \rightarrow \Omega(3,1)$ in class 1, $x_{3,1}\Omega(3,1)$ in 2 and $(1\text{-}x_{3,1})\Omega(3,1)$ in 3,

$\Omega(2,1) \rightarrow \Omega(2,1)$ in class 1, $x_{2,1}\Omega(2,1)$ in 1 and $(1\text{-}x_{2,1})\Omega(2,1)$ in 2.

The break-up death rate may thus be written as

$$D_B(i) = \sum_{k=1}^{i-1} \Omega_B(i,k),\ i = 2 \,..\, \mathrm{N}, \tag{A.39}$$

and the break-up birth rate must thus be written as

$$B_B(i) = \sum_{k=i+1,\, i\neq N}^{N} \Omega_B(k,i) + \sum_{k=1,\, i\neq N}^{i} x_{i+1,k}\Omega_B(i+1,k) + \sum_{k=1,\, i\neq 1}^{i-1} (1-x_{i,k})\Omega_B(i,k),\ i = 1 \,..\, \mathrm{N}, \tag{A.40}$$

Notice that the last term in eq (A.40) could have been defined as a negative term in the death rate, eq (A.39). It is just a matter of definition where it is put as long as the total change in the class, $B_B(i) - D_B(i)$, remains the same.

By writing out all the terms for all i one will get all the terms written in the test case. Further, eq (A.39) and eq (A.40) can be checked by taking the total volume balance for all the classes

$$\sum_{i=1}^{N} [(B_B(i) - D_B(i))\vartheta_i] = 0. \tag{A.41}$$

For a $N = 4$ case the terms for the volume balance are (simplified form used) written below. Note that the multiplication factors for the volumes are written in the right side column. These factors must be included when cancelling out terms of different sizes.

$i = 1$: $\Omega(2,1) + \Omega(3,1) + \Omega(4,1) + x_{2,1}\Omega(2,1)$ $\quad | \cdot \vartheta_1$

$i = 2$: $\Omega(3,2) + \Omega(4,2) + x_{3,1}\Omega(3,1) + x_{3,2}\Omega(3,2) + (1-x_{2,1})\Omega(2,1) - \Omega(2,1)$ $\quad | \cdot \vartheta_2$

$i = 3$: $\Omega(4,3) + x_{4,1}\Omega(4,1) + x_{4,2}\Omega(4,2) + x_{4,3}\Omega(4,3) + (1-x_{3,1})\Omega(3,1) + (1-x_{3,2})\Omega(3,2) - \Omega(3,1) - \Omega(3,2)$ $\quad | \cdot \vartheta_3$

$$i = 4: (1 - x_{4,1})\Omega(4,1) + (1 - x_{4,2})\Omega(4,2) + (1 - x_{4,3})\Omega(4,3) \quad | \cdot \vartheta_4$$
$$-\Omega(4,1) - \Omega(4,2) - \Omega(4,3)$$

Cancelling terms of same sizes, inserting $x_{i,k} = 2^{1+k-i}$ and using $\vartheta_{i+1} = 2\vartheta_i$ gives:

$$i = 1: \Omega(2,1) + \Omega(3,1) + \Omega(4,1) + 2^{1+1-2}\Omega(2,1) \quad | \cdot 1$$

$$i = 2: \Omega(3,2) + \Omega(4,2) + 2^{1+1-3}\Omega(3,1) + \quad | \cdot 2$$
$$2^{1+2-3}\Omega(3,2) - 2^{1+1-2}\Omega(2,1)$$

$$i = 3: \Omega(4,3) + 2^{1+1-4}\Omega(4,1) + 2^{1+2-4}\Omega(4,2) + \quad | \cdot 4$$
$$2^{1+3-4}\Omega(4,3) - 2^{1+1-3}\Omega(3,1) - 2^{1+2-3}\Omega(3,2)$$

$$i = 4: -2^{1+1-4}\Omega(4,1) - 2^{1+2-4}\Omega(4,2) - 2^{1+3-4}\Omega(4,3) \quad | \cdot 8$$

This simplifies to:

$$i = 1: 2\Omega(2,1) + \Omega(3,1) + \Omega(4,1) \quad | \cdot 1$$

$$i = 2: 2\Omega(3,2) + \Omega(4,2) + 0.5\Omega(3,1) - \Omega(2,1) \quad | \cdot 2$$

$$i = 3: 2\Omega(4,3) + 0.25\Omega(4,1) + 0.5\Omega(4,2) - 0.5\Omega(3,1) - \Omega(3,2) \quad | \cdot 4$$

$$i = 4: -0.25\Omega(4,1) - 0.5\Omega(4,2) - \Omega(4,3) \quad | \cdot 8$$

All terms above cancels out which indicates that the terms for birth and death are correct. For the $\Omega(3,1)$ term we see that we have one term in the 1st class, half a term in the 2nd class which is of course pre-multiplied with the factor 2 for belonging to the 2nd class and finally a factor 4 for the 3rd class multiplied by a negative half term. The cancellation is thus as follows

$$\Omega(3,1): 1 \cdot 1 + 2 \cdot 0.5 + 4 \cdot (-0.5) + 8 \cdot 0 = 0, \qquad \text{(A.42)}$$

where the volume factor is multiplied with the size of $\Omega(3,1)$ in each class. Thus, since all terms cancels out similarly it is shown that for the $N = 4$ case the 1st term of eq (A.41) equals the 2nd term.

A.6 Coalescence in population balance

When two equal sized particles coalesce the resulting particle will be of one class higher than the two colliding particles. Thus,

$$\vartheta_i + \vartheta_i \rightarrow \vartheta_{i+1}. \tag{A.43}$$

Note that this is only true if and only if we use eq (A.9) with the factor 2 between the classes. When two unequal sized particles collide the coalesced particles will be of a size larger than the largest colliding particle but smaller than the class above the largest particle. It has to be smaller than the next class since this class is twice the volume of the class below, i.e. twice the volume of the largest particle. This clearly demonstrates the advantage of using the factor 2 when dividing the coalescence population into classes. When two particles collide the resulting particle will always be placed in the same class as the largest particle and the class above. When using a factor lower than 2 this may not be the case. If we assume i to be the largest of the two particles colliding this gives

$$\vartheta_i + \vartheta_j \rightarrow x_{i,j}\vartheta_i + (1 - x_{i,j})\vartheta_{i+1} = (x_{i,j}2^{i-1} + (1 - x_{i,j})2^i)\vartheta_1 . \tag{A.44}$$

We may also write the two colliding particles as multiples of the base form (class 1)

$$\vartheta_i + \vartheta_j = (2^{i-1} + 2^{j-1})\vartheta_1 . \tag{A.45}$$

Combining eq (A.9), eq (A.44) and eq (A.45) gives

$$x_{i,j} = 1 - 2^{j-i}, \; i \geq j, \tag{A.46}$$

where $x_{i,j}$ is the fraction in class i and $(1 - x_{i,j})$ is the fraction in class $i + 1$.

A test case with $N = 4$ gives the following coalescence terms (simplified form used, $\Omega_C(\vartheta_i, \vartheta_j)$ is written as $\Omega(i, j)$):

$\Omega(1, 1)$, $\Omega(2, 1)$, $\Omega(3, 1)$, $\Omega(2, 2)$, $\Omega(3, 2)$, $\Omega(3, 3)$,

Size 4 does not coalesce and $\Omega(i, j) = \Omega(j, i)$. Further note that for a $\Omega(i, i)$ coalescence two particles are removed from class i.

Each of the terms above must be assigned to different classes:

$\Omega(1, 1) \rightarrow x_{1,1}\Omega(1, 1)$ in class 1 and $(1 - x_{1,1})\Omega(1, 1)$ in class 2,

$\Omega(2, 1) \rightarrow x_{2,1}\Omega(2, 1)$ in class 2 and $(1 - x_{2,1})\Omega(2, 1)$ in class 3,

$\Omega(3, 1) \rightarrow x_{3,1}\Omega(3, 1)$ in class 3 and $(1 - x_{3,1})\Omega(3, 1)$ in class 4,

$\Omega(2, 2) \rightarrow x_{2,2}\Omega(2, 2)$ in class 2 and $(1 - x_{2,2})\Omega(2, 2)$ in class 3,

$\Omega(3, 2) \rightarrow x_{3,2}\Omega(3, 2)$ in class 3 and $(1 - x_{3,2})\Omega(3, 2)$ in class 4,

$\Omega(3, 3) \rightarrow x_{3,3}\Omega(3, 3)$ in class 3 and $(1 - x_{3,3})\Omega(3, 3)$ in class 4.

For the $\Omega(i, i)$ coalescence one must also include the factor $1/2$ in the $\omega_C(i, i)$ expression to avoid counting each collision twice, Laider & Meiser (1982). The coalescence death rate may thus be written as

$$D_C(i) = \sum_{j=1}^{N-1} \Omega_C(\vartheta_i, \vartheta_j) + \Omega_C(\vartheta_i, \vartheta_i), \; i = 1 \,..\, \text{N-1}, \tag{A.47}$$

and the coalescence birth rate must be written as

$$B_C(i) = \sum_{j=1,\, i \neq N}^{i-1} x_{i,j}\Omega_C(\vartheta_i, \vartheta_j) + \sum_{j=1}^{i-1} (1 - x_{i-1,j})\Omega_C(\vartheta_{i-1}, \vartheta_j), \; i = 2 \,..\, \text{N}. \tag{A.48}$$

By writing out all the terms for all i one will get all the terms written in the test case. Further, (A.47) and (A.48) can be checked by taking a volume balance

$$\sum_{i=1}^{N} [(B_C(i) - D_C(i))\vartheta_i] = 0. \tag{A.49}$$

For a $N = 4$ case the terms for the volume balance are (simplified form used):

$i = 1: -\Omega(1,1) - \Omega(2,1) - \Omega(3,1) - \Omega(1,1) \quad | \cdot \vartheta_1$

$i = 2: x_{2,1}\Omega(2,1) + (1 - x_{1,1})\Omega(1,1) - \Omega(2,1) - \Omega(2,2) - \Omega(2,3) - \Omega(2,2) \quad | \cdot \vartheta_2$

$i = 3: x_{3,1}\Omega(3,1) + x_{3,2}\Omega(3,2) + (1 - x_{2,1})\Omega(2,1) + (1 - x_{2,2})\Omega(2,2) - \Omega(3,1) - \Omega(3,2) - \Omega(3,3) - \Omega(3,3) \quad | \cdot \vartheta_3$

$i = 4: (1 - x_{3,1})\Omega(3,1) + (1 - x_{3,2})\Omega(3,2) + (1 - x_{3,3})\Omega(3,3) \quad | \cdot \vartheta_4$

Cancelling terms, removing $x_{i,i} = 0$ terms and using $\vartheta_{i+1} = 2\vartheta_i$ gives:

$i = 1: -\Omega(2,1) - \Omega(3,1) \quad | \cdot 1$

$i = 2: x_{2,1}\Omega(2,1) - \Omega(2,1) - \Omega(2,3) \quad | \cdot 2$

$i = 3: x_{3,1}\Omega(3,1) + x_{3,2}\Omega(3,2) + \Omega(2,1) - x_{2,1}\Omega(2,1) - \Omega(3,1) - \Omega(3,2) \quad | \cdot 4$

$i = 4: \Omega(3,1) - x_{3,1}\Omega(3,1) + \Omega(3,2) - x_{3,2}\Omega(3,2) \quad | \cdot 8$

Inserting $x_{i,j} = 1 - 2^{j-i}$ and cancelling terms gives:

$i = 1: -\Omega(2,1) - \Omega(3,1) \quad | \cdot 1$

$i = 2: -0.5\Omega(2,1) - \Omega(2,3) \quad | \cdot 2$

$i = 3: -0.25\Omega(3,1) + 0.5\Omega(2,1) - 0.5\Omega(3,2) \quad | \cdot 4$

$i = 4: 0.25\Omega(3,1) + 0.5\Omega(3,2) \quad | \cdot 8$

All terms above cancels out which indicates that the terms for birth and death are correct. For the $\Omega(3,1)$ term the cancellation is as follows

$$\Omega(3,1) : 1 \cdot (-1) + 2 \cdot 0 + 4 \cdot (-0.25) + 8 \cdot 0.25 = 0. \qquad \text{(A.50)}$$

A.7 Incorporation into the transport equation

The transport equation with source terms eq (A.7) is solved numerically by using the fractional time step method, Berge & Jakobsen (1998), and by splitting the convective, diffusive and source terms into their components in the coordinate directions and solving them sequentially. Strang (1968) pointed out that the accuracy of such a splitting depends on the accuracy of how each individual term is numerically solved and on the accuracy of the splitting itself. The splitting used can be shown to be of second order in time.

As an explicit method is used to solve the source terms care has to be taken with the timestep needed for the integration. It is very likely that the timestep needed for the source terms is quite different from what is needed for the flow and pressure fields. Further, the timestep needed for the source terms may vary greatly between different population classes and likewise between different locations in the grid.

Thus, the change and size of the source terms have to be carefully monitored.

Symbols

a	exponent in incomplete gamma function
B_B	birth from break-up, $1/(m^3 s)$
B_C	birth from coalescence, $1/(m^3 s)$
c_1	constant in order of unity, -
c_3	constant, -
c_f	coefficient, -
d_i, d_j	diameters of bubbles in classes i and j, m
$\overline{d_{v,i}}$	diameter of average fluid particle of class i, m
D_B	death from break-up, $1/(m^3 s)$
D_C	death from coalescence, $1/(m^3 s)$
f_{BV}	breakage volume fraction, -
i, j, k	class numbers, -

N	total number of classes, -
n_i	number in class i, $1/m^3$
$P(a, x)$	incomplete gamma function
$P_C(\vartheta_i, \vartheta_j)$	coalescence efficiency for particles of volumes ϑ_i and ϑ_j colliding, -
$Q(a, x)$	(complementary) incomplete gamma function
S	source terms, $1/(m^3 s)$
S’	source terms, $kg/(m^3 s)$
t	time, s
t	integration variable, see eq (A.18), -
$\bar{u}$	Favre averaged velocity, m/s
$\overline{u_i}$, $\overline{u_j}$	average velocities for classes *i* and *j*, m/s
$\overline{u_{ij}}$	relative velocity between particles of classes *i* and *j*, m/s
We_i	Weber number for fluid particle of class *i*, -
We_{ij}	Weber number for collision between fluid particles of classes *i* and *j*, -
x	volume fraction, -
x	lower limit in incomplete gamma function
$x_{i,j}$	coalescence between classes *i* and *j* gives a volume fraction in class *i*, -
$x_{i,k}$	break-up of class *i* gives a volume fraction of second particle, ϑ_j, into class *i-1*, -
y	multiplication factor, see eq (A.10), -
z	exponent in gamma function
α	volume fraction, -
β	constant, $\beta \cong 2.05$

$\bar{\beta}$	constant, $\beta = 2.41$
$\Gamma(a)$, $\Gamma(z)$	gamma function
$\Gamma(a, x)$	part of complimentary incomplete gamma function
γ	added mass parameter, -
γ	constant, see eq (A.17), -
γ'	constant, see eq (A.15), $m^{2/3}$
$\gamma(a, x)$	part of incomplete gamma function
ε	eddy dissipation, m^2/s^3
ε_G	void fraction, -
ϑ	volume, m^3
ϑ_1, ϑ_2, ϑ_3	volume of fluid particles of class sizes 1, 2 and 3, m^3
ϑ_i, ϑ_j, ϑ_k	volume of fluid particles of class *i, j* and *k*, m^3
λ	eddy diameter, *m*
ξ	size ration, $\xi = \lambda / d_i$, -
ξ_{ij}	size ration, $\xi_{ij} = d_i / d_j$, -
ξ_{min}	minimum size ration for break-up, -
ρ	density, kg/m^3
ρ_i	density of class *i*, kg/m^3
ρ_G, ρ_L	gas, liquid phase density, kg/m^3
σ	surface tension, N/m
χ_C	critical breakage energy, -
Ω'	integral part of $\overline{\Omega}_B(\vartheta_i, \vartheta_i f_{BV})$, -
Ω_1'	part of Ω', -

$\Omega(i, j)$ same as $\Omega_C(\vartheta_i, \vartheta_j)$, $1/(m^3 s)$

$\Omega(i, k)$ same as $\Omega_B(\vartheta_i, \vartheta_k)$, $1/(m^3 s)$

Ω_B break-up rate, $1/(m^3 s)$

$\Omega_B(\vartheta_i, \vartheta_i f_{BV})$ corrected break-up rate, see eq (A.29), $1/(m^3 s)$

$\overline{\Omega}_B(\vartheta_i, \vartheta_i f_{BV})$ break-up rate of size ϑ_i into a daughter fraction $\vartheta_i f_{BV}$ and a second particle with the remaining volume (or mass), $1/(m^3 s)$

$\Omega_C(\vartheta_i, \vartheta_j)$ coalescence rate between particles of volumes ϑ_i and ϑ_j, $1/(m^3 s)$

$\omega_C(\vartheta_i, \vartheta_j)$ collision rate between particles of volumes ϑ_i and ϑ_j, $1/(m^3 s)$

References

Berge, E. & Jakobsen, H.A. (1998). A regional scale multi-layer model for the calculation of long-term transport and deposition of air pollution in europe. *Tellus*, **50**, 205-223.

Laider, K,J. & Meiser, J.H. (1982). Physical chemistry. The Benjamin/Cummings Publishing Company, Inc. Menlo Park, California, USA, 19-21.

Luo, H. (1993). Coalescence, breakup and liquid circulation in bubble column reactors. Dr. ing. Thesis, Department of chemical engineering, Trondheim, Norway.

Luo, H. & Svendsen, H.F. (1996). Theoretical model for drop and bubble breakup in turbulent dispersions. *AIChE Journal*, **42**, No. 5, 1225-1233.

Press, W.H., Teukolsky, S.A., Vetterling, W.T. & Flannery, B.P. (1992). Numerical recipes in FORTRAN, Cambridge University Press, 2nd ed., New York, USA.

Strang, G. (1968). On the construction and comparison of difference schemes. *SIAM J. Numer. Anal.*, **5**, No. 3.